SAPIENZA
UNIVERSITÀ DI ROMA

Ph.D. in Sustainable Development and International Cooperation

Small scale hybrid concentrated solar power – biomass system. Development, time dependent modelling and validation.

Eileen Tortora

Supervisor: Prof. Alessandro Corsini

Engineering is not merely knowing and being knowledgeable, like a walking encyclopedia; engineering is not merely analysis; engineering is not merely the possession of the capacity to get elegant solutions to non-existent engineering problems; engineering is practicing the art of the organized forcing of technological change... Engineers operate at the interface between science and society…

Dean Gordon Brown

Engineering: where the noble semi-skilled laborers execute the vision of those who think and dream. Hello, Ooompa-Loompas of science.

Sheldon Cooper

The Big Bang Theory – The Loobenfeld Decay

Acknowledgements

Before the scientific memories about my PhD course, I want to share here my social memories too. This works contains most of the experiences I have had the opportunity to experiment, and I hope that somebody will read it besides have read these acknowledgments (every reference to facts, things or persons, are purely casual and involuntary ☺).

First of all I want to thank my parents Astrid and Luigi, my sister Cecilia and my brother Daniele, who have always sustained and withstanded me, often lightening my duties. I owe you the successes I have obtained in my life and much, much more.

Secondly I want to thank my husband Stefano, for his continuous support to my academic career, his fundamental help and his capacity to properly amuse me in the harder times.

I also want to acknowledge all my friends who cheerfully call me Prof. and all the persons who have shared with me portions of this path.

Finally, I want to pose the attention on the two academic realities I have experienced: the full-comfort wide and sometimes solitary environment of Latina 10 in Latina and the subtropical micro-cosmic crammed full environment of Stanza 21. There are several persons to remember, and for each one, with the thanks for the things they have taught me and the good times spent together, I have a special thought.

Prof. Rispoli, for his precious pearls of knowledge.

Alessandro, as he “belives in it”, even if I don’t belong to the TurboExpo group.

Domenico, for his continuous researches and hunger of ~~knowledge~~ good food.

Paolo, for his lessons of equilibrium between duty and hilarity.

Giovanni, my sheldonian perfidious kindred spirit.

Stefano M., my best gossip spy.

Eleonora, co-ruler of the Latina 10 fort.

Stefano B., for his entertainment with drinking stories.

Fabrizio, for constantly giving me the opportunity to train my throwing abilities.

Andrea, for his great capability to inspire jokes.

Esmeralda, for not applying any diminutive to my name.

Preface

The present work was inspired by the recurrent news about the need of a sustainable fashion for each development sector, the need to pull down greenhouse gas emissions recurring to renewable energies and about the idea that the green economy may help us to come out from the economic crisis. The energy issue has been pointed out, highlighting its problems when including it in a sustainable development scenario. Particular attention has been played to the renewable energy sources, underlying their advantages, problems and solutions.

Another food for thought was the idea that the key for turning the present fossil-fuel economy to a clean tech one, powered by renewable energy, is to give up the approach of replacing individual technologies, but replacing and create whole new systems. The challenge is not to invent a new technology, but to conceive a fully operational system. Thinking about new systems requires an enable technology, an innovative business model, a careful market-adoption strategy and a favorable government policy.

In view of these preliminary remarks, the present work proposes a small scale fully renewable based energy system for cogeneration, able to

supply energy either in on and off-grid systems. The power system was analyzed trough models developed in a transient simulation software, which allows to analyze the plant behavior under hourly-variable operating conditions during a one year period. As developing new systems is more important than developing new technologies, the chosen devices used for the plant are all traditional or large experienced technologies arranged in an innovative shape.

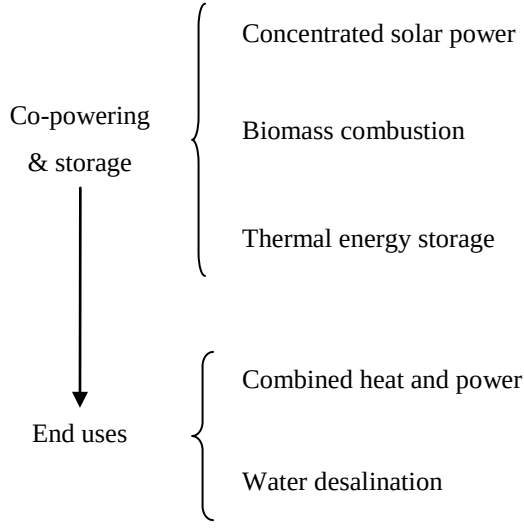

Following the solutions to the renewable energy flaws, mainly related to the intermittent and unpredictable nature of renewable energy sources, the main system components are:

*a **parabolic trough field**, chosen as it is one of the third generation technology and is the most mature technology among concentrating solar power technologies;*

*a **thermal storage** equipped to the solar filed, in order to minimize the collected solar energy dump;*

*a **biomass furnace**, to provide a complementary and spinning resource for the solar field to compensate the sun radiation fluctuations;*

*a **saturated steam Rankine cycle** (RC) for the electric energy conversion via a **steam engine**.*

The novelties of the study can be summarized as:

- *small solar field size, in opposition to the current multi-MW trends, to reduce the footprint impact;*
- *biomass compensation of the sun fluctuations, in place of the usual fossil fuel methods;*
- *saturated steam RC in place of superheated steam, allowing a reduced heat requirement to drive the RC, resulting in a smaller solar field;*
- *a reciprocating steam engine in place of a steam turbine, in order to exploit a wider steam characteristics range. Moreover, it works without any lubricant need. It is worth noting that nowadays steam engines are not more much exploited and are produced by only one company in the world.*

The paths followed during the present study are sketched in the following map.

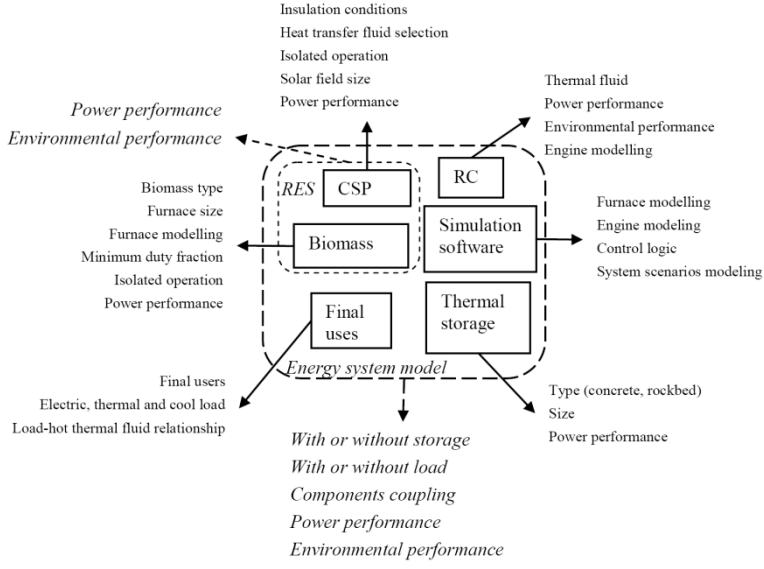

Map of the tackled issues

The modelled energy system has been analyzed under several aspects. Beginning from the renewable energy sources, the solar section has been

initially analyzed by looking at the meteorological data and selecting the heat transfer fluid. At this stand point, with fixed design specifications for the parabolic troughs, isolated operation transient simulations of the solar field were made with the selected software, in order to determine the solar field size and its energy performance. Concerning the biomass side, an identical procedure has been conducted except for the creation of an in-house model for the biomass furnace. Hence, the CSP and biomass systems are coupled and power and environmental performance have been determined.

Subsequently, thermal energy storage block and the Rankine cycle have been studied and modelled to be integrated with the RES system. In particular for the TES section a selection has been made between concrete and rock-bed thermal energy storage. In addition, an in-house model for the steam engine has been created for the purpose.

Moreover the end uses have been inspected, pinpointing direct, i.e. electric and thermal energy loads, and indirect, i.e. water desalination, end uses. To draw out the simulations of the energy system in a load tracking configuration the relations which bond the needed thermal fluid flow rate to obtain both the desired electric and thermal output.

Finally the whole system has been investigated, evaluating power and environmental performance for three configurations:

- *a baseline configuration with a constant power output production;*
- *an end-users electric and thermal power tracking configuration;*
- *a desalting configuration.*

The results show the plant versatility in several duty settings, making it suitable for different applications either in on or off-grid working conditions.

Abstract

Proceeding from the sustainable development principle and the current energy issues, in the present work a small-scale fully renewable power plant was designed, modelled in a time-dependent environment and validated. The plant is design in order to produce both thermal and electric power either in on- or off-grid configuration.

With respect to the state of the art, the power plant is composed by standard and well-known technologies. The novelties brought with the present study are entailed in the arrangement and size of the technologies themselves. Thus the selected parabolic trough solar field is a small size one, i.e. 1,2 MW, on the contrary of the usual multi-MW design. Moreover, the solar section is co-powered with a biomass furnace in place of the typical fossil fuel power generators. Finally, a steam engine is used in a saturated steam Rankine cycle substituting the most common configuration based on steam turbine and superheated steam cycle.

In order to properly evaluate the plant performances, a time-dependent simulation tool was used, allowing to take into account the meteorological variations during a one year period, which has a direct influence on the solar field, affecting the whole system behaviour.

Three different working configurations were proposed, with the aim to assess the plant flexibility to different working conditions, e.g. off-grid or grid-connected. In particular the proposed models are a baseline configuration with constant power outputs, an electric or thermal power tracking scenario coupled with end-users load, and a desalt scenario for electric power and desalted seawater production.

The study shows the capability of the plant to follow different managements, demonstrating its suitability to work in several environments, thus it is effectively reproducible in different countries.

Sommario

Partendo dal principio di sviluppo sostenibile a dalle attuali questioni energetiche, il presente lavoro propone un impianto di piccola taglia completamente alimentato da fonti rinnovabili, mostrandone progettazione, modellazione non stazionaria e validazione. L'impianto è progettato per fornire potenza elettrica e termica lavorando indifferentemente in presenza o assenza di collegamento alla rete elettrica.

Rispetto allo stato dell'arte, l'impianto è composto da tecnologie standard e di comprovato funzionamento. La novità apportata dal presente risiede nella composizione e nella taglia delle tecnologie stesse. In tal senso, il campo di concentratori parabolici selezionato è di piccola taglia, i.e. 1,2 MW, rispetto alle usuali dimensioni multi-MW. Inoltre, la sezione solare è coadiuvata da una fornace a biomasse, invece che da uno dei più comuni impianti per la generazione di potenza da fonti fossili. Infine, è stato considerato un motore alternativo a vapore in un ciclo Rankine a vapore saturo al posto delle più usuali turbine a vapore funzionati in cicli a vapore surriscaldato.

Per la valutazione corretta delle prestazioni dell'impianto è stato utilizzato uno strumento per simulazioni non-stazionarie, permettendo di tenere in considerazione le variazioni delle condizioni meteorologiche durante lo spazio temporale di un anno, le quali hanno influenza diretta sul campo solare, condizionando il comportamento dell'intero sistema.

Sono state proposte tre diverse configurazioni dell'impianto con l'intento di valutare la flessibilità dell'impianto in condizioni di lavoro diverse, e.g. in presenza o assenza di connessione alla rete elettrica. In particolare, i modelli prospettati consistono in una configurazione di base con produzione di potenza costante, una configurazione con inseguimento del carico elettrico e termico di utenze diverse e, una configurazione per la produzione di acqua dissalata.

Lo studio mostra la capacità dell'impianto di seguire i tre diversi tipi di gestione, dimostrando la sua idoneità a lavorare in ambienti e condizioni vari variabili, attestandone quindi la riproducibilità in Paesi diversi.

Table of contents

Chapter 3 Hybrid system components, design and basic thermodynamics

Chapter 4 Analyses of hybrid system process

Acronym list

BIG/GT	Biomass integrated gasifier/gas turbine
BOD	Biological oxygen demand
CHP	Combined heat and power
COD	Chemical oxygen demand
CPC	Compound parabolic concentrator
CSP	Concentrating solar power
DG	Distributed generation
DNI	Direct normal insulation
DSG	Direct steam generation
ED	Electrodialisis
HTF	Heat transfer fluid
IEA	International energy agency
ISCCS	Integrated solar combined cycle power system
LFR	Linear Fresnel reflector
MED	Multi effect distillation
MSF	Multi stage flash
MVC	Mechanical vapour compression
OECD	Organisation for economic co-operation and development
ORC	Organic rankine cycle
PCM	Phase change material
PV	Photovoltaic
R&D	Research and development
RC	Rankine cycle
RD&D	Research, development and demonstration
RES	Renewable energy source
RO	Reverse osmosis
SCA	Solar collector assembly
SEGS	Solar energy generator system
TES	Themal energy storage
TVC	Thermal Vapour Compression
VC	Vapour compression
VVC	Vacuum vapour compression

Nomenclature

Am	Real combustion air mass
A_{tm}	Theoretical combustion air mass
Bc	Biomass consumption
c	Angular coefficient
C	Carbon ratio in biomass composition
C_C	Cold fluid heat capacitance rate
C_H	Hot fluid heat capacitance rate
C_{max}	Maximum heat capacitance rate
C_{min}	Minimum heat capacitance rate
c_p	Specific heat
C_r	Heat capacitance rate ratio
e	Combustion air excesss
e	Steam admission degree
E	Energy
ef	Steam engine effect
ETAo	Operational efficiency
G_m	Gas mass per kg of fuel
H	Hydrogen ratio in biomass composition
h	Enthaply
Hi	Low heating value
k	Steam engine adiabatic exponent
$\dot{m}$	Mass flowrate
n	Combustion air index
n	Steam engine rotational frequency
NTU	Number of transfer units
P	Power
pa	Steam engine admission pressure
Pi	Steam engine indicated power
P_{ltot}	Steam engine total limit power
p_{mi}	Steam engine indicated average pressure
p_{ml}	Steam engine limit average pressure
ps	Steam engine discharge pressure
$\dot{Q}$	Heat exchange
r	Steam engine admission degree

S	Sulphur ratio in biomass composition
T	Temperature
$T_{eg,fur}$	Flame gas temperature
$T_{o,sol,in}$	Inlet oil temperature to solar field
$T_{o,sol,out}$	Outlet oil temperature from solar field
UA	Overall heat transfer coefficient
V	Steam engine cylinders capacity
z	Steam engine pressure admission ratio
γ	Steam engine piston run fraction dedicated to the compression
γ_{SET}	Biomass furnace design set point
$\gamma(t)$	Biomass furnace effective set point
Δh	Enthaply drop
ΔT	Temperature gap
ε	Heat exchanger effectiveness
εv	Steam engine volume expansion ratio
ζ	Pistons shaft encumbrance fraction
η	Efficiency
μ	Steam engine cylinders dead space volume

Subscripts

35	35% rate
O	Oxygen ratio in biomass composition
b	Biomass
b+	Additional biomass
c	Condenser
cool	Cooling water
d	Demand
del	Double effect, lower limit
deu	Double effect, upper limit
eco	Economizer
eg	Exhaust gas
el	Electric
ev	Evaporator
F	Hot thermal fluid
fur	Biomass furnace
g	Global

gen	Biomass generator
in	Input value
out	Output value
o	Oil
se	Steam engine
sel	Single effect, lower limit
seu	Single effect, upper limit
stack	Stack (chimney)
TESc	Thermal energy storage charge
TESd	Thermal energy storage discharge
th	Thermal
w	Water/steam

Chapter 1

Sustainable development and renewable energy sources

1.1 Innovation driven sustainable development

Sustainable development has become part of the lexicon of modern society. From an international perspective, sustainable development is a concept that is routed in the 1972 Stockholm Conference on the Human Environment where international concern on environment and development was first highlighted. Efforts to save this issue culminated in 1987, in the pioneering report of the World Commission on Environment and Development [1] "Our Common Future" which first advanced the notion of sustainable development as "meeting the needs of the present generation without compromising the ability of future generations to meet their own needs". This report proved to be a catalyst for the global movement for sustainable development capped by the 1992 Earth Summit in Rio de Janeiro where governments and members of key sectors of society forged a consensus to implement an action agenda for sustainable development, now popularly known as Agenda 21. The U.N. Commission for Sustainable Development was then established to coordinate the implementation of Agenda 21 and to further develop the principles and practice of sustainable development.

The sustainable development principle offers a vision of progress that integrates immediate and longer-term objectives, local and global action, and regards social, economic and environmental issues as inseparable and interdependent components of human progress, Figure 1.

Sustainable development will not be brought about by policies only: it must achieve a continuous long-term improvement of quality of life through the creation of sustainable communities able to manage and use

resources efficiently, able to tap the ecological and social innovation potential of the economy and, in the end, to ensure prosperity, environmental protection and social cohesion. Economic growth requires a secure and reliable energy supply, but is sustainable only if it does not threaten the environment or social welfare. Environmental quality is more readily protected if basic economic needs are also met, and social development needs both economic growth and a healthy environment. The correlated policies are potentially complementary but sometimes they conflict, thus demanding for trade-offs.

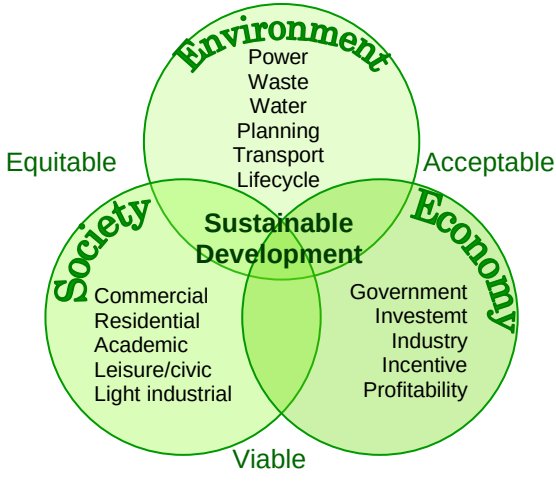

Figure 1: Sustainable development issues [2].

To warrant a sustainable development, the European Union (EU) strategy sets overall objectives and concrete actions for seven key priority challenges for the coming period until 2010, many of which are predominantly environmental [3]:

- climate change and clean energy;
- sustainable transport;
- sustainable consumption & production;
- conservation and management of natural resources;
- public health;

- social inclusion, demography and migration and
- global poverty and sustainable development challenges.

The path to a more sustainable energy future is not static. It must be continuously redefined and rebalanced with revised forecasts, reassessment of progress, identification of new problems and the development of new technical solutions and technologies. All countries, developed and developing, will need to design their own policy mix; it is clear that national circumstances will affect the scope for action and the appropriate policy choices in and between countries [4].

Furthermore, the adoption of the sustainability principle in the economy sector will lead to business and environmental advantages, driving innovation. Figure 2 shows in a simple way the advantages achievable by the application of the sustainability principle to the economy sector, turning to *green economy.*

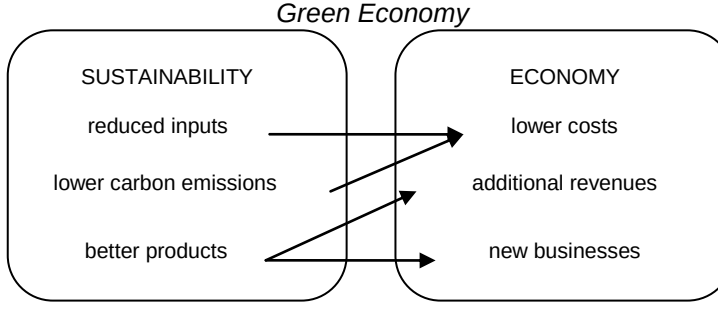

Figure 2: Green economy advantages.

To sum up, smart companies now treat sustainability as innovation's new frontier and a medium to exit well from the economic recession. In fact, by treating sustainability as a goal today, early movers will develop competencies that rivals will be hard-pressed to match. That competitive advantage will stand them in good stead, because sustainability will always be an integral part of development. The *green-innovation* process go through five distinct stages of change, which face different challenges and must develop new capabilities to tackle them. The five stages are [5]:

- viewing compliance as opportunity,

- making value chains sustainable,
- designing sustainable products and services,
- developing new business models, and
- creating next-practice platforms.

There are several environmental regulations of different level. Although it's tempting to adhere to the lowest environmental standards for as long as possible, it's smarter to comply with the most stringent rules, and to do so before they are enforced, to enjoy first-mover advantages in terms of fostering innovation. In fact, enterprises that focus on meeting gold standards gain more time to experiment with materials, technologies, and processes. Moreover, companies that enforce a single norm at all their manufacturing facilities worldwide benefit from economies of scale and can optimize supply chain operations. Finally it enhances the reputation with consumers, policy makers.

The second step in the green economy process is the reduction of non-renewable resources consumption, e.g. coal, oil, and natural gas. The efficiency increase extends from manufacturing facilities and offices to the value chain. The interested areas are supply chains, operations, workplaces and returns. At this stage, corporations work with suppliers and retailers to develop eco-friendly raw materials and components and reduce waste. The initial aim is usually to create a better image, but most corporations end up reducing costs or creating new businesses as well. That's particularly helpful in difficult economic times, when corporations are desperate to boost profits.

At the third stage the attention is paid to consumers who prefer eco-friendly offerings, and to the advantages that the businesses can score over rivals by being the first to redesign existing products or develop new ones. The needed competencies must be turned to the pinpoint the most environmental unfriendly products and services, and to manage the knowhow to scale both supplies of green materials and the manufacture of products. The opportunities of this step are applying new techniques and technologies in the product development.

The fourth step entails the development of new business models, which requires exploring alternatives to current ways of doing business as well as understanding how companies can meet customers' needs differently.

Finally, executives must question the implicit assumptions behind current practices to develop innovations that lead to next practices. Turning to the energy topic, an interesting next-practice platform is

emerging at the intersection of the internet and energy management. Called the smart grid, it uses digital technology to manage power generation, transmission, and distribution from all types of sources along with consumer demand. The smart grid will lead to lower costs as well as the more efficient use of energy. The concept has been around for years, but the huge investments going into it today will soon make it a reality. The grid wilt allow companies to optimize the energy use of computers, network devices, machinery, telephones, and building equipment, through meters, sensors, and applications. It will also enable the development of cross-industry platforms to manage the energy needs of cities, companies, buildings, and households.

1.2 The role of renewable energy, a view

Energy plays an important role in each dimension of sustainable development: economic, social and environmental. Energy services underpin economic activity. They enable basic needs, such as food and shelter, to be met, and they contribute to social development by improving education and public health. Access to modern energy services can also be environmentally beneficial, for example, by reducing deforestation and decreasing pollution caused by inefficient appliances and processes. But there can be conflicts: growing energy use can increase absolute levels of pollution and involves swifter resource depletion. Sustainable development is about finding the right trade-offs.

Thus, energy is a strategic commodity, and ensuring its availability is one important aspect of governments' ultimate responsibility for national security and economic growth. National circumstances and policies will determine the mix of fuels necessary to contribute to the collective energy security, to the economic growth, and to address the challenge of achieving sustainable development. But producing, transporting and using energy carries both economic and environmental costs. Each country will choose the mix of fuels it considers most appropriate, i.e. oil, gas, coal, nuclear or renewables. The power required today to satisfy worldwide demand is about 12.5 TW [6]; end-use energy only, excludes losses in production and transmission). In terms of primary energy, about 35% is from oil, 27% from coal, 23% from natural gas, 6% from nuclear, and the rest from biomass, sunlight, wind, and geothermal. Delivered electricity is a little over 2 TW of the end-use total.

When discussing the energy issue, some considerations must be done about the world population growth, the increasing development of some countries, fossil fuels and the green house gases emissions.

Population growth affects the size and composition of energy demand, directly and through its impact on economic growth and development. World population is projected to grow from an estimated 6,5 billion in 2006 to around 8,2 billion in 2030 - an average rate of increase of 1% per year, Figure 3. By 2030, 52% of the world's population will be in non-OECD Asia (Organisation for Economic Co-operation and Development), down slightly from 53% today. China will remain the world's most heavily populated country, with more than 1,46 billion people, though India's population all but reaches China's by 2030 [7].

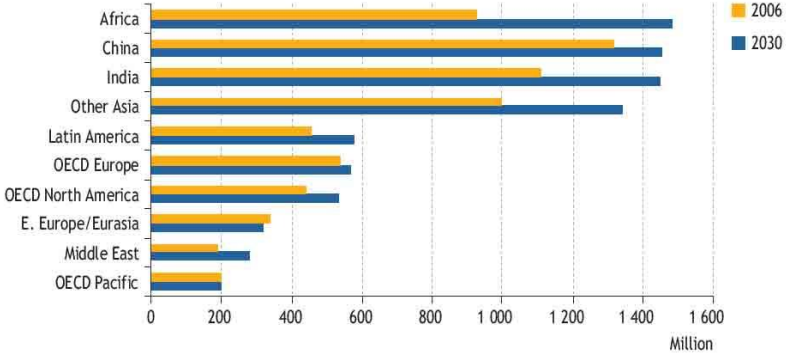

Figure 3: Population by geographic region [7].

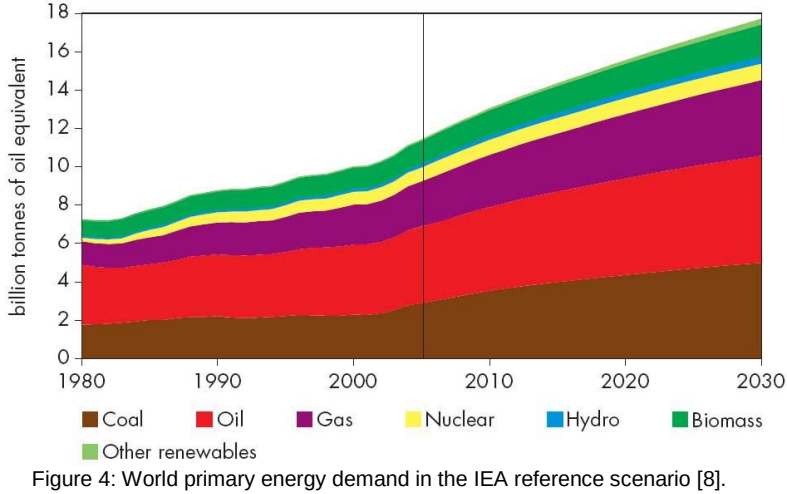

Figure 4: World primary energy demand in the IEA reference scenario [8].

Fossil fuels, i.e. oil, natural gas and coal, remain the worldwide dominant sources of primary energy in the IEA (International Energy Agency) Reference Scenario[1], Figure 4 and Figure 5, and coal sees the biggest increase in demand among all primary energy sources in absolute terms between 2005 and 2030, closely followed by natural gas and oil [8]. The increase share of "other renewables", category that includes wind, solar, geothermal, tidal and wave energy, rises from less than 1% to about 2%.

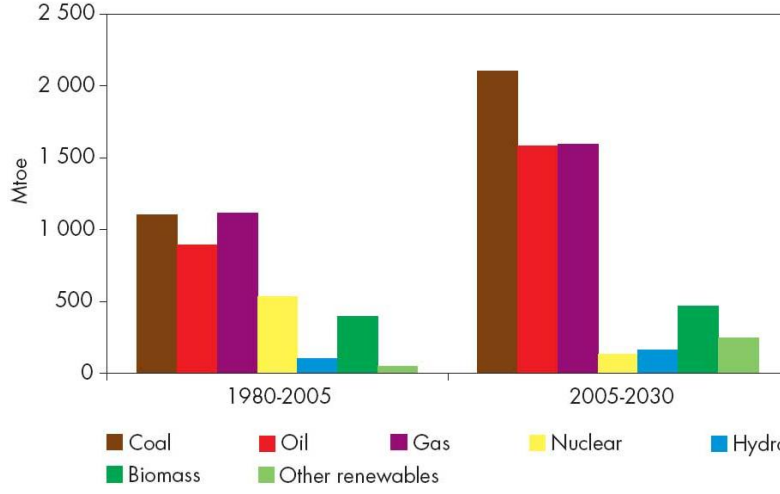

Figure 5: Increase in world primary energy demand by fuel in the IEA reference scenario [8].

Extremely rapid economic expansion in many countries outside the OECD is the main reason why energy demand has accelerated in recent years. Developing countries are projected to contribute around 74% of the increase in global primary energy consumption between 2005 and 2030, Figure 6. Their economies and populations grow much faster than those of the industrialized countries, pushing up their energy use. China and India alone account for 45% of the increase in energy use.

In some cases, i.e. China and India, the population growth is strictly related to the economic growth. This demand is mainly satisfied recurring to the most economic sources, i.e. fossil fuels. Energy developments in

[1] The reference scenario assumes that there are no new energy-policy interventions by governments.

China and India are transforming the global energy system by dint of their sheer size and their growing weight in international fossil-fuel trade. Similarly, both countries are increasingly exposed to changes in world energy markets. Their economic growth has pushed up sharply their energy needs as becoming richer, citizens use more energy to run offices and factories and buy more electrical appliances and cars. Thus the life quality improvement is based on energy needs that must be accommodated and supported by the rest of the world.

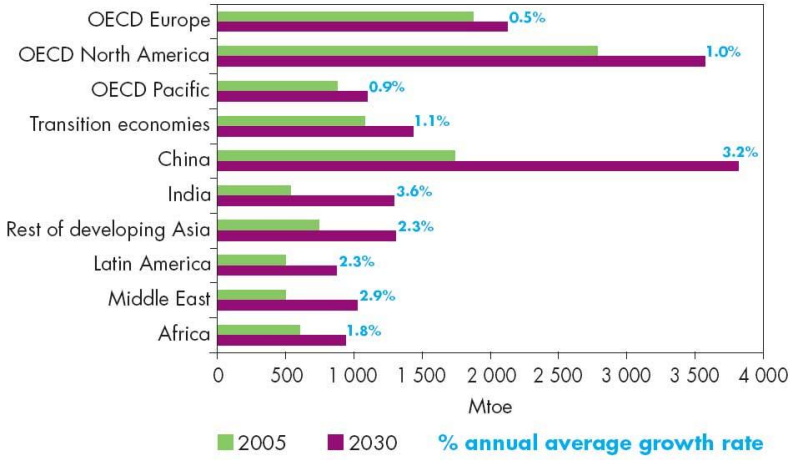

Figure 6: Primary energy demand by region in the reference scenario [8].

The consequences for China, India, the OECD and the rest of the world of unfettered growth in global energy demand are, however, alarming. If governments around the world stick with current policies the world's energy needs would be well over 50% higher in 2030 than today. Globally, fossil fuels continue to dominate the fuel mix. These trends lead to continued growth in energy related emissions of carbon-dioxide and to increased reliance of consuming countries on imports of oil and gas, much of them from the Middle East and Russia. Both developments would heighten concerns about energy security and climate change [8].

From the energy security point of view, oil is the world's vital source of energy and will remain so for many years to come, even under the most optimistic of assumptions about the pace of development and deployment of alternative technology. But the sources of oil to meet rising demand, the cost of producing it and the prices that consumers will need to pay for

it are extremely uncertain, perhaps more than ever. The surge in prices in recent years culminating in the price spike of 2008, coupled with much greater short-term price volatility, have highlighted just how sensitive prices are to short-term market imbalances. They have also alerted people to the ultimately finite nature of oil (and natural gas) resources [7].

Looking at the climate change problems, Figure 7, the rise in fossil-energy use drives up related emissions of carbon dioxide by 57% between 2005 and 2030 in the IEA reference scenario [8]. Preventing catastrophic and irreversible damage to the global climate ultimately requires a major decarbonization of the world energy sources. The energy sector will have to play the central role in curbing emissions, through major improvements in efficiency and rapid switching to renewables and other low carbon technologies, such as carbon capture and storage.

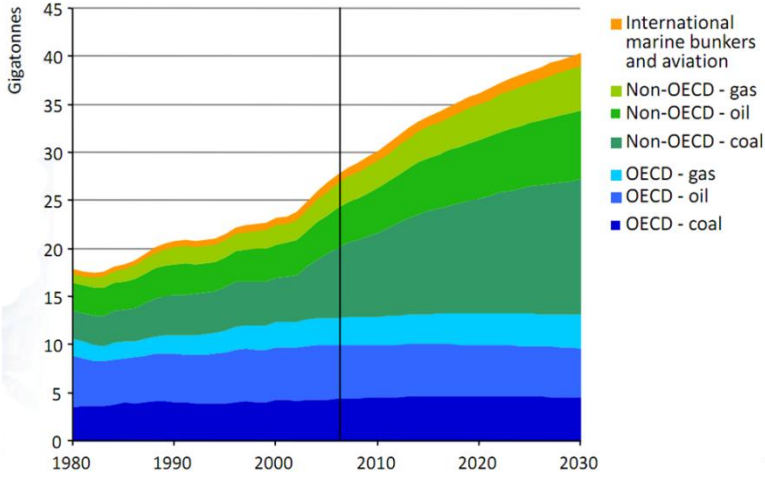

Figure 7: Energy related CO2 emissions in business as usual scenario [9].

The challenge for all countries is to put in motion a transition to a more secure, lower-carbon energy system, without undermining economic and social development. Vigorous, immediate and collective policy action by all governments is essential to move the world onto a more sustainable energy path. Obviously, deciding that action is needed is easy; taking actions and properly linking them is much harder. The first step is defining the areas where action is needed. From the perspective of IEA Member countries, these areas include [10]:

- energy security;
- improving energy efficiency;
- using more renewable energy;
- making markets work;
- technology, including research, development and deployment;
- access to energy;
- transportation; and
- environment, health and safety.

Table 1: Classification of the possible sources of sustainable energy [11].

Primary	Secondary	Tertiary	Qaternary	Quintary
Gravitation				
Earth-Moon	Tides	Grid		
Nuclear				
Natural terrestrial fission	Geothermal	Steam	Grid	
Anthropogenic Fusion	Steam	Grid		
Solar fusion	Electromagnetic radiation	Biomass	Steam	Grid
		Photochemistry	Grid	
		Terrestrial PV	Grid	
		Space PV	Microwaves	Grid
	High temperature solar	Steam	Grid	
	Low temperature solar	Warm air	Grid	
	Climate	Water (hydro)	Grid	
		Waves	Grid	
		Wind	Grid	

The sustainable energy primary sources of harvestable energy which impact the earth are two: gravitational and nuclear, Table 1. Gravitational arises from the Earth–Moon interaction, is manifested in the tides which can be harnessed, but are predictably intermittent and will require energy storage to interface smoothly with the electric grid. Nuclear processes may become manifest in three basic ways [11].

- Fusion driven solar heat radiation which, each day on average, deposits a few hundred watts per square-meter of near-visible electromagnetic radiation on the surface of the Earth and drives

not only photosynthesis but also both climate (with its winds, rains, and waves) and all direct human photon capture and conversion (whether photovoltaic or high temperature thermal2 or low temperature thermal).

- Deep nuclear decay within the planetary interior which drives geothermal processes.
- Human-mediated nuclear processes such as controlled fission or (potentially) fusion.

Renewable energies are essential contributors to the energy supply portfolio as they contribute to world energy supply security, reducing dependency on fossil fuel resources, and provide opportunities for mitigating greenhouse gases. The principle constraint in advancing renewable energy over the last few decades has been cost-effectiveness. With the exception of large hydropower, combustible biomass (for heat) and larger geothermal projects (>30 MWe), the average costs of renewable energy are generally not competitive with wholesale electricity and fossil fuel prices, Figure 8, [12]. On the other hand, several renewable energy options for specific, small-scale applications can now compete in the marketplace, including hot water from solar collectors and electricity from small hydro and other technologies. The biggest challenge facing renewable energy technologies is to advance the state-of-the-art to the point where more renewable options can generate energy at costs that are competitive with conventional sources.

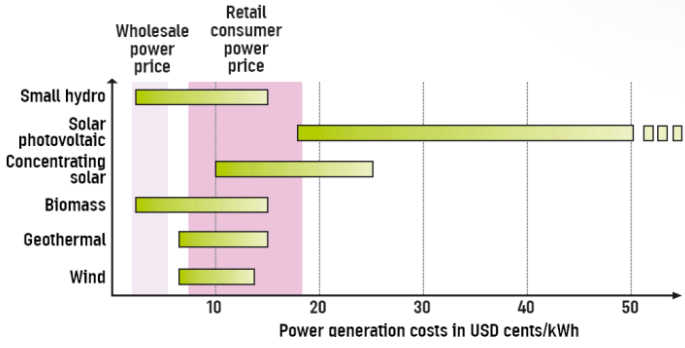

Figure 8: Cost-competitiveness of selected renewable power technologies [12].

With worldwide adoption of stricter environmental standards and guidelines for greenhouse gas emissions, it is becoming clear that renewable energy systems will be credited for their inherent advantage in lowering emissions. These environmental benefits will contribute towards making the delivered costs more palatable and are already the driving force behind policy initiatives in many IEA member countries. Nevertheless, achieving substantial technology breakthroughs to improve cost-competitiveness remains a priority. In many IEA member countries, past policy initiatives to support renewable energy concentrated on research and innovation, market deployment and market-based energy. It is imperative to ensure that market-oriented policies complement technology initiatives.

Based on experience to date, the following observations can be made regarding deployment:

- Significant market growth in renewable technologies results from a combination of policies that address specific barriers and/or complement existing policies. For example, in Japan, photovoltaic (PV) technology was supported by extensive RD&D investments to increase the competitiveness of the technology, through demonstration projects (to increase public awareness and acceptance), through financial incentives (to reduce the purchase price of PV systems) and by requiring utilities to accept, through net metering, excess power generated by PV systems at the retail price of electricity. In Spain, wind technology is supported by feed-in tariffs, low-interest loans, capital grants, and local support for manufacturing of turbines.
- Longevity and predictability of policy support are important to overall market success. In most cases, feed-in tariffs for renewable energy sources have an eight- to twenty-year time frame. The long-term support offered to biomass district heating plants in Austria provides an example. Conversely a ‘stop–and-go’ policy environment does not provide a sound basis to encourage the much-needed private sector involvement.
- With the trend towards market liberalization, early support policies for emerging renewable energy technologies must be tailored carefully to insure against the impact of a significant drop in overall energy prices.

Energy security and environment, as each other sector, are affected by the present financial and economic crises. Investment in new-build renewable energy assets in the power sector grew tremendously over recent years, recording year-on-year growth of 85% in 2007, Figure 9.

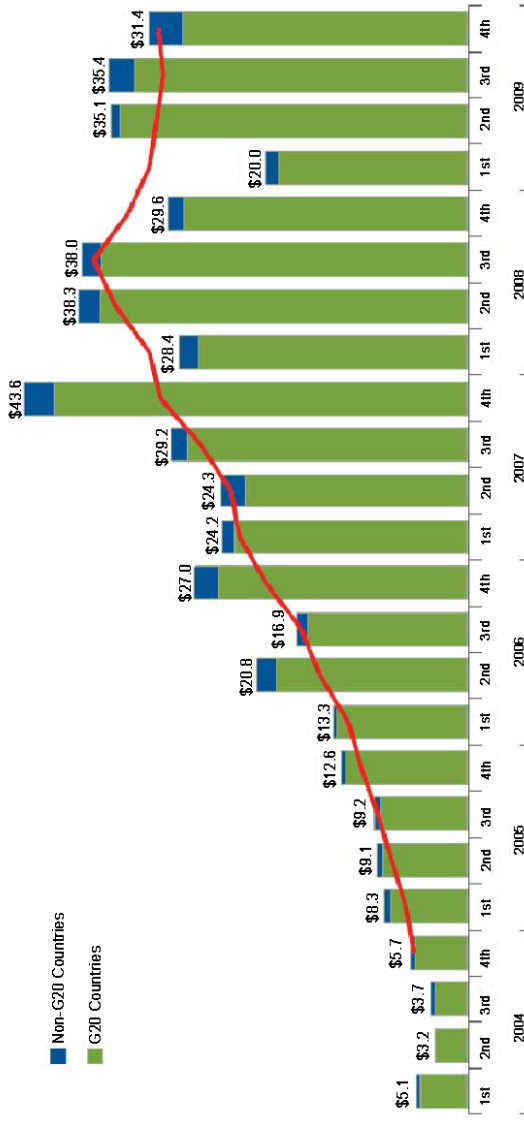

Figure 9: Global investment in renewable based power generation (billion $) [13].

Activity in the sector continued to grow rapidly until the third quarter o 2008, but then fell away as the financial crisis dried up sources of project finance and lower fossil-fuel prices reduced the economic incentive to invest in renewables [14].

Economic recession and financial crisis have brought reduced energy demand and reduced investments [14]. Nevertheless, the reduced energy demand, despite the lowered energy related greenhouse gases emission, might discourage long-term investments in low-carbon and more energy-efficient technologies, pushing up the risk of higher emissions and energy prices when the demand will rise up. However, it is worth noting that investments in renewable energy have had a 6,6% drop down in 2009 with respect to 2008, while gas and oil industries lost 19% of their investments in the same period. In the United States of America in the first 2010 trimester capital venture have invested 1,9 billion $ in renewables, which amounts to an 83% increase with respect to 2009. Concerning Europe, the renewable energy industry turnover is doubled from 2008 to 2009, Figure 10, amounting to 70 billion € [15].

Looking at Italy, in 2008-2009 the amount of 6,5 billion € have been invested on 389 projects, for an overall nominal power of 4127 MW [13].

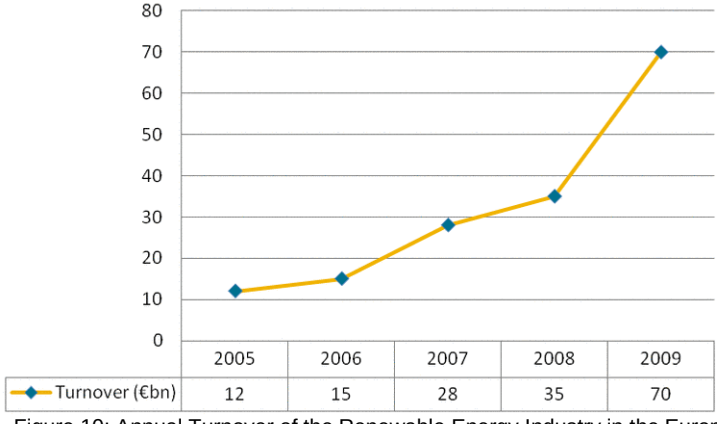

Figure 10: Annual Turnover of the Renewable Energy Industry in the Europe [15].

1.3 A survey of renewable energy sources technical barriers

Renewable energy technologies do not have a long story yet. For this reason there are still many technical bottleneck to be solved before its total penetration on the energy market. In this section the main renewable energy technologies are classified by generations [12].

The **first generation** technologies emerged from the industrial revolution at the end of the 19th century. This category includes devices which easily employ the renewable sources: hydropower, biomass

combustion, and geothermal power and heat. These sources are still in widespread use.

Hydropower is an extremely flexible technology from the perspective of power grid operation. Moreover, as most large plants were built many years ago, their facility costs have been fully amortised making it one of the lowest cost options in today's energy market. Nevertheless, most of the sites suitable for large plants have been already employed. Also a small-hydropower technology exists. At present, only 5% of the global hydropower potential has been exploited through small-scale sites. The principal barriers to exploiting more fully small hydro capacity worldwide, are access to transmission systems and environmental and social concerns.

Biomass combustion for heat and power is a fully mature technology. It offers both an economic fuel option and a ready disposal mechanism of municipal, agricultural and industrial organic wastes. One of the problems of biomass is that material directly combusted in cook stoves produces pollutants, leading to severe health and environmental consequences; although improved cook stove programs are alleviating some of these effects. A second issue is that burning biomass emits carbon dioxide, even though biomass combustion is generally considered to be "carbon-neutral" because carbon is absorbed by plant material during its growth, thus creating a carbon cycle. First-generation biomass technologies can be economically competitive, but may still require deployment support to overcome public acceptance and small-scale issues.

*Geotherma*l power plants can operate 24 hours per day, providing base-load capacity. The world potential capacity for geothermal power generation is estimated at 85 GW over the next 30 years. However, geothermal power is accessible only in limited areas of the world, the largest being the United States, Central America, Indonesia, East Africa and the Philippines. Challenges to expanding geothermal energy include very long project development times, and the risk and cost of exploratory drilling.

Afterwards researchers improved the renewable energy capture devices and the used materials, leading to a **second generation** consisting of solar heating and cooling, wind power, modern forms of bioenergy, and solar photovoltaic. These are now entering markets as a result of RD&D investments since the 1980s.

Solar thermal collectors are already widely used, primarily for hot water production. In principle, larger systems can be used for residential space heating and, in combination with absorption heat pumps, for

cooling. However significant cost reductions are needed before the latter application will become cost-effective.

Wind technology has become very reliable, operating with availabilities of more than 98% and having a design life of 20 years or more. Moreover, as the costs of wind turbines have steadily declined, technical reliability has increased. The factors that currently limit wind energy's market penetration include variability, public acceptance and grid reliability. However, recent developments in electricity market reform, which promote better grid integration and improved management of natural cycles of renewables, diminish the technological barriers that have constrained market penetration. In the area of wind energy, continued RD&D is essential to provide the necessary reductions in cost and uncertainty to realize the anticipated level of deployment. Other RD&D priorities include increasing the value of forecasting power performance, reducing uncertainties related to engineering integrity, improvement and validation of standards, reducing the cost of storage techniques, enabling large-scale use, and minimizing environmental impacts. Further expansion of wind power will promote significant reductions in greenhouse gases.

The *photovoltaic* (PV) market has grown extensively since 1992. RD&D efforts, together with market deployment policies, have effectively produced impressive cost reductions: every doubling of the volume produced prompted a cost decrease of about 20%. In the near term, RD&D efforts will focus on improving the balance-of-system components for both grid connected and stand-alone applications.

More *modern forms of bioenergy* include biomass-based power and heat generation, co-firing, biofuels for transport and short rotation crops for energy feedstocks. These are more advanced and each has its own unique benefits. Biomass is attractive for use either as a stand-alone fuel or in fuel blends, such as co-firing wood with coal, or mixing ethanol or biodiesel with conventional petroleum-based fuels. Anaerobic digestion has strong potential in countries with ample resources. Electricity generated from biomass is based on steam turbine technology. Co-firing is a low-cost and low-risk way of adding biomass capacity. Biofuels from agricultural biomass production is another well-developed conversion technology. The primary barriers to increased use of biomass on a larger scale are the cost of systems required for dedicated feedstock production, harvesting, and transportation, as well as the fuel conversion technologies.

Finally, there is a **third generation**, which is still under development and include concentrating solar power, ocean energy, enhanced geothermal systems, and integrated bioenergy systems.

Concentrating solar power (CSP) consists of three main types of technologies to support electricity production based on thermodynamic processes: parabolic troughs, parabolic dishes and solar central receivers. Current RD&D efforts concentrate on parabolic trough technology. To achieve progress, much larger resources are needed than what is currently offered in public programs. Optimal conditions for CSP are an arid or semi-arid climate, limiting its usefulness to southern Europe, north and southern Africa, the Middle East, western India, western Australia, the Andean Plateau, north-eastern Brazil, northern Mexico and the US Southwest.

Over the last 20 years, *ocean energy technology* received relatively little RD&D funding. However, there is renewed interest in the technology, and several concepts now envisage full-scale demonstration prototypes around the British coast. But ocean energy technologies must still solve two major problems concurrently: proving the energy conversion potential and overcoming a very high technical risk from a harsh environment. Other non-technical barriers include resource assessment, energy production forecasting and design tools, test and measurement standards, environmental impacts, arrays of farms of ocean energy systems, and dual-purpose plants that combine energy and other structures.

Enhanced geothermal systems, known as hot dry rock, utilize new techniques to exploit resources that would have been uneconomical in the past. These systems are still in the research phase, and require additional RD&D for new approaches and to improve conventional approaches, as well as to develop smaller modular units that will allow economies of scale on the manufacturing level. Several technical issues need further government-funded research and close collaboration with industry in order to make exploitation of geothermal resources more economically attractive for investors. These are mainly related to exploration of reservoirs, drilling and power generation technology, particularly for the exploitation of low-temperature cycles.

The *biomass integrated gasifier/gas turbine* (BIG/GT) is not yet commercially employed, but substantial demonstration and commercialization efforts are ongoing worldwide, and global interest is likely to lead to market deployment within a few years. Overall economics of biomass-based power generation should improve considerably with BIG/GT systems as opposed to steam turbine systems.

The bio-refinery concept for biomass feed stocks also has potential to meet a large proportion of future energy demand, particularly once dedicated crops tailored to biorefinery requirements are developed. Current RD&D efforts focus on reducing the costs of dedicated plantations, mitigating potential environmental impacts of bio-refineries and creating an integrated bio-energy industry that links bio-energy resources with the production of a variety of other energy and material products.

Table 2: Technical barriers to renewable energy sources exploitation and current solutions.

Technical barriers	Current solutions
unpredictability of the renewable energy production	technological innovations
low energy-density	combination of complementary renewable energy sources and energy storage
irregular source distribution	smart grids development
integration in conventional grids	use of small-size devices
mismatchings between end users load and energy availability in off-grid configurations	distributed generation promotion

Table 2 provides a summary of the technical barriers to the renewable energy exploitation and the current keys to handle these bottlenecks.

As a matter of fact, few recent studies assert the possibility to supply the whole Europe's, North Africa's [16] and World's [17] energy demand only recurring to renewable sources. In particular, Table 3 and Table 4 show the worldwide available power, the number of devices and the required space needed to meet the energy requirement of the world within 2030, exclusively recurring to renewable energy sources.

Energy Technology	Power Worldwide [TW]	Power in high energy locations [TW]	Power in likely-developable locations [TW]	Current power delivered as electricity [TW]
Wind	1·700 [a]	72-170 [b]	40-85 [c]	0,02
Wave	42,7	2,7 [e]	0,5	0,000002
Geothermal	45	2 [g]	0,07-0,14	0,0065
Hydroelectric	1,9	1,9	1,6	0,32
Tidal	3,7	0,8	0,02	0,00006
Solar PV	6·500 [h]	1·300 [i]	340	0,0013
CSP	4·600 [j]	920 [j]	240 [j]	0,00046

The data are estimated in the hypothesis of energy used in conversion devices, in locations where the energy resources are high, in likely-developable locations, and in delivered electricity in 2005 or 2007 (for wind and solar)

a) Accounts for all wind speeds at 100 m over land and ocean.
b) Locations over land or near the coast where the mean wind speed is 7 m/s at 80 m and at 100 m.
c) Eliminating remote locations.
e) Wave power in coastal areas.
g) Includes estimates of undiscovered reservoirs over land.
h) Assuming use of 160 W panels and areas over all latitudes, land and ocean.
i) Assuming use of 160 W panels and areas between 50S and 50N.
j) Scaling solar PV resources relative land area requirements.

Table 3: Power available in energy resources worldwide [17].

Table 4: Number of plants or devices needed to power the world total energy in 2030 [17].

Energy Technology	Rated power of one plant or device [MW]	Percent of 2030 power demand met by plant/device	Number of plants needed World	Footprint area (% of global land area)	Spacing area (% of global land area)
Wind turbine	5	50	3,8 million	0,000033	1,17
Wave device	0,75	1	720˙000	0,00026	0,013
Geothermal plant	100	4	5˙350	0,0013	0
Hydroelectric plant	1˙300	4	900 [a]	0,407 [a]	0
Tidal turbine	1	1	490˙000	0,000098	0,0013
Roof PV system	0,003	6	1,7 billion	0,042 [b]	0
Sola PV plant	300	14	40˙000	0,097	0
CSP plant	300	20	49˙000	0,192	0
Total		100		0,74	1,18
Total new land				0,41 [c]	0,59 [c]

A given partitioning of the demand among plants or devices is assumed. Also shown are the footprint and spacing areas required to power the world, as a percentage of the global land area $1{,}466 \cdot 10^8$ km^2

a) about 70% of the hydroelectric pklants are already in place.
b) The footprint area for rooftop solar PV does not represent an increase in land since the rooftops already exist and are not used for other purposes
c) Assumes 50% of the wind is over water, wave and tidal are in water, 70% of hydroelectric is already in place, and rooftops solar does not require new land.

1.3.1 Co-powering and storage

The conventional remedial strategy to attenuate the renewable energy fluctuations is to plug the supply gap providing alternative capacity, known as spinning reserve [18]. Whereas among the solutions devoted to RES electric grid integration, it is worth mentioning the use of high capacity energy storage to buffer in time the energy surplus [19] [20], or the combination of different sources with complementary intermittencies [21] [22] [23] [24].

- Hybrid systems can be considered as a reasonable solution. In particular, when looking at the solar technology, several fossil fuel based integration options are commonly cited [25], which include:
- the Solar Energy Generator System (SEGS) power plants in California [26] with electric powers between 30 and 80 MWe, which are based on cylindro-parabolic concentrators with additional fossil fuel burners or natural gas boilers to supply a steam cycle,
- the Integrated Solar Combined Cycle Power System (ISCCS), such as PAESI [27] [28] [29] or ISSCS Nevada, USA [30] [31] based on efficient combined cycles with a better fuel conversion efficiency and reduced electricity production costs (by as much as 42%) compared to the present SEGS plants [26], and
- concepts using high efficiency parabolic solar concentrators, delivering solar heat at an exergy level sufficient to preheat or to fully heat the compressed air of the gas turbine of a combined cycle or to supply heat for endothermic fuel reforming [32].

It is important to note that these advanced concepts have been designed for multi-MW plants aiming at a centralized production, with the associated power transport losses and costs, and with limited possibilities to use the waste heat (cogeneration to meet either heat and/or cold demand).

Looking at remote areas, the complementary aspect is becoming popular for power generation applications due to advances in renewable energy technologies and subsequent rise in prices of petroleum products, and due to the possibility of attenuating fluctuations in produced power. Commonly, it consists of a mix of two or more energy sources used jointly to provide increased system efficiency as well as greater balance in energy supply. Different patterns of intermittency are observed from different technologies, and from the same technology used at different sites. Once these differences in intermittency patterns are known, it is possible to identify complementary patterns between different sites or

technologies, and thus plan the development of intermittent renewables to better match the electricity demand pattern. In literature, several papers have studied the design and planning of hybrid renewable energy systems [33] [34] [35].

To make an example, it has been demonstrated that the complementary intermittencies of wind and solar power in California, along with the flexibility of hydro, make it possible for a true portfolio of renewables to meet a significant portion of California's electricity demand. In particular, combining at least four renewables, wind, solar, geothermal, and hydroelectric power in optimal proportions would allow California to meet up to 100% of its future hourly electric power demand assuming an expanded and improved transmission grid [36].

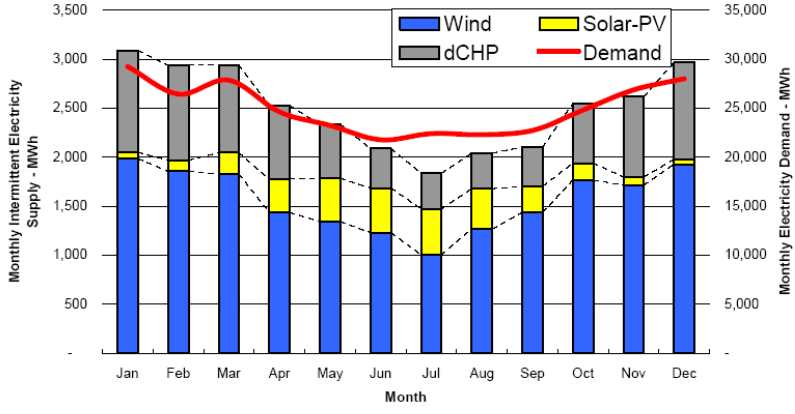

Figure 11: Comparison of electric demand and intermittent electricity supply by month in England and Wales [21].

Moreover, Figure 11 demonstrates how the electricity generated from a combination of intermittent technologies can match demand on a monthly basis. In this example, the total hourly electricity demand for each month has been calculated (red line), while the total electricity generated by wind, solar PV and combined heat and power (CHP) for each month has also been calculated (coloured bars) [21]. In this case, the total amount of electricity generated from intermittent renewables equals 10% of the total annual electricity demand for England & Wales. For each month, however, the contribution from intermittent renewables may be slightly higher or lower than the 10% annual average target. Electricity generated from offshore wind accounts for around 65% of total

intermittent generation, while CHP accounts for around 25% and solar PV accounts for around 10% of total intermittent generation.

Looking at the energy storage alternatives, the basic idea is to provide a buffer to balance fluctuations in supply and demand, maximizing the renewable energy conversion of the peak production periods. Energy storage embraces a wide range of energies, technologies, scales and applications. Energy may be converted to stored form in chemical, electrical, kinetic, potential or thermal media. It can be converted for end use directly, for example when heat is taken from a thermal energy store, or indirectly via an energy conversion system, for example when electricity is generated via the turbine generator of a pumped hydro storage system. Energy storage systems are generally described as either electrical or thermal. Electrical energy storage embraces all the technologies and systems where the external interface is electrical. The energy storage medium itself may use one of a number of technologies, including electrochemical systems, kinetic energy storage and potential energy storage. The electrical interface is an essential element of electrical energy storage systems and is provided by a power conversion system. The power conversion system can represent more than 25% of the overall cost of a complete electrical energy storage system. In contrast, thermal energy storage systems utilize either the sensible or latent heat capacity of materials to provide a heating or cooling resource, which can be replenished as required. Electrical energy storage systems find ready application in a diverse range of markets. They include traction and propulsion, the ubiquitous automotive starting, lighting and ignition sector, standby power, remote area power supplies and in electrical power systems. In contrast, thermal energy storage has a somewhat more restricted applications domain, principally embracing the built environment, industry and certain other niche markets

A demonstration of the weight of thermal energy storage (TES) in renewable energy systems is provided in Figure 12 [37], which shows the charge-discharge transient behaviour of a CSP system on a typical summer day-time. When the power from the CSP (P_{CSP}) attains the design power input to the evaporator ($P_{ev,sol}$), the surplus heat (P_{TESc})is stored during a charging sub-cycle that lasts about 10 hours. When the direct normal insulation (DNI) decrease, the TES discharge cycle is switched on. The cycle takes place over a time interval of 8 hours. The behaviour of the power input from TES (P_{TESd}) is shown by the grey area. It is remarkable that the TES is able to establish a buffer of the solar thermal input.

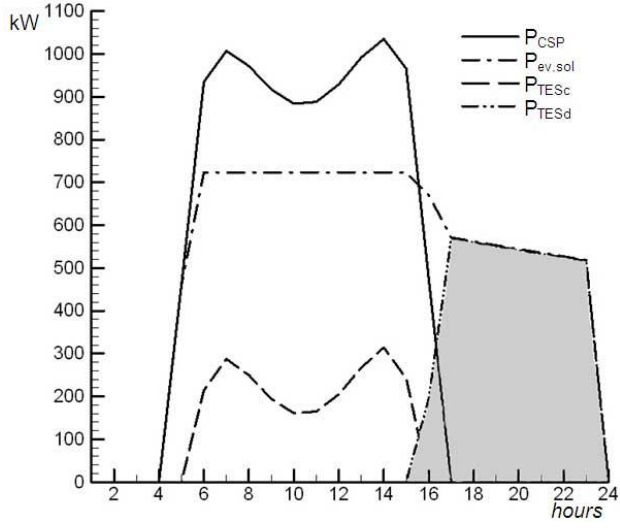

Figure 12: Storage charge-discharge behaviour of a CSP system on typical summer day time [37].

1.3.2 Renewable energy management: smart grids

Modern society is dependent on flexible electrical energy, available on demand and at an affordable cost. Most of our electrical energy is produced by converting the carbon stored in coal or natural gas into heat energy and then via a turbine into mechanical energy. As the percentage of renewables in a given grid edges above 10-15%, the problems of integration begin to multiply due to intermittency issues [38]. At present, in most distribution networks, particularly those in the developed world, consumers can have as much electrical energy as they require whenever it is needed; generators provide the flexibility. Currently, nuclear stations and less-expensive coal or combined cycle gas turbines are used for base load, while coal and gas fuelled generators and pumped storage plants are used for balancing during peak demand. Many renewable resources are *intermittent or variable* by nature, producing power inconsistently and somewhat unpredictably, while on the other end of the transmission line, consumers demand power variably but predictably throughout the day. The Independent System Operator (ISO) monitors this demand, turning on or off additional generation when necessary. As such, predictability of energy supply and demand is essential for grid management. For natural gas or hydroelectricity, supplies can be throttled relatively easily. But

with a wind farm, power output cannot be ramped up on demand. In some cases, a single wind farm that is providing power steadily may see a drop in or complete loss of wind for a period. For this reason, grid operators generally pay less for energy provided from wind or solar power than from a conventional, predictable resource. Nowadays, renewable generation is normally only a small percentage of the total and consequently is always allowed to generate, with a negligible role in balancing, but in a low carbon future, we will have to find a way of balancing supply and demand without resorting to coal and gas fuelled generators, contemporarily facing the variable nature of renewables.

More specifically, all electric grids can fall victim to sudden drops in voltage caused by a short-circuit within the transmission system. While the fault is usually speedily isolated by automatic protection systems, typically within milliseconds, until that point the voltage on the transmission system falls (in theory to zero at the point of the fault). The effect of this voltage drop becomes less severe the further it is away from the source of the problem, but its effects can be significant over several hundred kilometres. Conventional generating capacity uses synchronous generators, which respond well to short-lived voltage dips and are able to rapidly change the amount of reactive power they produce or consume. Reactive power, which is produced predominantly by generating plants, and consumed by electricity consumers, is a complex concept, but it is essentially used by system operators to control voltage levels. The injection of reactive power into the grid by generating plant has the effect of counteracting the effect of voltage drops. Looking at the wind sector, which represents the larger fraction of grid-connected renewable energy although its highly unpredictable nature, many old or less advanced wind turbines are not able to react in such a fashion, consuming large amounts of reactive power, which can exacerbate the voltage dip. Instead, in order to protect their power electronics, they are designed to shut down instantaneously in the event of such a drop in voltage. This is a significant problem in grids with high renewable penetration rates. The solution to this problem is higher technical standards for renewable energy generators to meet, enhancing grid codes by requiring that renewable energy generating equipment has low voltage ride trough (LVRT) capability and reactive power control capability. These typically have three aspects:

- a voltage-time graph which defines an envelope defined by the extent of voltage drop-off and duration outside of which generators are permitted to disconnect from the grid;
- a requirement for the provision of reactive power during the fault; and

- a requirement for the restoration of active power after the fault.

Furthermore, the energy management has to become much smarter, with integrated communication systems and real time balancing between supply, demand, and storage.

The *Smart Grid* is a method of delivering electricity from suppliers to consumers using information technology and communication systems, which allows to save energy, reduce cost and maximize the use of national, local and domestic sources of low carbon energy. Key components of smart grids include s*torage technology*, *demand side management and enhanced grid communications systems* [39]. In particular, the storage is fundamental to fully employ the produced renewable energy when the supply exceeds the demand, shifting its release at times of peak demand. The storage can be centralized within the grid or distributed in individual homes or communities. Even with additional storage, systems will need to be in place to ensure that energy use is sensitive to the supply available and enhance the reliability of the network. If for example, renewable generation remains low for extended periods of time, in an unmanaged system all the stored energy could be used up leading to electricity supply problems. To avoid such scenarios, consumers could have *smart home* systems which receive pricing signals informing smart appliances that local energy costs are high and ideally that they should not operate. Finally, to balance the supply, demand, and storage, electricity grids will need an intelligent communication system. Such an information system would provide 'real time' electricity pricing to smart meters in homes and integrate all elements connected to the electrical grid. In a smart grid the above components are linked in to an intelligent network infrastructure, adapted to incorporate distributed generation. Such a network would have remote management and fault monitoring, and respond in real time to external factors such as changes in weather patterns and therefore electricity generation. Moreover, as smart grids are essentially a way to adapt the grid to incorporate low carbon intermittent electricity generation, there are several challenges involved in their development, and maintaining a secure and reliable energy supply system. In fact, there will be the need to manage an increasingly complex energy supply and demand mix made by:

- a larger average demand;
- the need of capacity to cope with (or be able to shift) an increase in peak demand due to electric vehicle charging;
- the deal of the increasing of distributed generation.

1.3.3 Renewable energy management: Distributed Generation and Combined Heat and power

Distributed generation (DG) represents an alternative paradigm of generating electricity (and heat) at, or close to, the point of demand. Alternate definitions of DG can be made according to size or location within the electricity network [40], but these implicitly classify DG as a function of an electricity system's characteristics. DG became almost extinct in the period to 1990. The primary reason for this was that the economies gained by building larger power stations outweighed the additional costs of transporting electricity to consumers. The fundamental benefit of DG is that it promises significant reductions in transportation cost. The precise potential for efficiency gains and emissions savings varies depending on the generation technology and the location of the generation unit. Technologies using renewable energy sources often need to be located distant from consumers to take advantage of localized energy resources. Overall, as smaller generation technologies reduce their capital and operating costs compared with larger generators their transportation benefits will encourage their further growth. The five DG key technologies, i.e. gas engines, diesel engines, gas turbines, micro-turbines, and fuel cells, are fossil fuel based. However, there are renewable based DG systems too [41].

Beside DG the use of Combined Heat and Power (CHP) systems providing energy directly to end users is currently becoming one of the options in the industrial, service and residential sectors [42] [43] [44], for its capability to produce heat and power more efficiently than with conventional power sets. They produce electricity allowing the exploitation of waste heat output to be used for district or process heating. A cogeneration system can return fossil fuel energy savings up to 30% and can reduce CO2 emissions correspondingly as compared with conventional systems. Also CHP configurations are mainly based on the use of conventional fossil fuels, such as natural gas, except for the small-scale power plants fed with biomass derived fuel (e.g. wooden or biogas), now gaining a significant share of the European energy market, and by the development of co-combustion schemes on large power plants [45] [46]. One serious challenge to the implementation of CHP systems is matching and sizing of the system to strongly and frequently varying load conditions without negative impacts on the efficiency [47].

1.4 Aim of the thesis

In this introductory chapter the energy issue has been pointed out, highlighting its problems when including it in a sustainable development

scenario. Particular attention has been played to the renewable energy sources, underlying their advantages, problems and solutions. The key for turning the present fossil-fuel economy to a clean tech one, powered by renewable energy, is to give up the approach of replacing individual technologies, but replacing and create whole new systems. The challenge is not to invent a new technology, but to conceive a fully operational system. Thinking about new systems consists of four interdependent and mutually reinforcing components: an enable technology, an innovative business model, a careful market-adoption strategy and a favourable government policy [48].

In view of the above mentioned elements, the present work proposes a small scale fully renewable based energy system for cogeneration, able to supply energy either in *on* and *off-grid* systems. The power system was analyzed trough models developed in a transient simulation software, TRNSYS®, which allows to analyze the plant behavior under hourly-variable operating conditions during a one year period. As developing new systems is more important than developing new technologies [48], the chosen devices used for the plant are all traditional or large experienced technologies arranged in an innovative shape.

Chapter 2

State of the art of renewable energy technologies

Renewable energies represent a concrete opportunity to rise from the economic crisis and to solve many energy and environmental problems. However, the randomness of energy availability represents a problem when there is the need to accurately match a defined load. As already explained in §1, the solution to this problem is represented by the co-powering, that is the possibility to mix two or more complementary renewable energy sources with different intermittency patterns, providing increased system efficiency as well as greater balance in energy supply [33] [34] [35]. For this reason it is fundamental to know the characteristics of the different sources and technologies.

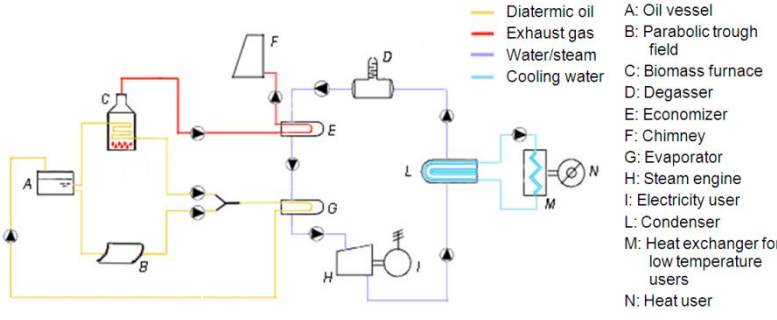

Figure 13: Main scheme of a hybrid CSP-biomass power plant.

Referring to the present study, the selected renewable energy sources are sun and biomasses. As represented in Figure 13 the studied power plant principally consists of two sections: the co-powering and thermal energy storage subsystem and the end users subsystem. The first one is composed by concentrated solar power, biomass combustion and thermal storage technologies. The second subsystem consists of the end uses of the produced energy, in the direct electric and thermal form and in the indirect form of desalted water.

2.1 Concentrated Solar Power systems

Classical optical theory predicts that light rays travelling parallel to the axis of a spherical mirror will reflect off the mirror and pass through the focus of the mirror located a distance R/2 from the mirror, where R is the radius of the mirror. The energy of all incident light rays combine at this point, effectively concentrating the light energy. This concentration produces heat, hence the name: concentrated solar power (CSP). So, in short, CSP systems use different mirror/reflector configurations to convert the sun's energy into high temperature heat. This heat can then be used directly or converted into electricity.

The main components of a CSP system are:

- The **solar collector field**: it is the array of mirrors or reflectors that actually collects the solar radiation and focuses it on to the solar receiver. The field is usually quoted in square metres which represents the surface area of the array, not the land use area.
- The **solar receiver**: it is the part of the system that transforms the solar radiation into heat. Sometimes this receiver is an integral part of the solar collector field. A heat transfer medium, usually water or oil, is used in the solar receiver to transport the heat to the energy conversion system.
- The **energy conversion system**: it is the final component in the system and converts the heat into usable forms of energy, in the form of electricity or heat.

The knowledge of the quantity and quality of solar energy available at a specific location is of prime importance for the design of any solar energy system. Although the solar radiation (*insolation*) is relatively constant outside the earth's atmosphere, i.e. about 1367 W/m^2, local climate influences can cause wide variations in available insolation on the

earth's surface from site to site. In addition, the relative motion of the sun with respect to the earth will allow surfaces with different orientations to intercept different amounts of solar energy. Figure 14 shows regions of high insolation where solar energy conversion systems will produce the maximum amount of energy from a specific collector field size. However, solar energy is available over the entire globe, and only the size of the collector field needs to be increased to provide the same amount of heat or electricity as in the shaded areas. It is the primary task of the solar energy system designer to determine the amount, quality and timing of the solar energy available at the site selected for installing a solar energy conversion system.

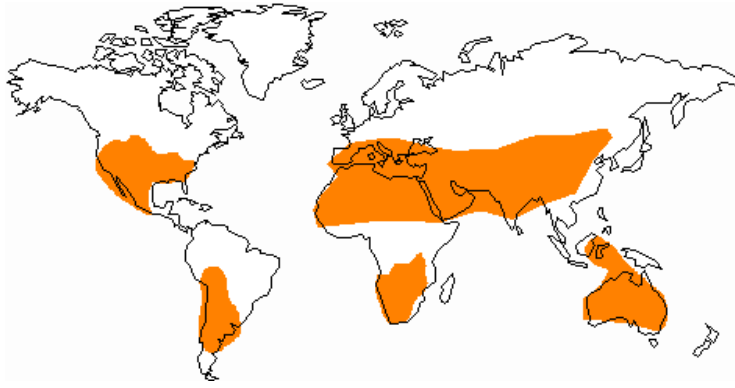

Figure 14: High insolation world's areas in which CSP is economic viable [49].

Solar thermal power uses direct sunlight, called 'beam radiation' or Direct Normal Irradiation (DNI). This is the sunlight that is not deviated by clouds, fumes or dust in the atmosphere and which reaches the Earth's surface in parallel beams for concentration. Suitable sites are those that get a lot of this direct sun - at least 2,000 kWh/m^2 of sunlight annually. The best sites receive more than 2,800 kWh/m^2 a year. Typical regions for CSP are those without large amounts of atmospheric humidity, dust and fumes. They include steppes, bush, savannas, semi-deserts and true deserts, ideally located within less than 40 degrees of latitude north or south. Therefore, the most promising areas of the world include the south-western United States, Central and South America, North and Southern Africa, the Mediterranean countries of Europe, the Near and Middle East, Iran and the desert plains of India, Pakistan, the former Soviet Union, China and Australia, Figure 14. In these regions, 1 km^2 of land is enough

to generate as much as 100-130 GWh of solar electricity a year using solar thermal technology. This is the same as the power produced by a 50 MW conventional coal or gas-fired mid-load power plant [50].

The solar collector intercepts the incoming insolation and changes it into a useable form of energy that can be applied to meet a specific demand. In particular, the temperature of the receiver increases until the convective and radiation heat loss from the receiver equals the absorbed solar energy. The temperature at which this occurs is termed "collector stagnation temperature". For control of the collector temperature at some point cooler than the stagnation temperature, active removal of heat must be employed. This heat is then available for use in a solar energy system. The heat removal is obtained by the circulation of a fluid in the receiver. The fluid may be water, air melted salts or diathermic oil. For removal of a large fraction of the absorbed solar energy as useful heat, the amount of heat lost from the receiver must be kept small. The most common way of reducing receiver heat loss at elevated temperatures is to reduce the size of the hot surface, i.e., the receiver, since heat loss is directly proportional to area of the hot surface. Concentrating collectors reduce the area of the receiver by reflecting, or refracting, the light incident on a large area, the collector aperture, onto an absorber of small area. With reduced heat loss, *concentrating collectors can operate at elevated temperatures and still provide significant quantities of useful thermal energy.* Furthermore, reflective surfaces are usually less expensive than absorbing, receiver, surfaces. Therefore, *large amounts of inexpensive reflecting surface area can placed in a field, concentrating the incident solar energy on smaller absorbing surfaces*. However, to obtain high efficiencies, concentrating collectors usually track the sun´s movement across the sky, adding significant cost to the construction of a concentrating collector system [49].

Table 5: Classification of solar concentrators.

Technological level	Concentrator type	Architecture type
Low	Fresnel mirror concentrators	Line-focus
	Compound parabolic concentrators	Line-focus
High	Solar tower/central receiver systems	Point-focus central receiver
	Parabolic dish/Stirling engines	Point-focus distributed receiver
	Parabolic troughs	Line-focus

There are two groups of concentrated solar power systems, Table 5, which differ for their technological level and for the architecture type. The mentioned technologies will be briefly described afterwards.

Table 6 offers a global view of the different plant characteristics, focusing on operating temperatures, concentration ratio, sun tracking type, net efficiency and type of operation. As can be seen, the best concentration ratio and efficiency are related to the parabolic dish technology, which is still under development, while most projected technology is the parabolic trough one, despite the lower efficiency and concentration ratio.

Spain is the leading country in CSP development, with 22 projects for 1,037 MW under construction, all of which are projected to come online by the end of 2010. Despite only 75 MW of CSP under construction, the U.S. continues to offer significant opportunity for CSP, with 8.5 GW in the pipeline and scheduled for installation by 2014. While parabolic trough represents more than 96% of all CSP projects currently under construction in Spain, the technology accounts for only 40% of the U.S. CSP pipeline. Backed by sufficient government incentives, Spanish CSP developers have not been compelled to take on major technology risk [51].

The sizes of the different plants ranges from 1 MW_e for parabolic dish installations to 10 MW_e for central receiver systems or 50 MW_e for parabolic trough systems. Generally, the efforts are toward the realization of plants with increased power, entailing higher land use and costs too. To the best of the author knowledge, only two studies in the open literature treat the possible downsizing of CSP plants, one supplying energy for the operation of a building with a 65 m^2 parabolic trough field [52] and one targeted to supply energy services to remote and isolated villages with a mini-hybrid solar-fossil power plant of a few kWe to a few tens of kWe [53].

In terms of power density the Andasol projects in Spain have an average footprint of about 12 m^2/kW, while the SEGS plants range between 9,29 and 6,26 m^2/kW [54], remarkably higher than those of conventional power generation schemes, i.e. 4 times the micro-turbine generator footprint in the range 0,15-1,5 m^2/kW (Aspen Systems Corporation Applied Management Sciences Group, 2000). To improve the power density, at present, the investigation areas target the up-grade of the optical and thermal efficiency of the solar components as well as the use of direct generation of steam (DSG) in the receivers [55] [56].

Table 6: Technical characteristics of solar thermal power plants [57]

Technology	Typical operating temperature [°C]	Concentration ratio	Tracking	Net efficiency a [%]	Type of operation	Installed capacity [MWel]	Annual ouput 2006 [GWhel]	Currently projected [MWel]
Parabolic + Fresnel trough	260-400	80-200	One-axis	9-14	commercial	354	988	1'100 (Spain) b 2'675 (worldwide) 513 Fresnel
Central receiver	500-800	500-1'000	Two-axes	13-18	commercial	10'250	-	46 (Spain) 566 (worldwide)
Parabolic dish	500-1'200	800-8'000	Two-axes	15-24	demo	-	-	800 (U.S.)

a) defined as electricity generated/solar energy intercepted
b) 12-15% fossil back up allowed to maintain the thermal storage temperature during non-generation periods

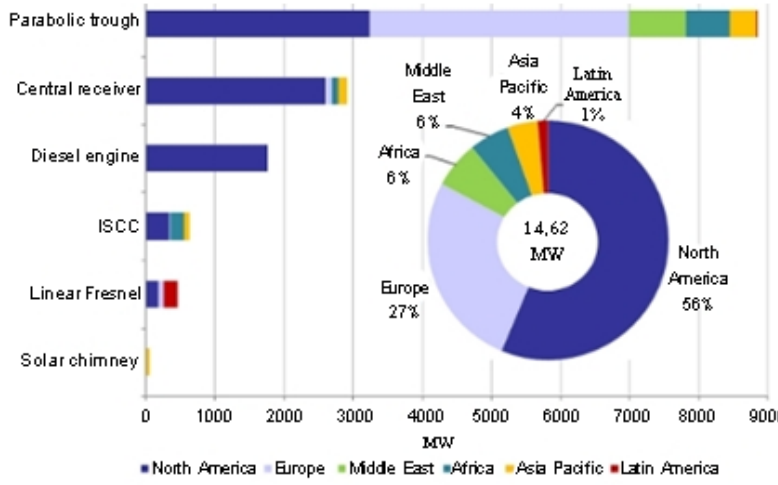

Figure 15: Regional CSP Pipeline by Technology [51].

2.1.1 Fresnel Mirror Concentrator

A Linear Fresnel Reflector (LFR) is a single-axis tracking technology that focuses sunlight reflected by long heliostats onto a linear receiver to convert solar energy to heat.

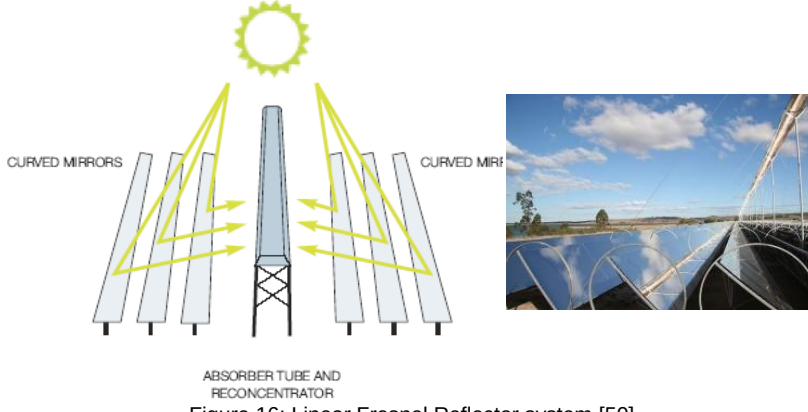

Figure 16: Linear Fresnel Reflector system [50].

The classical linear Fresnel system uses an array of mirror strips close to the ground to direct solar radiation to a single, linear, elevated, fixed receiver. Each mirror element is tilted at an angle so that all incident solar rays falling on them are reflected to a common focus. The Fresnel

reflector is composed of parabola slices mounted on a flat surface. The flat mounting surface has advantages with regard to practical engineering and construction.

The technology is seen as a lower cost alternative to trough technology for the production of solar steam for power generation. The main advantages of the Linear Fresnel collector, compared to trough collectors, are seen to be:

- Inexpensive planar mirrors and simple tracking system.
- Fixed absorber tube with no need for flexible high pressure joints.
- No vacuum technology and no metal-to-glass ceiling.
- One absorber tube with no need for thermal expansion bellows.
- Due to the planarity of the reflector strips, wind loads are substantially reduced so the reflector width for one absorber tube can easily be three times the width of parabolic trough.
- Due to direct steam generation no heat exchanger is necessary.
- Efficient use of land since the collectors can be placed close to one another.

2.1.1.1 Compound parabolic concentrator

The name, compound parabolic concentrator (CPC), derives from the fact that the CPC is comprised of two parabolic mirror segments with different focal points, Figure 17. The focal point for parabola *A* (F_A) lies on parabola *B,* whereas the focal point of parabola *B* (F_B) lies on parabola *A*. The two parabolic surfaces are symmetrical with respect to reflection through the axis of the CPC.

A Compound parabolic concentrator (CPC) makes use of the fact that when the rim of a parabola is tilted toward the sun, the rays are no longer concentrated to a point, but are all reflected somewhere below the focus. The rays striking the half of the parabola, which is now tilted away from the sun, are reflected somewhere above the focus. This can be seen in Figure 18, where the rays on the right-hand side are reflecting below the focus and the rays on the left-hand side are reflecting above the focus. If the half parabola tilted away from the sun is discarded, and replaced with a similarly shaped parabola with its rim pointed toward the sun, the result will be a concentrator that reflects (i.e. traps) all incoming rays to a region below the focal point.

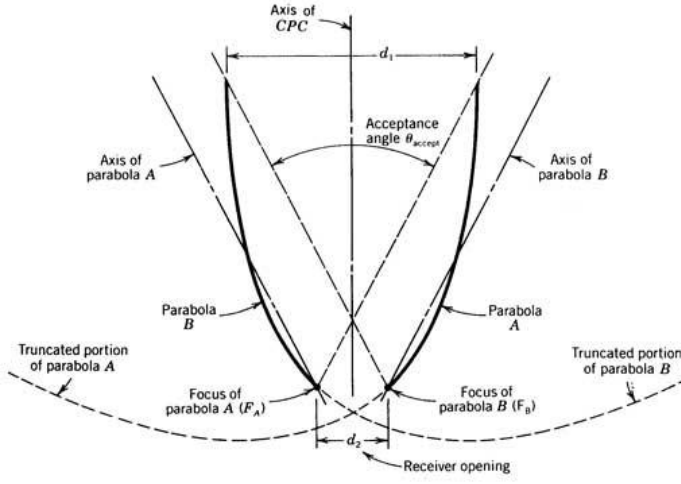

Figure 17:Compound parabolic concentrator (CPC) [49].

Since the rays are no longer concentrated to a single point, this design is called a *non-imaging concentrator.* A receiver placed in the region below the focus and the concentrator will trap the sun rays coming from any angle between the focal line of the two parabola segments. Receivers can be flat plates at the base of the intersection of the two parabola, or a cylindrical tube passing through the region below the focus.

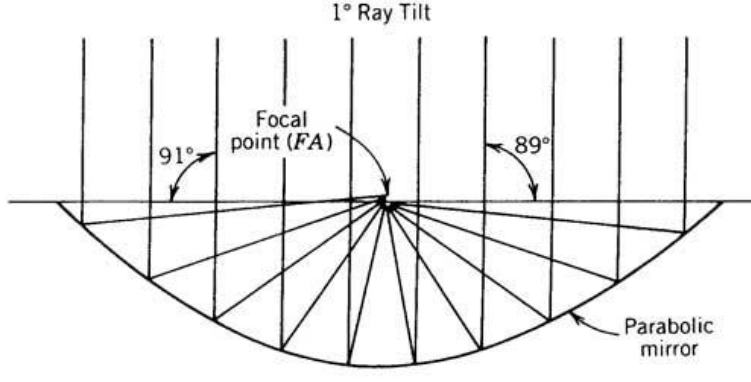

Figure 18: Off-axis light reflection from parabolic mirror [49].

In operation, the CPC is usually deployed with its linear receiver aligned along an East/West line. The aperture of the CPC is typically tilted toward the south so that the incident solar irradiance enters within the acceptance angle of the CPC. Provided the sun's apparent motion does not result in the incident solar irradiance falling outside the CPC's acceptance angle, the CPC's aperture need not be tracked. Typically, a CPC's aperture need not be tracked on an hourly basis throughout a day since the sun's declination does not change more than the acceptance angle throughout a day. However, the tilt of the CPC may have to be adjusted periodically throughout the year if the incident solar irradiance moves outside the acceptance angle of the CPC.

2.1.2 Solar Tower/Central Receiver

In this concentrating solar power (CSP) technology, there is a single receiver placed on top of a tower surrounded by hundreds of large, flat, mirrors (heliostats) which follow the apparent motion of the sun in the sky and which re-direct and focus the sunlight onto the receiver. The heliostats are provided with a two-axis tracking system. A heat-transfer fluid heated in the receiver is used to generate steam, which, in turn, is used in a conventional turbine generator to produce electricity. Some power towers use water/steam as the heat-transfer fluid. Other advanced designs are experimenting with molten nitrate salt because of its superior heat-transfer and energy-storage capabilities. If a gas or even air is pressurized in the receiver, it can be used alternatively to drive a gas turbine (instead of producing steam for a steam turbine). For gas turbine operation, the air to be heated must first pass through a pressurized solar receiver with a solar window.

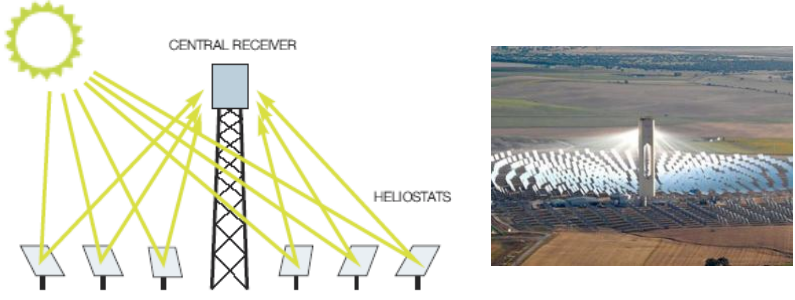

Figure 19: Power tower plant [50].

Power tower technology offers good longer-term prospects because of the high solar-to-electrical conversion efficiency. It is also intended to generate electricity by means of a Rankine cycle power plant. Individual commercial plants can be sized up to 200 MW. The main problem is the high costs and the extremely precise and complex installation requirements required to obtain maximum efficiency.

2.1.3 Parabolic Dish/Stirling Engine

A Stirling engine is a closed cycle regenerative gas engines. Stirling engines are unique heat engines because their theoretical efficiency is nearly equal to their theoretical maximum efficiency, known as the Carnot Cycle efficiency. Stirling engines are powered by the expansion of a gas when heated, followed by the compression of the gas when cooled. The Stirling engine contains a fixed amount of gas which is transferred back and forth between a "cold" and a "hot" end. The "displacer piston" moves the gas between the two ends and the "power piston" changes the internal volume as the gas expands and contracts. The gasses used inside a Stirling engine never leave the engine. There are no exhaust valves that vent high-pressure gasses, as in a gasoline or diesel engine, and there are no explosions taking place. Because of this, Stirling engines are very quiet. The Stirling cycle uses an external heat source, which could be anything from gasoline to solar energy to the heat produced by decaying plants. No combustion takes place inside the cylinders of the engine.

A dish Stirling system consists of a parabolic-shaped point focus concentrator in the form of a dish that reflects solar radiation onto a receiver mounted at the focal point. These concentrators are mounted on a pedestal and can pivot on two axes to follow the sun. This two-axis tracking mechanism allows the capture of the highest amount of solar energy at any time possible. The energy absorption enables fluid in the receiver to be heated to approximately 750°C. This is then used to generate electricity. Like all concentrating systems, they can be additionally powered by natural gas or biogas, providing firm capacity at any time.

It is a concentrating solar power (CSP) technology that produces relatively small amounts of electricity compared to other CSP technologies. Overall size typically ranges from 5 to 15 meters in diameter and 5 to 50kW of power output, with a peak efficiency of up to 30% (net).

Solar dish/engine systems are still under development, but represent a new opportunity for solar-thermal electricity. If there is inadequate power

or at night, the power system can operate in hybrid mode in which an alternative fuel can be burned to provide heat. A dish system can achieve much higher temperatures due to the higher concentration of light (as in tower designs). Higher temperatures lead to better conversion to electricity and the dish system is very efficient on this point. However, there are also some disadvantages. Heat to electricity conversion requires moving parts and this results in maintenance. In general, a centralized approach for this conversion is better than the decentralized concept in the dish design. Second, the (heavy) engine is part of the moving structure, which requires a rigid frame and strong tracking system. Furthermore, parabolic mirrors are used instead of flat mirrors and tracking must be dual-axis.

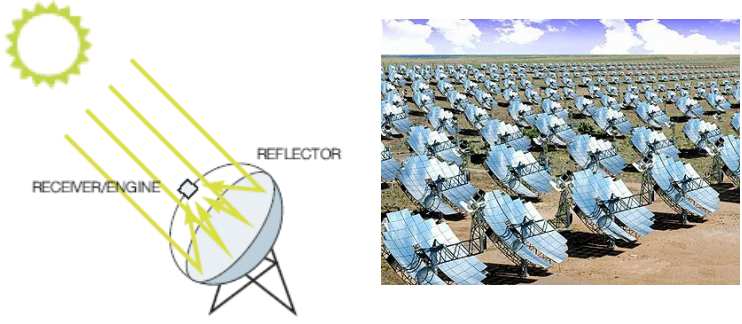

Figure 20: Dish/Stirling engine plant [50].

Aside from questions about the reliability of the Stirling motor, the dish Stirling is the quintessential thermal solar power plant:

- its two-axis tracking mechanism allows it to maximize solar energy collection.
- the generation threshold is relatively low.
- the unit ramps to grid synchronization within a minute.
- it has the highest efficiency of any solar generating technology.
- it requires the least amount of land in relation to peak capacity and energy production.
- its high engine-operating temperature allows air cooling, thus eliminating the need for cooling water.

The largest potential market for dish/engine systems is large-scale power plants connected to the utility grid. Their ability to be quickly installed, their inherent modularity, and their minimal environmental impact make them a good candidate for new peaking power installations. The output from many modules can be ganged together to form a dish/engine farm and produce a collective output of virtually any desired amount. In addition, systems can be added as needed to respond to demand increases. Hours of peak output are often coincident with peak demand. Although dish/engine systems do not currently have a cost-effective energy storage system, their ability to operate with fossil or bio-derived fuels makes them, in principal, fully dispatchable. This capability in conjunction with their modularity and relatively benign environmental impacts suggests that grid support benefits could be a major advantage of these systems.

2.1.4 Parabolic Trough

A parabolic trough is constituted by a long parabolic mirror through with a receiving tube in the focus line. Due to their parabolic shape, theses mirrors reflect and concentrate the sunlight directly upon the receiver tube, focusing the sun at about 80 times its normal intensity.

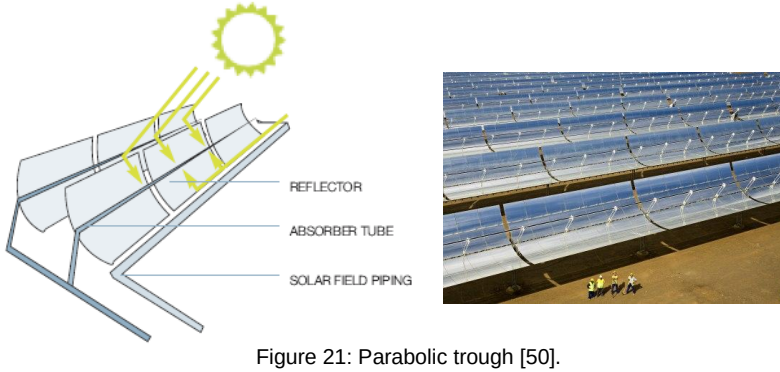

Figure 21: Parabolic trough [50].

The trough is usually aligned on a north-south axis, and rotated to track the sun as it moves across the sky each day. Alternatively the trough can be aligned on an east-west axis; this reduces the overall efficiency of the collector, due to cosine loss, but only requires the trough to be aligned with the change in seasons, avoiding the need for tracking motors. In any case, the latter are used to increase efficiencies. The concentrated energy is absorbed by a heat transfer fluid (HTF), usually oil that flows through

the receiving tube. This fluid is then used to generate steam which powers a standard turbine generator.

The process itself is economical and, for heating the pipe, thermal efficiency ranges from 60 to 80%. The overall efficiency from collector to grid, i.e. (Electrical Output Power)/(Total Impinging Solar Power) is about 20-25%. The basic component of a parabolic trough solar field is the solar collector assembly (SCA). A solar field consists of hundreds or potentially thousands of solar collector assemblies. Each solar collector assembly is an independently tracking, parabolic trough solar collector composed of the following key subsystems.

- *Concentrator metal support structure*, usually composed of steel beams and rods, which gives and maintains the parabolic form of the mirrors. Because the mirror itself is not geometrically rigid, the rigidity of the parabolic form wholly relies on the support structure. The technical difficulty is important due to the requirements on optical precision and wind resistance.

- *Mirrors or reflectors*, pieced up from several curved glass mirrors fixed on the support structure. Development efforts are aimed at reducing the thickness of the mirror, improving the reliability of the glass to metal seal, surface coatings on the mirrors to improve their performance and development of a composite concentrator modules with lightweight, front-surface mirrors instead of heavy (4 mm) glass mirrors that were originally used on the original SEGS plants.
- *Linear receiver or heat collection element*, composed of a stainless steel pipe with a glass tube surrounding it, with the space between evacuated to provide low thermal losses from the pipe. The pipe is coated with a material that improves the absorption of solar energy. The receiver collects the solar radiations reflected by the mirror, and transforms the energy into the heat conveyed out by the heat transfer fluid (HTF) that flows in the inner tube.
- *Tracking systems*, the mechanism that constantly maintains the orientation of the mirrors towards the moving sun.

The initial installation cost of parabolic trough solar collectors constitutes the main ingredient in the final cost of electricity produced by the power plant. And the main sources of cost (over 80%) of the collectors are the metal support structure, the parabolic mirror, the receiver (heat collector element), and the tracking system.

2.2 Thermal storage for solar technologies

In all production processes, it is economically inefficient to install production and distribution equipment with the capacity to accommodate for the maximum (short-term) demand. Furthermore, productivity decreases when production equipment cannot operate at full capacity in periods of reduced demand. Energy storage is employed to shift excess energy produced during times of high availability to times of low availability.

Thermal energy storage can serve at least five different purposes:

- energy conservation utilizing new renewable energy sources;
- peak shaving both in electric grids and district heating systems;
- power conservation by running energy conversion machines, for instance cogenerating plants and heat pumps, on full (optimal) load instead of part load. This reduces power demand and increases efficiency;
- reduced emissions of greenhouse gases, and
- freeing high quality electric energy for industrial value adding purposes.

There are basically three types of thermal storage devices being investigated at present by the international research society and some industrial players [49]:

- specific (sensible) heat storage, where a change of temperature occurs;
- latent heat storage (phase change materials), where a change of phase occurs; and
- thermo-chemical heat storage, where a reversible chemical reaction takes place.

2.2.1 Sensible heat storage

Sensible-heat storage of thermal energy is perhaps, conceptually, the simplest form of storing thermal energy. In its simplest configuration, cold fluid contained in an insulated tank is heated to some higher temperature by the hot fluid from the field of solar collectors, as shown in Figure 22. In most industrial solar energy systems, the fluid in the collector field and the storage tanks is the same. Thus no heat exchanger is shown between the collector field and storage in the following

discussions of sensible-heat storage. This is not the case with storage concepts such as latent heat storage where the storage medium undergoes a phase change.

The storage fluid in Figure 22 reaches some average temperature between the starting storage temperature and the hot collector fluid temperature. However, the quality (i.e. temperature) of the energy in storage is usually of interest. If the quantity of thermal energy delivered by the collector field is insufficient (e.g. partially cloudy days) to heat the entire storage to a temperature near that of the hot collector fluid, a significant loss in energy quality (i.e. second law availability) can occur in the storage subsystem. Energy quality is usually an important factor in the design of high-temperature solar thermal energy systems. Otherwise, there would be no need to operate the solar collectors at high temperatures that decrease collector efficiency. To avoid this, a multi-tank storage system can be used.

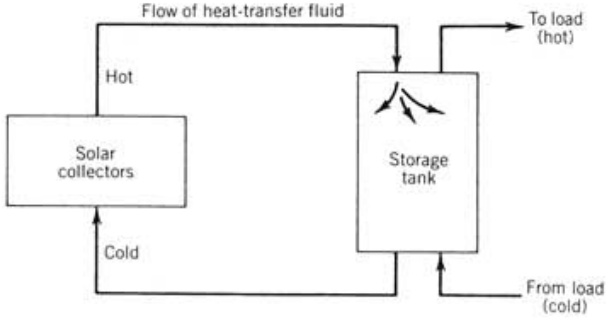

Figure 22: Single-tank sensible-heat storage [49].

2.2.1.1 Multi-tank storage

The term "multi-tank storage," refers to the type of sensible-heat storage system illustrated in Figure 23, except more than two tanks can be used.

There are direct and indirect systems. In the direct systems the solar thermal energy is stored in the same fluid used to collect it, while in the indirect system different fluids are used as the heat-transfer and storage fluids. The indirect system is used in plants where the heat-transfer fluid is too expensive or not suited for use as the storage fluid. In a *direct two-*

tank system, the fluid is stored in two tanks, one at high temperature and the other at low temperature. Fluid from the low-temperature tank flows through the solar collector or receiver, where solar energy heats it to the high temperature and it then flows back to the high-temperature tank for storage. Fluid from the high-temperature tank flows through a heat exchanger, where it generates steam for electricity production. The fluid exits the heat exchanger at the low temperature and returns to the low-temperature tank. In an *indirect two-tank system* the thermal energy storage is charged by taking hot, heat transfer fluid (HTF) from the solar field and running it through the heat exchangers. The storage fluid is taken from the cold storage tank and run counter currently through the heat exchangers. It's heated and stored in the hot storage tank for later use. Later, when the energy in storage is needed, the system simply operates in reverse to reheat the solar heat transfer fluid, which generates steam to run the power plant. It's referred to as an indirect system because it uses a fluid for the storage medium that's different from what's circulated in the solar field.

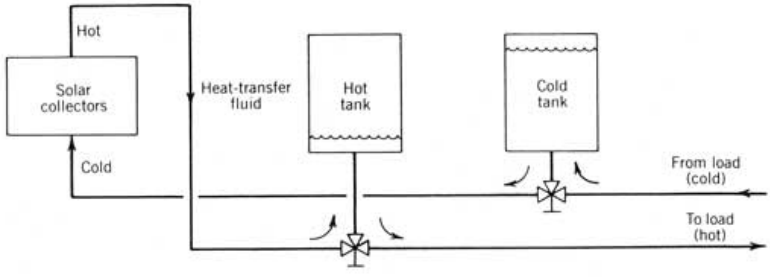

Figure 23: Two-tank sensible heat storage [49].

There is a potential for a multiple tank system to be lower cost than the corresponding two-tank system. In fact, if minimization of storage tank volume were the sole parameter, logic would drive the design to a very large number of tanks. In practice, however, many factors contribute to limit the number of tanks. Such factors include:

- *Complexity of control.* The complexity of controlling liquid levels and automatically switching tanks grows quickly as the number of tanks increases. The control strategy is especially complex on partially cloudy days.

- *Interconnecting plumbing*. The provision of a piping network interconnecting many tanks and provision for automatic valving can become quite expensive.
- *Heat loss.* Large tanks lose less heat per unit volume of hot fluid than do small tanks. In addition, the interconnecting piping network (especially the control valves) is a source of increased heat loss.

2.2.1.2 Thermocline energy storage

The ultimate reduction in storage tank volume is achieved when the storage tank volume equals the storage fluid volume. An attempt to achieve this is represented by a thermocline system in which both the hot and cold storage fluids occupy the same tank. Conceptually, the operation of a thermocline sensible-heat storage system is illustrated in Figure 24.

At the start of operation, the storage tank is full of cold fluid. As thermal energy, in the form of hot collector fluid, becomes available, cold storage fluid is withdrawn from the bottom of the storage tank and heated. The hot storage fluid is then put back into the top of the storage tank. If properly done, the less dense hot storage fluid will "float" on top of the cold storage fluid, creating what is termed a *thermocline*. This phenomenon actually occurs quite commonly in many fluid systems ranging from the ocean to residential hot-water heaters.

Thermocline energy storage systems have received much attention because of their potential for low cost resulting from minimized tankage volume. Moreover, stable thermoclines can be established and, with careful design of the tank inlet and outlet diffusers, momentum-induced mixing of the hot and cold fluids can be minimized, leading to a rather small transition region between the hot and cold fluid regions.

2.2.1.3 Mixed-media thermocline storage

Once the tank volume has been reduced to a minimum through use of, for example, a thermocline system, the next step in reducing the capital cost of the storage system is to reduce the cost of the storage fluid. Organic heat-transfer oils are typically used in high-temperature solar energy systems to avoid the cost of high-pressure plumbing systems. Unfortunately, most organic heat-transfer oils are expensive. Mixed-media thermocline storage systems seek to displace expensive heat-transfer oil inventory in storage with less expensive materials such as

rock. The mixed media concept reduces the quantity of oil used in the conventional thermocline storage by about 75%. Top and bottom manifolds are employed to distribute the heat transfer oil across the cross section of the tank.

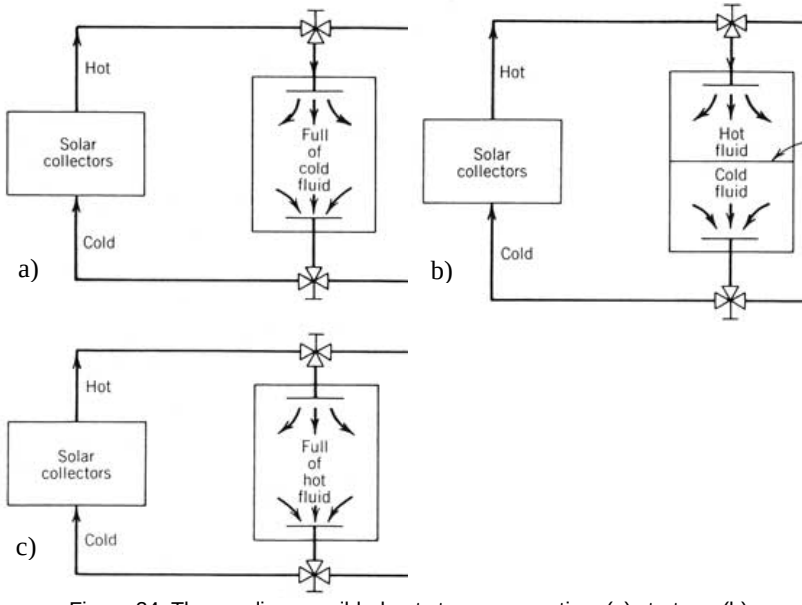

Figure 24: Thermocline sensible-heat storage operation: (a) start-up; (b) midday; (c) end of day [49].

2.2.1.4 High-temperature sensible heat storage

The ability to store high temperature thermal energy is basically limited by the availability of heat-transfer fluids. Above about 400ºC, most organic heat-transfer fluids tend to thermally decompose. For electric power generation and other high-temperature applications, therefore, fluids such as molten salts, liquid metals, and air (with an air-rock storage medium) are typically considered. Very few engineering prototype storage systems employing such high-temperature storage concepts have been constructed and tested. As such, there is very little information concerning the performance of high-temperature systems.

A basic problem afflicting storage concepts using molten salts and metals is solidification at low temperatures. Thus, unless auxiliary heat is provided, shut-down of the solar energy system can be complicated by the

solidification of the heat-transfer fluid. This can result in increased system complexity and cost if extensive heat tracing is required. Sensible heat storage employing molten salt has been tested at Sandia National Laboratories, but there are no commercial units of such storage available to the authors' knowledge [49].

High-temperature air systems typically employ some type of inert solid material such as rock to store thermal energy. These storage systems are conceptually similar to the air-rock thermal energy storage systems commonly used in solar residences.

2.2.1.5 Pressurized fluid storage

The cost of most of the common thermal energy storage systems is strongly influenced by the cost of the storage fluid. The cost of organic heat-transfer fluids can be quite high. The mixed-media storage concepts described previously represent one attempt to reduce storage fluid costs. The use of water or steam as a storage medium represents another way in which to reduce storage fluid costs. In addition, the use of water or steam as a storage fluid in a solar thermal electric system using a steam-driven power generation unit would permit elimination of the expense of a oil-water steam generator. However, although these advantages are significant, they are usually overwhelmed by the expense of the pressurized storage tank needed. For example, saturated water at 300ºC has a pressure of about 8,8 M Pa.

2.2.2 Latent heat storage

One limitation of a sensible-heat system is that the capability of most materials to store heat sensibly is small. Even water, which has a reasonably high heat capacity of 4,186kJ/kg K, is not a high-energy-density sensible heat storage medium. In addition, the materials most commonly used to store heat in a sensible-heat storage system, namely organic heat transfer oils, typically have heat capacities in the range of 0,5-0,7 times that of water. The motivation for using a latent heat-process as a thermal storage mechanism is to increase the energy density of storage and thus potentially reduce storage tank size and cost.

Since the storage material undergoes a transition from liquid to solid and vice versa, the storage material cannot be pumped through the collector field or the process. This results in the need for a heat exchanger within the storage system as shown. In addition, since the storage medium undergoes a phase change, the heat exchangers must be carefully

designed to accommodate the typically low thermal diffusivity of the solid material. The requirement for rather complex heat exchangers in latent heat storage concepts typically results in increased system costs compared to systems that use sensible heat storage.

Other characteristics that adversely affect design of a latent heat storage system include [58]:

- the cost of many of the more effective latent heat storage materials is high;
- some of the latent heat storage materials are not pure materials but mixtures that tend to separate into their component parts on repeated freeze-thaw cycling;
- some of the latent heat storage materials such as NaOH can react violently with the organic heat-transfer oils commonly used in solar thermal energy collectors; and
- supercooling of the latent heat storage material can occur on solidification.

Because of these problems and the availability of sensible heat storage systems, latent heat storage systems have not been widely used in high-temperature solar thermal energy systems.

2.2.3 Thermo-chemical energy storage

In thermo-chemical energy storage systems thermal energy is used to break chemical bonds in a reversible fashion. The rupture of the chemical bond requires large quantities of energy input, thus resulting in thermal energy storage. The product or products of the thermo-chemical reaction are typically un-reactive at ambient temperatures. At elevated temperatures the energy storing reaction reverses, forming the original chemical system with the release of heat.

The reason for interest in thermo-chemical energy storage systems are listed below.

- Chemical reactions are typically very energetic, thus allowing large quantities of energy to be stored in small quantities of material.
- The reverse, the energy-releasing chemical reaction, seldom proceeds at room temperature, thus the energy can be stored indefinitely, without energy loss, at ambient temperatures.

- Because of very high energy density and stability at low temperatures of some thermo-chemical energy storage systems, the stored thermal energy can be transported. An extreme case of transportability is the formation of a chemical fuel, such as hydrogen, which can be piped around the country and then burned (i.e., reacted with oxygen) to provide thermal energy.

2.2.4 Thermal energy storage media

2.2.4.1 Concrete

This system uses the standard heat transfer fluid (HTF) in the solar field. The heat transfer fluid passes through an array of pipes imbedded in the solid medium to transfer the thermal energy to and from the media during plant operation. The primary advantage of this approach is the low cost of the solid media. Primary issues include maintaining good contact between the concrete and piping, and the heat transfer rates into and out of the solid medium.

The used material in solid media, sensible heat storage systems is high-temperature concrete or castable ceramic materials. However, the high-temperature concrete is favoured because of lower costs, higher material strength, and easier handling. There is no sign of degradation between the heat exchanger pipes and storage material.

2.2.4.2 Phase-change material

Phase-change materials (PCMs) allow large amounts of energy to be stored in relatively small volumes, resulting in some of the lowest costs for storage media of any storage concept. Initially, PCMs were considered for use with parabolic trough plants that used a synthetic heat-transfer fluid designed to withstand high temperatures in the solar field. In this approach, thermal energy is transferred to a series of cascading heat exchangers containing PCMs that melt at slightly different temperatures. To discharge the storage, the flow of heat-transfer fluid is reversed, thus reheating the fluid. Testing proved this system to be technically feasible. However, further development of this concept is hindered by the following:

- complexity of the system
- thermodynamic penalty of going from sensible heat to latent heat and back to sensible heat

- uncertainty over the lifetime of phase-change materials.

The cost of such a system is driven by the cost of phase-change storage material, but also by the rate at which energy is charged or discharged from the material.

2.2.4.3 Molten-salt thermal storage

Molten nitrate salt is an excellent thermal storage medium. It is a mixture of 60 percent sodium nitrate and 40 percent potassium nitrate, commonly called saltpetre. It is non-flammable and nontoxic, and has already been used in the chemical and metals industries as a heat-transport fluid, so experience with such systems exists in non-solar applications. Using it in both the solar field and thermal energy storage system eliminates the need for expensive heat exchangers. It allows the solar field to be operated at higher temperatures than current heat transfer fluids allow. This combination also allows for a substantial reduction in the cost of the thermal energy storage system. Unfortunately, it can be a troublesome fluid to deal with because of its relatively high freezing point (220°C).

To keep the salt molten, a fairly complex heat trace system must be employed. Heat tracing is composed of electric wires attached to the outside surface of pipes. Pipes are kept warm by way of resistance heating. Also, valves can be troublesome in molten-salt service. Special packings must be used, oftentimes with extended bonnets, and leaks are not uncommon. Furthermore, freezing in the valve or packing can prevent it from operating correctly.

2.3 Biomass micro and small-scale CHP systems

Of all the renewable energy resources, biomass is plentiful and prominent as it is the world's fourth largest energy source, contributing to nearly 14% of the world's primary energy demand. For many developing countries, the contributions of biomass to their national primary energy demands are much higher, from about 20% to over 90%. Biomass energy systems contribute to both energy and non-energy policies. The life cycle of a sustainable biomass energy system has a nearly neutral effect on the atmospheric carbon dioxide concentration. Therefore, sustainable biomass utilisation has been considered as one of the most attractive options for addressing CO2 concerns [59] [60] [61].

2.3.1 Configurations

The energy use of biomass can be achieved with several technologies and energy conversion chains, Figure 25, which differ mainly for the biomass characteristics, the physical principles applied for the conversion and for the obtainable products. The three major conversion chains are based on :

- Thermo-chemical processes: combustion, pyrolysis, gasification;
- biochemical processes: digestion and fermentation;
- mechanical extraction: esterification.

Various technologies have been developed for energy conversion in biomass-fuelled CHP systems. Basically, these include a primary conversion technology that converts biomass into hot water, steam, gaseous or liquid products and a secondary conversion technology that transforms these products to heat and power. The major biomass energy conversion technologies are listed in Table 7. Direct combustion, gasification, pyrolysis and digestion are the most adopted conversion systems.

In anaerobic digestion, organic matter is decomposed by bacteria in the absence of oxygen to produce methane and other by-products. The resulting biogas is composed of 60-65% methane and 30-35% carbon dioxide, with the rest a mixture of other gases (mostly nitrogen). After appropriate treatment, biogas can be used directly for cooking and heating, or used in secondary conversion technologies such as gas engines and turbines. High-moisture biomass feedstocks are especially well-suited for the anaerobic digestion process. The advantage of anaerobic digestion over thermo-chemical processes is that it produces a concentrated nitrogen fertilizer, and also neutralizes wastes that would otherwise be dumped into the environment [62].

Gasification is a high-temperature thermo-chemical conversion process designed to produce a combustible gas. After appropriate treatment, the result of gasification -- called producer gas -- can be burned directly for cooking or heat supply, or used in secondary conversion technologies such as gas turbines and engines to produce electricity or mechanical work [63].

Air gasification produces a low-heating-value gas that is suitable for boiler, engine, and turbine operations. Oxygen gasification produces a medium-heating-value gas suitable for limited pipeline transit. Such a medium-value gas can also be produced by pyrolytic or steam gasification. Gasification with air is more widely used since it does not

include the cost or hazard of oxygen production and use, nor the complexity and cost of multiple reactors.

Commercial implementation of biomass gasification is still problematic, however, and few gasification processes have proved economically viable so far. Overall, gasification currently is best suited for large installations (>10 MW) where electricity is in high demand and commands premium prices [64].

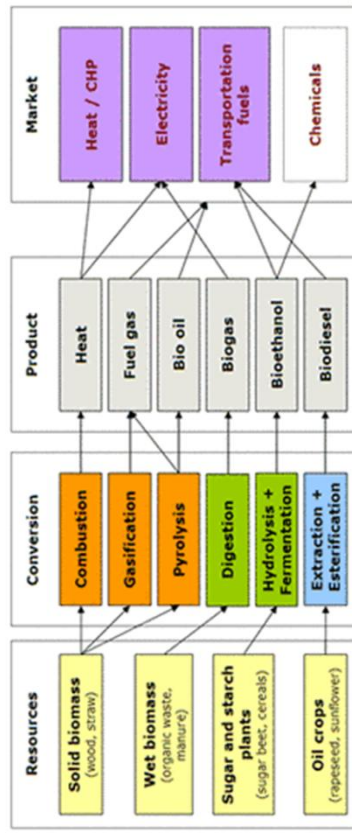

Figure 25: Biomass energy conversion chains [64].

In pyrolysis, biomass is exposed to high temperatures in the absence of air, causing the biomass to decompose [65]. The end product is a mixture of solids (char), liquids (oxygenated oils), and gases (methane,

CO, and CO_2). The goal of pyrolysis is to produce a liquid fuel, called bio-oil or pyrolysis oil, which can be used for heating or power generation. The main benefit of pyrolysis, relative to combustion and gasification, is that its liquid fuel product is easier to transport than either solid or gaseous fuels. This means that the pyrolysis plant does not have to be near the end-use point of the bio-oil, but can instead be located near the biomass supply, resulting in lower fuel transportation costs [63].

Table 7: Major energy conversion technologies of biomass-fuelled CHP systems [66].

Primary technology	**Secondary technology**
Combustion producing steam, hot water	Steam engine; steam turbine; Stirling engine; Organic Rankine Cycle (ORC)
Gasification producing gaseous fuels	Internal combustion engine; micro-turbine; gas turbine; fuel cell
Pyrolysis producing gaseous, liquid fuels	Internal combustion engine
Biochemical/biological processes producing ethanol, biogas	Internal combustion engine
Chemical/mechanical processes producing biodiesel	Internal combustion engine

Table 8: Number and power of biomass plants in Italy [67].

	2008		2009	
	N°	MW	N°	MW
Biomass type				
Solid	110	1˙068	122	1255
Solid waste	65	619	69	782
Solid biomass	45	449	53	473
Biogas	239	365	272	378
From waste	193	306	194	299
From depuration mud	11	5	20	10
From animal wastes	19	12	28	17
From agriculture and forestry activities	16	40	31	52
Bio-fuels	12	121	42	385
Raw vegetables oil	8	54	35	302
Other bio-fuels	4	66	7	82

Direct combustion facilities, which burn biomass directly to generate electricity, provide more than 90% of the energy generated from biomass worldwide. This is largely because direct combustion is a well-understood, well-developed, and widely available technology that can be easily integrated with existing infrastructure [63]. Direct combustion devices range from small domestic stoves to the largest boilers used in

power and cogeneration plants. The major types of large-scale biomass boilers use either fixed-bed combustion systems, fluidised-bed combustion systems, or pulverised fuel systems. In dedicated biomass operations, the boiler's fuel is 100% biomass, while in co-fired operations, multiple fuels are burned in the same boiler. For coal-based power facilities, co-firing with biomass may be one of the least expensive renewable energy options [65]. Co-firing often leads to reduced CO_2, SO_2, and NO_x emissions, and in many countries it is the most economic way to meet CO_2 reduction targets. In addition, it may be relatively inexpensive to modify existing fossil-fuel equipment for co-firing operations.

Among all the described biomass technologies, 'combustion' and 'steam turbine' technologies are the most widely used combination, particularly for large-scale and medium-scale biomass-fuelled CHP systems [68]. In the mean time, the combination of 'combustion' and 'Organic Rankine Cycle (ORC)' technologies is receiving more and more attention in the development of small-scale biomass fuelled CHP systems.

Table 8 shows the number and power of Italian biomass plants in years 2008 and 2009. As evident solid biomass and biogas are the prevailing sectors, although bio-fuel plants show the higher growth, either in the number of plants and in their power. Moreover, solid biomass plants have an average power of 9 MW.

2.3.2 Environmental impact

The environmental effects of biomass vary by feedstock and conversion technology. In general, biomass can be a climate-neutral power source as long as the plant material that formed the feedstock is allowed to re-grow. This is because an equivalent amount of CO_2 emitted during combustion will be captured by the next generation of plants as they grow.

In terms of air pollution, biomass feed stocks can offer improvements over fossil fuels. Biomass is naturally low in sulphur and therefore generates low SO_2 emissions when burned. However, if burned in the open air, some biomass feed stocks emit relatively high levels of NO_x (given the high nitrogen content of plant material), CO, and particulates. Nevertheless, there exist emissions control equipments that can reduce the level of such emissions. Therefore, the air pollution impact of bio-energy plants depends on whether facilities have installed such devices as selective catalytic reduction equipment (for NO_x), electrostatic precipitators (for particulates), and catalytic oxidizers (for VOCs, CO,

and NO_x). Finally, some forms of biomass may release toxins such as dioxins and heavy metals if the feedstock is contaminated. For example, organic municipal solid waste could contain inorganic materials such as plastics, and urban waste wood could contain material that has been treated with resins and varnishes.

The land and wildlife habitat impacts of biomass vary by feedstock and depend on how the feedstock is cultivated and gathered. For example, dedicated energy crops would have limited environmental impact if they were planted on degraded farmland and managed sustainably (e.g., using native plant species, low chemical and fertilizer inputs, and little irrigation). On the other hand, planting switchgrass on undisturbed lands or harvesting trees for fuel from forests of high conservation value would have a negative impact on wildlife habitat.

Finally, some observers claim that certain forms of biomass may discourage reuse, recycling, and composting of natural resources. For instance, using urban waste wood as an energy feedstock may reduce the incentive to reuse or recycle these wood products, thereby reducing the cost of disposal and increasing the demand for virgin wood [62].

2.4 Water desalination technologies

Water is an essential element for all socio-economic development and for maintaining healthy ecosystems. Drinking water distribution on hearth, Figure 26, emphasizes development differences among countries. Today, majority of the health issues are owing to the non-availability of clean drinking water. In the recent decades, most parts of the world receive insufficient rainfall resulting in increase in the water salinity. The pollution of water resources is increasing drastically due to a number of factors including growth in the population, industrialization, urbanization, etc. These activities adversely affected the water quality in rural areas and agriculture. By 2025, 1800 million people will be living in countries or regions with absolute water scarcity, and two-thirds of the world population could be under stress conditions [69].

While Europe is by large considered as having adequate water resources, with the exception of several small islands [20], water scarcity and drought is an increasingly frequent and widespread phenomenon in the European Union. The long term imbalance resulting from water demand exceeding available water resources is no longer uncommon. It was estimated that by 2007, at least 11 % of Europe's population and 17 % of its territory had been affected by water scarcity, putting the cost of droughts in Europe over the past thirty years at EUR 100 billion. The

Commission expects further deterioration of the water situation in Europe if temperatures keep rising as a result of climate change. Water is no longer the problem of a few regions, but now concerns all 500 million Europeans [70].

Desalination is becoming a major option for water supply, frequently associated to renewable energy sources, both in electric and thermal fashion [71] [20]. Desalination units driven by RES, such as those driven by solar and wind energy, guarantee friendly to the environment, cost effective and energy efficient production of desalinated water. Some applications involve CSP technology, always associated to Multi Stage Flash and Multi Effect Distillation plants, usually on the large scale production [72] [73] [74].

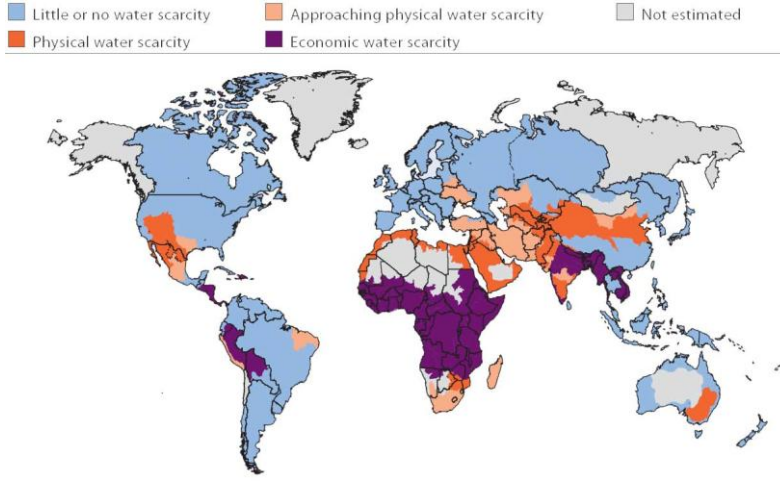

Figure 26: Areas of physical and economical water scarcity [69].

Table 9: Classification of desalination methods.

Electric desalination methods	Thermal desalination methods
Reverse Osmosis (RO)	Multi-Stage Flash (MSF)
Mechanical Vapour Compression (MVC)	Multiple-Effect Evaporator (MED)
Electrodialisis (ED)	Thermal Vapour Compression (TVC)

Desalination processes are divided in two categories which differ for the employed power form, that is electric or thermal, Table 9.

Reverse osmosis is a membrane process which exploits the osmosis principle, involving the transfer of a solvent through a semi-permeable membrane under the influence of a concentration gradient. In reverse osmosis, an increase in the pressure applied to the saline solution beyond the osmotic pressure drives a flow of water in the opposite direction to the normal osmotic flow. More precisely, water from a pressurized saline solution (sea water in this instance) is separated from the dissolved salts by flowing through a water-permeable membrane. The permeate (the liquid flowing through the membrane) is encouraged to flow through the membrane by the pressure differential created between the pressurized feed water and the product water, which is at near-atmospheric pressure. The remaining feed water continues through the pressurized side of the reactor as brine. As the water passes through the membrane, the remaining feed water increases in salt concentration. This water is discharged from the vessel in a controlled manner in order to ensure problems such as precipitation of supersaturated salts and increased osmotic pressure across the membranes does not occur. No heating or phase change takes place. The major energy requirement is for the initial pressurization of the feed water [75].

In the mechanical vapour compression (MVC) desalination system, the water vapour is compressed by means of a mechanical device, electrically driven in most cases. The MVC process comprises two different versions: Vapour Compression (VC) in which the evaporation effect takes place at manometric pressure, and Vacuum Vapour Compression (VVC).in which the mechanical compressor creates a vacuum in the vessel and then compressed the vapour taken from the vessel and condenses it inside a tube bundle. The compression is mechanically powered by something such as a compression turbine. As vapour is generated, it is passed over to a heat exchanging condenser which returns the vapour to water. The resulting fresh water is moved to storage while the heat removed during condensation is transmitted to the remaining feedstock [75].

Electrodialysis (ED) is an electrochemical separation process, in which ions are transferred through ion selective membranes by means of a direct current voltage, leaving the product water behind. ED involves the movement of water through a filtering membrane. Instead of using pressure to overcome the membrane's resistance, as in the RO system, pre-treated water is pumped between electrodialysis cells by means of a low voltage direct current (DC) electrical field. An electrodialysis cell

consists of a large number of feed (diluate) compartments and concentrate (brine) compartments through which the feed water for desalination is pumped. These compartments are separated by membranes that are permeable to either positive ions (cations) or negative ions (anions). The cations and anions migrate through the appropriate membranes by the influence of the DC electrical field, forming compartments of electrolyte-enriched wastewater and electrolyte depleted product water.

The basic electrodialysis unit consists of several hundred cell-pairs bound together with electrodes on the outside and is referred to as a membrane stack. Feed water passes simultaneously in parallel paths through all of the cells to provide a continuous flow of desalinated water and brine to emerge from the stack. Depending on the design of the system, chemicals may be added to the streams in the stack to reduce the potential for scaling.

The raw feedwater must be pre-treated to prevent materials that could harm the membranes or clog the narrow channels in the cells from entering the stack. The feed water is circulated through the stack with a low pressure pump with enough power to overcome the resistance of the water as it passes through the narrow passages [75].

Multiple stage flash (MSF) distillation is the most widely used desalination process, in terms of capacity. In this process, as well as in all distillation processes, the seawater is heated, producing water vapor that is in turn condensed to form fresh water. The water is heated to the boiling point to produce the maximum amount of water vapour.

There are two configurations concerning MSF process. The first one, the "once through" consists of two sections: the heat rejection section and the brine heater, which are in common with the second MSF configuration, the "brine recirculation", which presents a heat recovery section between the other two sections.

In both processes, the seawater is heated in the brine heater. In the brine recirculation process the seawater is taken into the plant and fed through the heat rejection stage. The function of this section is to reject thermal energy from the plant and to allow to the product water and brine to exit the plant at the lowest possible temperature. The feed water is mixed with the large mass of water which is recirculated round the plant, known as the "brine recirculation" flow. Then the feed water passes through a number of heat exchangers (stages), from 4 up to 40 stages, raising its temperature.

After passing through the last stage of the recovery section the water is heated up to its terminal temperature in the brine heater. MSF plants usually operate at top brine temperatures of between 90-120 ºC, depending on the feed water treatment. The brine then enters the first heat recovery stage through an orifice, thus reducing the pressure. As the brine was already at its saturation temperature, it will become superheated for a lower pressure and flashes to give off water vapour. It is then passed up through a demister into the condenser where the vapour is condensed and the produced distillate is dripped into a collector. This process continues right down to the bottom stage of the plant in the rejection section, where part is rejected as "blowdown" and the rest is mixed with the incoming make up (feed water) and then recycled once again via the brine recirculation pump. The distillate condensed in each of the condensers is collected in a distillate train [75].

The Multi Effect Distillation (MED) process is similar to the MSF process; the majority of the distillate is produced by boiling. A MED consists of several consecutive cells (or effects) maintained at decreasing levels of pressure (and temperature) from the first (hot) cell to the last one (cold). This permits the feed water to undergo multiple boiling phases without supplying additional heat after the first effect.

The incoming feed water is pumped into the plant through a number of pre-heaters located in each effect (evaporator) in order to raise its temperature. This feed water is sprayed onto the surface of the evaporator tubes to form a thin film to promote rapid boiling and evaporation. This reaction takes place as the feed water flows down from tube to tube due to gravity. Inside these tubes runs heating steam that is obtained from a boiler or another source. The vapour produced outside the tubes due to evaporation then goes, in part, to heat the incoming feed and in part to provide the heat supply for the second effect which is at lower pressure and receives its feed from the brine of the first effect. From the second effect the vapour itself is condensed (product water) while at the same time giving up heat to evaporate a portion of the remaining feed water in the next effect. This process is repeated in a series of effects, usually 8-16 effects in large plants, gradually operated at lower temperatures. This is accomplished by maintaining the effects at successively lower pressure (or higher vacuum by means of an air ejector). In the last cell, the produced steam condenses on a conventional shell and tubes heat exchanger. This exchanger, called "distillate condenser" is cooled by sea water. At the outlet of this condenser, part of the warmed sea water is used as make-up of the unit and the other part is rejected to the sea. Brine

and distillate are collected from cell to cell till the last one from where they are extracted by centrifugal pumps [75].

Vapour compression desalination refers to a distillation process where the evaporation of sea or saline water is obtained by the application of heat delivered by compressed vapour. Since compression of the vapour increases both the pressure and temperature of the vapour, it is possible to use the latent heat rejected during condensation to generate additional vapour. The effect of compressing water vapour can be done by two methods.

In the process, the feed water is preheated in a heat exchanger, or a series of heat exchangers, by the hot discharge of the brine blowdown and the distillate. The hot feed water enters the evaporator, where it is heated up to its boiling point and some of it is evaporated. The vapour formed in the evaporator is sent to the compressor where its pressure and consequently its saturation temperature are raised. The compressed vapour is then fed back into the evaporator to be condensed, providing the thermal energy to evaporate the applied seawater on the other side of the tubes. The distilled water produced by this condensation leaves the plant through the pre-heaters as the product water [75]

Chapter 3

Hybrid system components, design and basic thermodynamics

The aim of this study is to conceive, design and model a fossil-fuel-free micro-power system by the combination of standard technologies in a novel arrangement, trying to overthrow footprint, complexity, and costs when compared to the common energy plants. The proposed plant, analyzed through transient simulations, will be able to supply electric and thermal energy just exploiting renewable energy sources. To promote the diffusion of the studied system the solar source has been chosen as main energy supply. Nevertheless, its intermittency fashion in energy delivery has conducted to a biomass co-powering approach of the plant and to the introduction of a thermal energy storage for the time shifting of the energy delivery. Moreover the use of the produced energy has been investigated, considering end-users loads for electric and thermal energy in one case and the thermal energy employment for seawater desalination in another case.

3.1 Power plant rationale

The power plant blocks and their basic connections are shown in Figure 27, and briefly described in this paragraph. A closer examination for each element is given in the following paragraphs.

Concerning the *renewable energy collection* block, the third-generation technologies considered are the concentrating solar power and integrated bio-energy systems [12]. The adopted co-powering choice was mainly motivated by the availability of solar and bio-energy options world-wide, giving opportunity of replication of the proposed energy

plant. In particular the parabolic trough device is preferred in this study as currently it is the most proven technology among CSP systems for the power generation [76].

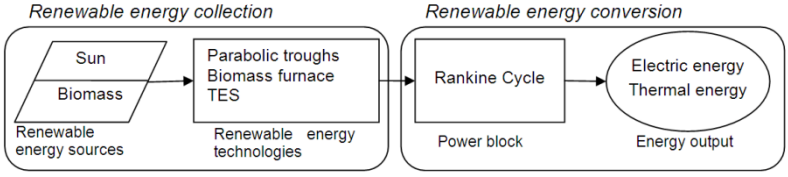

Figure 27: Power plant basic.

and Table 11 support this choice, demonstrating that among the CSP technologies, in spite of its lower concentration ability, parabolic trough plants have comparable values of annual solar and thermal cycle efficiencies and capacity factor. Troughs require less land on equal energy production basis. Furthermore, the modularity of the trough technology, with respect to the central receiver technology, permits to more deliberately choose the solar field size. However, to pursue the micro scale size of the plant, either the solar field has been down-sized with respect to the usual multi-MW size of the plant.

A critical aspect of CSP power generation, common to other RES, is given by the un-predictable nature of solar radiation which typically leads to the mismatch with respect to the power demand and problems in the grid-connection. In fact the continuous adaption of the generation electrical energy to the actual power consumption within a network is an important task in electric power supply business. Since every unexpected variation in power consumption has to be compensated almost immediately. There are several solutions to reduce the intermittency of the delivered power by RES, One of those is to plug the supply gap providing alternative capacity, known as spinning reserve [18].

Table 10: Comparison for main CSP technologies [77]

	Central receiver	Dish/Stirling	Trough
Applications	Grid-connected plants, high temperature process heat (Highest single unit solar capacity to date: 20 MWe under construction, Total capacity ~50MW with at least 100MW under development)	Stand-alone, small off-grid power systems or clustered to larger grid-connected dish parks (Highest single unit solar capacity to date: 100 kWe, Proposals for 100MW and 500 MW in Australia and US)	Grid-connected plants, mid to high-process heat (Highest single unit solar capacity to date: 80 MWe. Total capacity built: over 500 MW and more than 10 GW under construction or proposed)
Advantages	Good mid-term prospects for high conversion efficiencies, operating temperature potential beyond 1,000°C (565°C proven at 10 MW scale) Storage at high temperatures Hybrid operation possible Better suited for dry cooling concepts than troughs Better options to use non-flat sites	Very high conversion efficiencies – peak solar to net electric conversion over 30% Modularity Most effectively integrate thermal storage a large plant Operational experience of first demonstration projects Easily manufactured and mass-produced from available parts No water requirements for cooling the cycle	Commercially available – over 16 billion kWh of operational experience; operating temperature potential up to 500°C (400°C commercially proven) Commercially proven annual net plant efficiency of 14% (solar radiation to net electric output) Commercially proven investment and operating costs Modularity Good land-use factor Lowest materials demand Hybrid concept proven Storage capability
Disadvantages	Projected annual performance values, investment and operating costs need wider scale proof in commercial operation	No large-scale commercial examples Projected cost goals of mass production still to be proven Lower dispatchability potential for grid integration Hybrid receivers still an R&D goal	The use of oil-based heat transfer media restricts operating temperatures today to 400°C, resulting in only moderate steam qualities

Table 11: Performance data for various CSP technologies [78].

	Capacity unit [MW]	Concentration	Peak solar efficiency [%]	Annual solar efficiency[3] [%]	Thermal cycle efficiency [%]	Capacity factor[2] (solar) [%]	Land use [m²/MWh y]
Central receiver	10-150	300-1'000	20 d 35 p	8-10 d 15-25 p	30-40 ST 45-55 CC	25-70 p	8-12
Dish-Stirling	0,01-0,4	1'000-3'000	29 d	16-18 d 18-23 p	30-40 Stirl 20-30 GT	25 p	8-12
Trough	10-200	70-80	21 d	10-15 d 17-18 p	30-40 ST	24 d 25-70 p	6-8

d) demonstrated
p) projected
ST) steam turbine
GT) gas turbine
CC) combined cycle

[2] The capacity factor is calculated as the ratio between the yearly solar operating hours and the yearly hours with an incident radiation greater than zero.

[3] The solar efficiency is calculated as the ratio between the net power generation and the incident beam radiation.

Application	Type	Typical size range	Fuels	Ash [%]	Water content [%]
Manual	Wood stoves	2 – 10 kW	dry wood logs	<2	5-20
	Log wood boilers	5 – 50 kW	log wood, sticky wood residues	<2	5-30
Pellets	Pellet stoves and boilers	2 – 25 kW	wood pellets	<2	8-10
Automatic	Understoker furnaces	20 – 2.5 MW	wood chips, wood residues	<2	5-50
	Moving grate furnaces	150 – 15 MW	all wood fuels, most biomass	<50	5-60
	Pre oven with grate	0,02 – 1.5 MW	dry wood (residues)	<5	5-35
	Understoker with rotating grate	2 – 5 MW	wood chips, high water content	<50	40-65
	Cigar burner	3 – 5 MW	straw bales	<5	20
	Whole bale furnaces	3 – 5 MW	whole bales	<5	20
	Straw furnaces	0,1 – 5 MW	straw bales with bale cutter	<5	20
	Stationary fluidised bed	5 – 15 MW	various biomass, d < 10 mm	<50	5-60
	Circulating fluidised bed	15 – 100 MW	various biomass, d < 10 mm	<50	5-60
	Dust combustor, entrained flow	5 – 10 MW	various biomass, d < 5 mm	<5	<20
Co-firing (biomass covers less than 10% of fuel input)	Stationary fluidised bed	tot. 50 – 150 MW	various biomass, d < 10 mm	<50	5-60
	Circulating fluidised bed	tot. 100 – 300 MW	various biomass, d < 10 mm	<50	5-60
	Cigar burner Dust	straw 5 – 20 MW	straw bales	<5	20
	Combustor in coal boilers	tot. 0,1 – 1 GW	various biomass,d < 2 – 5 mm	<5	<20

Table 12: Most used furnaces for biomass combustion [79].

Other solutions are to combine different sources with complementary intermittencies [22] [21] [23] [80], or to provide high capacity energy storage to buffer the supply [19] [20], absorbing the supply peaks and releasing the energy in a controlled way over a longer period. In this study the RES intermittency bottleneck has been bypassed equipping the solar field with a Thermal Energy Storage (TES) device and by combining a biomass technology to the CSP sub-system. Furthermore, the TES reduces the thermal transient effects extending the life expectancy of components [81]. The solar-biomass hybridization allows an improved power output modulation and permits to operate the CSP modules close to design duty-point [82] [41] [83].

Concerning the biomass section, direct combustion has been chosen as it is a well-understood, well-developed, and widely available technology that can be easily integrated with existing infrastructure [63]. Furthermore, direct combustion devices are used in a wide range of applications, from small domestic stoves to the largest boilers used in power and cogeneration plants, with sizes varying from 2 kW up to 1 GW, Table 12.

Considering the *renewable energy conversion* block, a low enthalpy saturated steam Rankine Cycle (RC) was selected to obtain electric and thermal energy. In particular, the lack of a superheating section is due to the efforts to simplify the plant as much as possible. Moreover, the steam is expanded in a reciprocating engine, chosen to cope with the small-size turbine limitations in terms of operating flexibility and insensitivity to modest saturated steam quality, i.e. wet steam [84] [85]. The direct output of the plant are electric and thermal energy.

The paths followed during the present study are sketched in the map of tackled issues map shown in Figure 28. The modelled energy system has been analyzed under several aspects.

Beginning from the renewable energy sources, the solar section has been initially analyzed by looking at the meteorological data and selecting the heat transfer fluid. At this stand point, with fixed design specifications for the parabolic troughs, isolated operation transient simulations of the solar field were made with the selected software, in order to determine the solar field size and its energy performance. Concerning the biomass side, an identical procedure has been conducted except for the creation of an in-house model for the biomass furnace. Hence, the CSP and biomass systems are coupled and power and environmental performance have been determined.

Subsequently, thermal energy storage block and the Rankine cycle have been studied and modelled to be integrated with the RES system. In particular for the TES section a selection has been made between concrete and rock-bed thermal energy storage. In addition, an in-house model for the steam engine has been created for the purpose.

Moreover the end uses have been inspected, pinpointing direct, i.e. electric and thermal energy loads, and indirect, i.e. water desalination, end uses. To draw out the simulations of the energy system in a load tracking configuration the relations which bond the needed thermal fluid flow rate to obtain both the desired electric and thermal output.

Finally the whole system has been investigated, evaluating power and environmental performance of several configurations.

As the tackled issues are numerous, only the most relevant paths are reported in the present study.

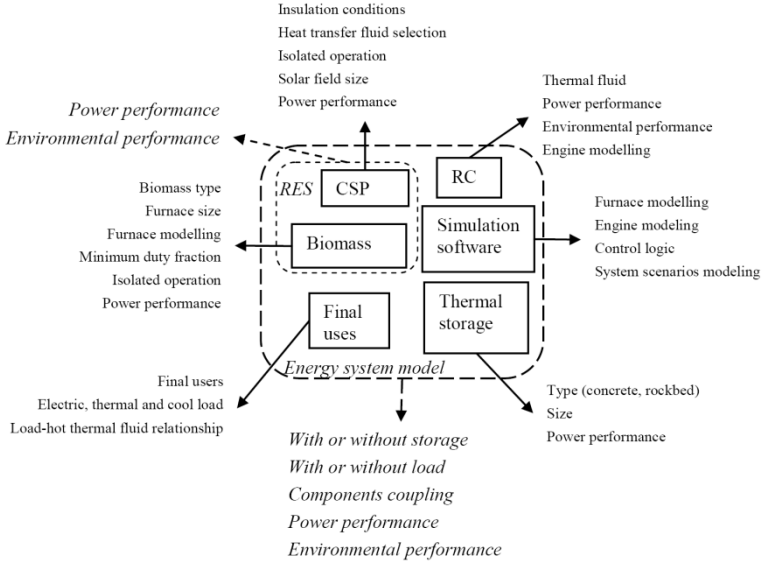

Figure 28: Map of tackled issues.

3.2 Time dependent input data

3.3 Parabolic trough field design

3.3.1 Weather data

The insulation and weather input data [86] are spread over a year period with an hourly distribution, and are referred to Rome's latitude, i.e. 41°54'39"24 N, as indicative of a central Italian location. The hourly weather data are generated by the Solar Energy Laboratory (SEL) by the application of a weather data generator given the monthly average values of solar radiation, dry bulb temperature, humidity ratio, and wind speed.

The hourly data, integrated on each month, are validated by the comparison with the monthly weather data obtained from the European Solar Radiation Atlas (ESRA) [87].

Looking at the *solar radiation*, Figure 29, the compared values have the same shape, even if not coincident. In particular the SEL data are on the average higher than the ESRA data. The maximum shift in the monthly direct normal insulation (DNI) value is registered in November with a difference of 4,43 MJ/m^2 d in October.

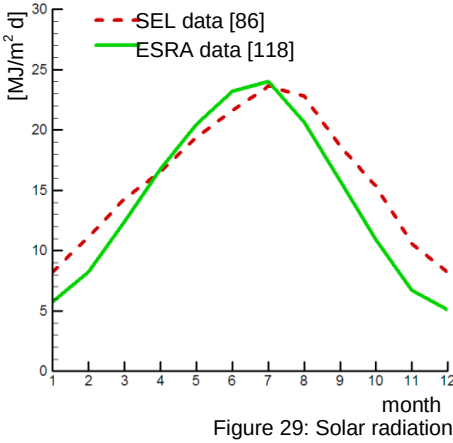

Month	SEL data MJ/m^2 d	ESRA data MJ/m^2 d
January	8,21	5,76
February	11,16	8,24
March	14,29	12,38
April	16,56	16,78
May	19,40	20,48
June	21,60	23,22
July	23,65	24,01
August	22,82	20,63
September	18,68	15,73
October	15,34	10,91
November	10,58	6,70
December	8,17	5,08

Figure 29: Solar radiation data comparison.

The *average temperature* curves, Figure 30, have the same shape. The maximum value difference between the two data sets is of 1,09 °C.

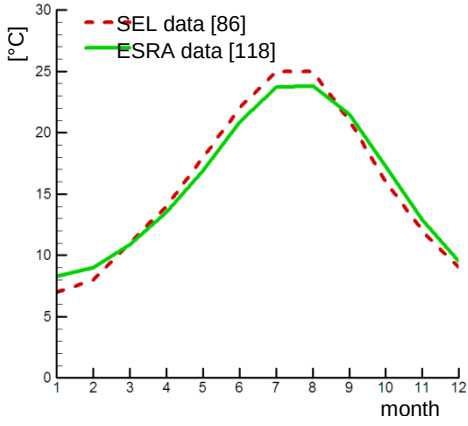

Month	SEL data °C	ESRA data °C
January	7,00	8,3
February	7,99	9
March	11,00	10,9
April	14,00	13,5
May	17,99	16,9
June	22,00	20,9
July	25,00	23,7
August	25,00	23,8
September	21,01	21,5
October	16,00	17,3
November	12,01	12,9
December	9,00	9,5

Figure 30: Average temperature data comparison.

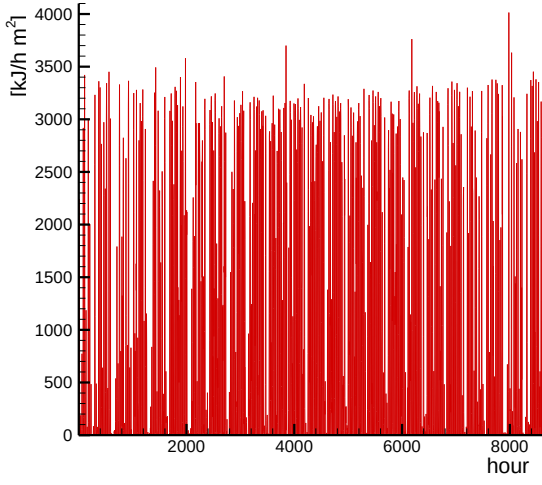

Figure 31: Hourly DNI for Rome [86].

The most important weather datum for a CSP plant is the DNI as it is the only useful component of the solar radiation for the concentrated solar power devices. The maximum DNI value, 733,68 MJ/m^2, occurs in the month of July, while the minimum value of 253,04 MJ/m^2 occurs in December. The annual DNI for Rome is 5˙760 MJ/m^2.

The data are available in a hourly time step, Figure 31, and show a continuous value variation. The DNI is equal to zero for 4˙136 hours a year, and the maximum reached value is 4˙014 kJ/h m^2. Looking at the DNI occurrence, Figure 32, excluding DNI values lower than 500 kJ/h/m^2, the most frequent values are in the range 2˙900-3˙300 kJ/h/m^2, with 661 corresponding hours.

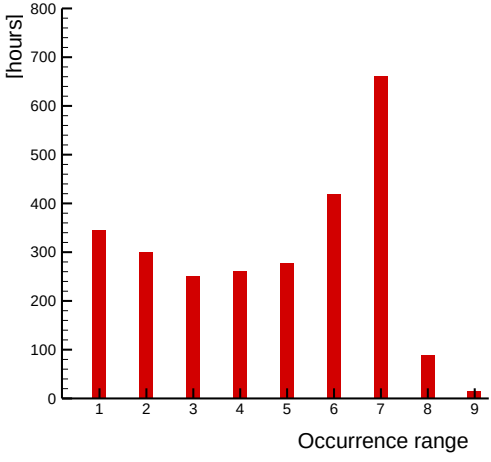

Occ.	DNI [MJ/h m^2]	Hours
0	0< < 0,5	2010
1	0,5≤ <0,9	344
2	0,9≤ <1,3	299
3	1,3≤ <1,7	251
4	1,7≤ <2,1	261
5	2,1≤ <2,5	276
6	2,5≤ <2,9	419
7	2,9≤ <3,3	661
8	3,3≤ <3,7	88
9	3,7≤ <4,1	14

Figure 32: DNI occurrence.

3.3.2 Hot thermal fluid

The industrial heating of solids, liquids or gases is commonly carried out by a system of indirect heat transmission *via* a heat transfer fluid that transfers heat from a heat source to the point of use.

The advantages of an indirect system are:

- precision in temperature control;
- uniformity of heating avoiding local overheating;
- multiuse from one heat source, and
- maximum safety due to the separation of the user and the heat source.

Mineral heat transfer oils are used in modern plants for the industrial transmission of heat from a heat source to one or more users, for the following advantages [88]:

- they operate in a wide range of temperatures (from ambient temperature to 553 – 673 K);
- they may operate at atmospheric pressure, thus avoiding the need of high pressures which would require expensive plant;
- they provide excellent lubrication that ensures low wear on pumps and valves;
- they have a protective capacity that ensures the absence of rust on metallic surfaces;
- they have a low pour point that allows starting the plant in the cold;
- low vapour tension that reduces the risk of vapour formation, and
- use of a non-toxic, non-corrosive fluid that does not give collection or recovery problems.

In this scenario, a density of diathermic oils has been compared on the basis of the working temperature range, Table 13. Among these, *Dowtherm A* and *Therminol VP-1* have the most suitable temperature range, with a higher maximum temperature, which allows a higher security level in case of an unexpected over-production of the solar field. Finally, *Dowtherm A* fluid has been chosen for its additional environmental characteristics.

Table 13: Mineral oils working temperature comparison.

Name	Temperature range [K]	Reference
Essotherm 500	max 588	[89]
Jaritherm DBT	273-623	[90]
Therminol VP-1	285-673	[91]
Dowtherm A	288-673	[92]

The *Dow Chemical Company* "Dowtherm A" oil [92], is an eutectic mixture of two biphenyl (C12H10) and diphenyl oxide (C12H10O), and may be used in systems employing either liquid phase or vapour phase heating. It is stable, does not decompose readily at high temperatures, has low viscosity throughout the entire operating range, minimizing start-up and pumping problems, and is non-corrosive to common metals and

alloys. Table 14 summarizes the main physical properties of *Dowtherm A* fluid, while Figure 33 shows its liquid properties curves.

Table 14: Physical properties of Dowtherm A fluid [92].

Properties	
Atmospheric Boiling Point	530.25 K
Freezing Point	285 K
Flash Point	386,15 K
Fire Point	391,15 K
Auto Ignition Temperature	872,15 K
Density	1˙056 kg/m^3 @ 298,15 K
Volume Contraction upon Freezing	6.63%
Volume Expansion upon Melting	7.10%
Heat of Fusion	98.2 kJ/kg
Critical Temperature	770,15 K
Critical Pressure	31.34 bar
Critical Volume	3.17 l/kg
Heat of Combustion	36,053 kJ/kg
Molecular Weight (Average)	166.0

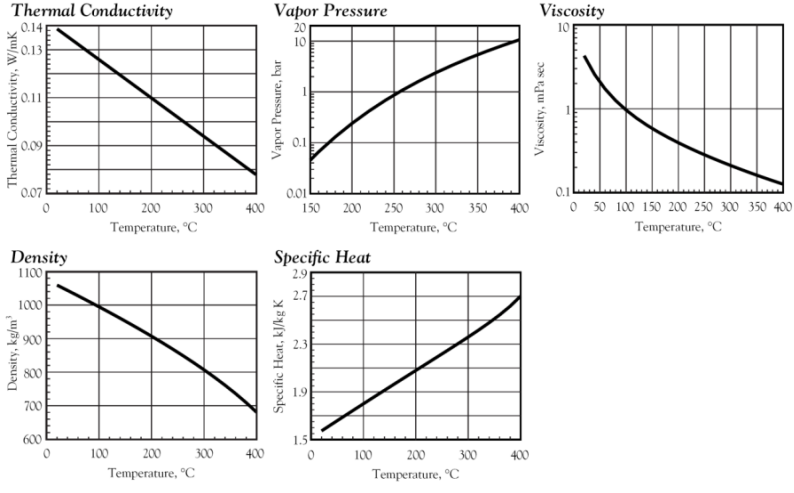

Figure 33: Liquid Properties of Dowtherm A [92].

From the environmental point of view, *Dowtherm A* fluid has a 5-day BOD[4] of 1,70 parts/part, 62% of its theoretical oxygen demand. Its COD[5]

[4] Biological Oxygen Demand

is 2,53 parts/part. This indicates that it is biodegradable and non-persistent in the environment. There is no evidence that harmful products are formed as a result of biodegradation. Once its bacteria are acclimated, a waste treatment system should achieve a high degree of removal of fluid before the wastewater effluent reaches the receiving body of water. The water solubility of this material is very low, i.e. only 14 ppm at ambient temperatures, and if amounts exceeding this limit are mixed with water, the medium will settle to the bottom. Of course, turbulence and the presence of other materials may affect the physical condition of the solution. It is also possible that an emulsion may form under certain conditions. Data indicate that a large percentage of the medium present in water will be stripped out during aeration in the primary stage of a waste treatment facility. Finally, both components of *Dowtherm A* fluid, biphenyl and diphenyl oxide, bio-concentrate in trout, but that when these trout are exposed to fresh water, the compounds disappear from their tissues in a relatively short time. Should this material be discharged into a body of water, it may bioc-oncentrate in fish, but at a significantly lower level than compounds such as polychlorinated biphenyl. Furthermore, because of the speed with which the material is cleared from the tissues and biodegrades, it is unlikely to pose a serious problem [92].

3.3.3 Solar collectors data

The solar field is made up of 32 parabolic trough collectors, Figure 34, of 36 m of length and 2,3 m of aperture width. Its gross collecting surface is 2˙580 m^2 and the rotating axis of the collectors is oriented east-west.

The chosen field extension is consistent with the Italian feed in tariff for thermodynamic solar plants [93], which sets a minimum solar field extension of 2˙500 m^2. The field is designed to give a constant HTF output temperature of 573,15 K, modulating the output flow rate to face the sun DNI variations. The field peak power is 1˙294 kW for direct solar irradiance of 1˙000 W/m^2 and 298,15 K ambient temperature.

[5] Chemical Oxygen Demand

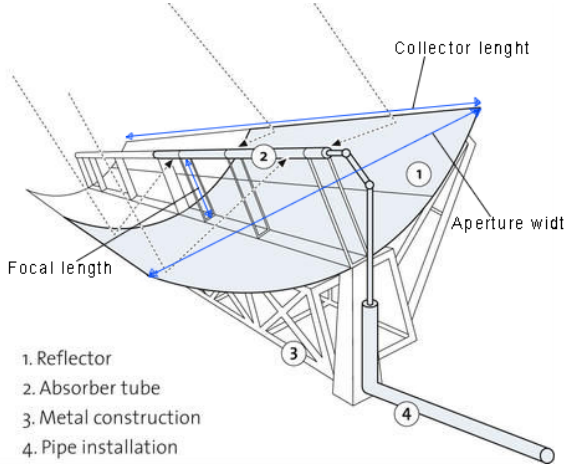

Figure 34: Collector geometry scheme.

Table 15: Parabolic trough field design data.

Collectors	
Length of SCA	36 m
Aperture width	2,3 m
Focal length	0,76 m
Collectors per row	5
Number of rows	6
Row-spacing	6,9 m
Total field area	2˙580 m^2
Number of collectors	30
Wind speed limit for tracking	13,7 m/s
Orientation	
Direction	South
Min tracking angle	-90 degrees
Max tracking angle	90 degrees
HTF flow rate	
Pump max flow rate	31˙000 kg/h
Turn down ratio (min flow ratio)[6]	0,03

[6] Flow rate fraction, with respect to the maximum flowrate, under which the system is turned down. In this case the minimum allowed flow rate corresponds to 930 kg/h, i.e. the 3% of the 31˙000 kg/h maximum flowrate.

3.3.4 Power plant thermodynamics

Oil side

The initial aim of the plant is to work on constant duty conditions, maximizing the solar contribution by using direct thermal energy supply and employing thermal energy storage. The biomass co-powering is used to compensate direct or stored energy output from the solar field, although the biomass furnace supplies a constant contribution of the 35% of its nominal power (i.e. 325,5 kW of 930 kW) in order to avoid start-ups problems. The desired result is a constant power output of 135 kW of electric energy and 900 kW of thermal energy.

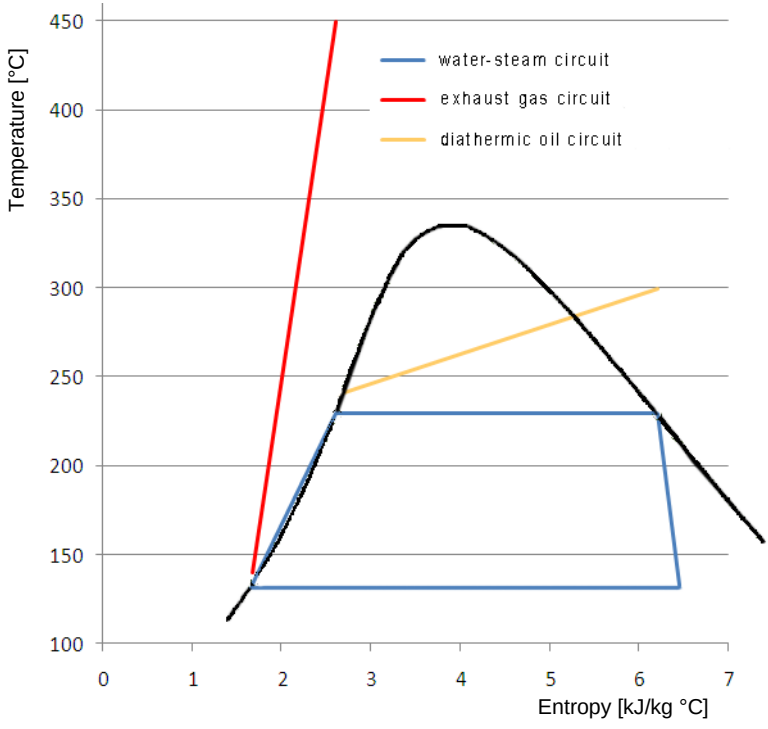

Figure 35: Temperature-Entropy diagram of the thermodynamic cycle.

Anticipating what is afterwards described, the biomass furnace supplies 2,39 kg/s of oil mass flow rate. As the evaporator oil mass flow rate amounts to 6,82 kg/s, then the solar field desired flow rate is of 4,43

kg/s. The oil temperatures at the solar field extremes amount to 240 at the inlet and 573,15 K at the outlet. Figure 35 shows the temperature-entropy diagram of the thermodynamic cycle involving both biomass and solar field contribution to the preheating and evaporator sections.

Table 16: Solar field thermodynamic data summary.

Inlet temperature	$T_{o,sol,in}$	513,15 K
Outlet temperature	$T_{o,sol,out}$	573,15 K
Desired mass flow rate	$m_{o,sol}$	4,43 kg/s

Obviously the solar field is not able to constantly furnish the designed flow rate, but it will vary in every time step, reaching higher and lower values. In case of excess flow rate, the difference is sent to the thermal energy storage, While in case of deficit the supply will first be requested to the thermal energy and then to an additional biomass furnace contribution, The control logic will be deeply analyzed in § 4.

3.4 Thermal energy storage

Oil side

The thermal energy storage consists of parallel equally spaced tubes in a concrete matrix with HTF flowing through in two possible directions, Figure 36: flow down (normally charge flow entering hot) and flow up (normally discharge flow entering cold).

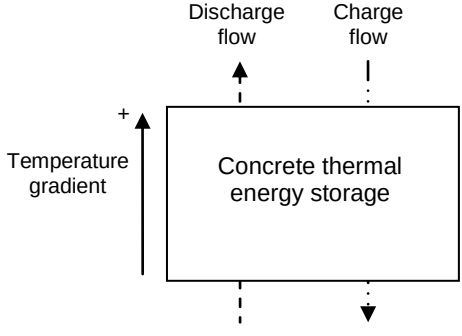

Figure 36: Thermal energy storage scheme.

The design data, shown in Table 17, have been defined by the comparison with the parabolic trough field with oil concrete storage system example contained in the solar thermal energy conversion (STEC) Release Examples [94], in which a 220˙000 m^2 solar trough field is simulated. The concrete storage device of the example has been scaled down by considering solar field extension, oil temperatures oil flow rates.

Table 17: Concrete storage design data.

Total cross sectional area of pipes	1,5 m^2
Length of storage	114 m
Concrete specific heat	0,9638 kJ/kg K
Concrete total mass	4˙543˙990 kg
Overall heat transfer coefficient at reference flow rate	124˙847 kJ/h K
Reference flow rate	5˙489 kg/s
Overall loss coefficient	10 kJ/h K
Power capacity	70 MW

The design has been performed with the objective to effectively extend the daily duty time of the solar contribution to the energy conversion. Figure 37 shows a summer day solar field and TES power behaviour with respect to the design energy goal. It is evident that the solar power contribution (P_{CSP}) exceeds the requested power level (100%) for several hours during the day. The surplus power is then stored ($P_{TES,c}$) and turned back when the direct solar power decreases, guaranteeing paying back with additional 8 hours of full-solar operation of the system.

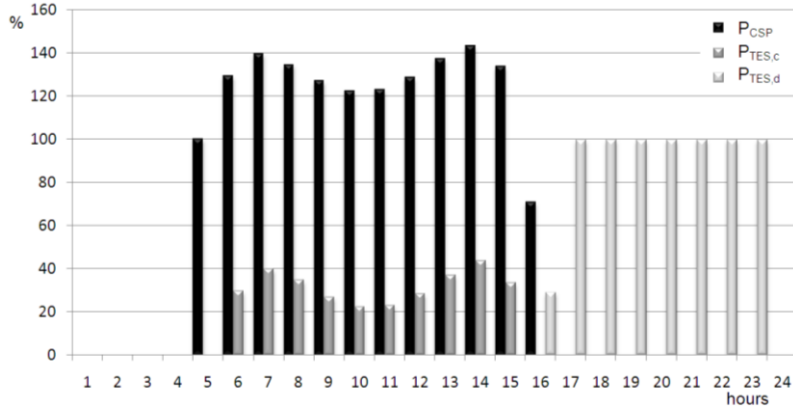

Figure 37: Storage charge-discharge behaviour of a CSP system on a typical summer day.

3.5 Biomass co-powering system

3.5.1 Biomass data

As far as the biomass is concerned, the thermo-chemical characteristics are shown in Table 18. The values are typical of pine wood derived woody pellet, with a lower heating value of about 18 MJ/kg and high carbon and oxygen ratios.

Table 18: Biomass characteristics [95].

Hi [MJ/kg]	Carbon [%]	Hydrogen [%]	Oxygen [%]	Sulphur [%]	Humidity [%]
18,30	49,80	8,10	38,30	0,04	5,50

3.5.2 Biomass furnace

The designed furnace is a prismatic multi-tube diathermic fluid heater suitable for the combustion of solid fuels. Compatible fuels are:

- wooden biomass (plant waste from agricultural and forestry activities and from the first processing phase of agricultural and food products);
- waste from the processing of un-treated wood and cork;
- waste from the working of treated wood and similar (glued chipboard or multi-ply and products finished with resins of the type and in the quantity admissible according to legislation on the re-use of waste).

Table 19: Biomass furnace design data.

Heat input	1˙163 kW
Generator rating	930 kW
Combustion chamber volume	7 m^3
Flue gas side pressure drop	7,4 mbar
Oil side pressure drop	950 mbar
Installed electrical power	6,75 kW

The generator rating is of 930 kW with a heat input of 1˙163 kW, Table 19. The heater is designed for a maximum operating temperature of 573,15 K and a maximum operating pressure of 8 bars. The forced circulation of the diathermic fluid is provided by a pump suitable for oils

at temperatures of up to 623,15 K and sized for a flow-rate corresponding to a maximum thermal head of 313,15 K.

The operation of these boilers can be either on-off, with the possibility of calibrating the combustion system to outputs below the maximum level, or with continuous modulation from 50 to 100% or from 25 to 100% of the heat input [96].

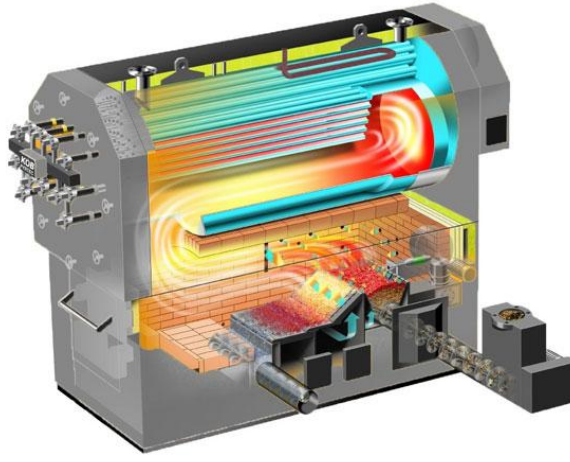

Figure 38: Biomass furnace device [97].

3.5.3 Thermodynamics

Gas side

The calculations are made in the hypothesis of the 35% rate of the biomass furnace duty. The heat input power from the burned biomass must provide heat to increase the diathermic oil temperature in the furnace itself, $P_{fur,35}$= 407,05 kW, and the water preheating in the economizer, taking $Q_{eco,eg}$=230,39 kW. Finally, the residual heat must be dispersed. In the hypothesis of a $T_{eg,fur}$=1˙273,15 K temperature of for the gas in the furnace and by imposing an economizer outlet gas temperature of $T_{eg,eco,out}$= 413,15 K from the economizer, the gas outlet temperature from the furnace $T_{eg,fur,out}$, coinciding with the gas economizer inlet temperature $T_{eg,eco,in}$, is calculated by matching the gas flow rate, $\dot{m}_{eg}$ of the two power equations for furnace and economizer:

$$\dot{P}_{fur} = \dot{m}_{eg} \cdot c_{p,eg} \cdot \Delta T_{eg,fur}$$

$$\dot{Q}_{eg,eco} = \dot{m}_{eg} \cdot c_{p,eg} \cdot \Delta T_{eg,eco}$$

The gas specific heat is assumed at a mean temperature value[7] of 900 K, $c_{p,eg}$ = 1,121. The resulting equation to calculate the gas temperature at the furnace outlet and economizer inlet is:

$$T_{eg,fur,out} = \frac{\dot{Q}_{eg,eco} \cdot T_{eg,fur} + \dot{P}_{fur} \cdot T_{eg,eco,out}}{\dot{P}_{fur} + \dot{Q}_{eg,eco}} = 723{,}98\ K.$$

At this standpoint, the gas flow rate value is determined as:

$$\dot{m}_{eg} = \frac{\dot{P}_{fur}}{c_{p,eg} \cdot \Delta T_{eg,fur}} = 0{,}66\ \frac{kg}{s}$$

and it is possible to calculate the energy to be dispersed in the stack to return the gas temperature to 293,15 K as:

$$\dot{Q}_{stack} = \dot{m}_{eg} \cdot c_{p,eg} \cdot \Delta T_{eg,stack} = 88{,}95\ kW.$$

The global power exchanged from the gas is then obtained as the sum of the furnace, economizer and stack powers, and amounts to $P_{eg,tot}$=726,39 kW. This value also corresponds to the power emitted from the burned biomass, allowing determining the biomass flow rate:

$$\dot{m}_b = \frac{P_{eg,tot}}{H_i} = 0{,}04\ \frac{kg}{s}.$$

Then the gas mass per kg of fuel (G_m) is calculated as:

$$G_m = \frac{\dot{m}_{eg}}{\dot{m}_b} = 16{,}63\ \frac{kg_{air}}{kg_{fuel}}$$

allowing to deduce the air mass (A_m):

$$A_m = G_m - 1 = 15{,}63\ \frac{kg_{air}}{kg_{fuel}}$$

the air index (n):

$$n = \frac{A_m}{A_{tm}} = 2{,}3$$

[7] The assumed specific heat value for the exhaust gases is based on the values scheduled for air. The author has become aware too late that the initial the reference to 900 K as mean temperature was erroneously maintained in the followed calculations.

and the excess of air as (e):

$$e = (n - 1) \cdot 100 = 130$$

where A_{tm} is the theoretical combustion air mass calculated as [98]:

$$A_{tm} = 0{,}11484 \cdot C + 0{,}34204 \cdot H + 0{,}4302 \cdot S - 0{,}0431 \cdot O = 6{,}85 \ \frac{kg_{air}}{kg_{fuel}}.$$

Oil side

The oil temperature in the furnace varies in the range 513,15- 573,15 K, thus the oil temperature gap is ΔT_o= 60 K

The oil specific heat ($c_{p,o}$) at the average temperature of 543,15 K is [92]:

$$C_{p,o} = 2{,}273 \ \frac{kJ}{Kg \ K}$$

As the exchanged heat between gases and oil must be equal to $P_{gen,35}$= 325,50 kW, the oil mass flow rate can be determined as:

$$\dot{m}_o = \frac{P_{gen,35}}{c_{p,o} \cdot \Delta T_{o,fur}} = 2{,}39 \ \frac{kg}{s}$$

Table 20: Biomass furnace data summary.

Gas side		
Yielded heat	$P_{fur,53}$	407,05 kW
Temperature at the burner	$T_{eg,fur}$	1˙273,15 K
Temperature after heat exchange with oil	$T_{eg,fur,out}$	680,2 K
Mass flow rate	m_{eg}	0,66 kg/s
Oil side		
Acquired heat	$P_{gen,35}$	325,5 kW
Inlet temperature	$T_{o,fur,in}$	513,15 K
Outlet temperature	$T_{o,fur,out}$	573,15 K
Mass flow rate	m_o	2,39 kg/s

3.6 Rankine Power cycle

This paragraph presents the reference Rankine power cycle. It is based on the utilization of steam, as water steam has the benefit of a large latent heat of vaporization. This is used in many ways, primarily using the change in phase for energy storage and energy release.

Power systems utilizing water/steam also have the benefit of combustion external to the power prime mover. These so called “external combustion engines” differ from gas turbines or diesel combustion where the working fluid (providing power to a turbine or piston) is also directly involved in the combustion. The obvious advantage of external combustion engines is enormous fuel flexibility. All varieties of biomass, waste fuels, and industrial by-products can be burned in incinerators or waste fuel boilers to make steam. Another form of waste which is often used to make steam is waste heat. As in the case of waste fuels, unusable heat from combustion or from cooling operations can be captured in boilers/heat exchangers designed for that purpose, in some cases utilizing more than 50% of the otherwise discarded energy [84].

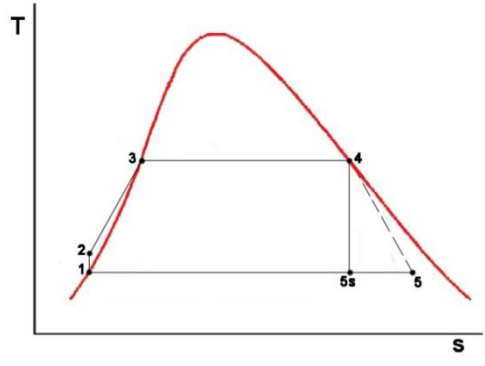

	1	2	3	4	5
T [K]	406,73	407,15	503,29	503,29	407,15
P [bar]	3,00	28,00	28,00	28,00	3,04
ρ [kg/m^3]	931,78	932,75	827,10	13,99	1,85
u [kJ/kg]	561,27	562,06	987,39	2604,02	2345,94
h [kJ/kg]	561,60	565,06	990,78	2804,11	2509,69
s [kJ/kg K]	1,67	1,67	2,61	6,21	6,46
x	0,0	0,0	0,0	1,0	0,9

Figure 39: Temperature-Entropy diagram of power cycle at reference state.

Figure 39 shows the temperature-entropy diagram of the power cycle at reference state. In general, the biomass furnace exhaust gases heat the feed-water in the economizer, while the HTF heats the preheated water in the evaporator, generating dry steam at 503,29 K and 28 bar pressure. All is done by direct heat exchange. After the evaporation, the steam flows into the reciprocating steam engine, where it is expanded to 407,15 K and 3 bar pressure, generating rotation of the axis that will be transmitted to the generator. The expanded wet steam is then condensed at 407,15 K and 3 bar pressure, producing a thermal power output available at a constant temperature of 353,15 K, which typically matches with the temperature demand of district heating networks. Hence, the feed-water is pumped again at the outlet of the condenser and flows back into the economizer, where it completes the cycle.

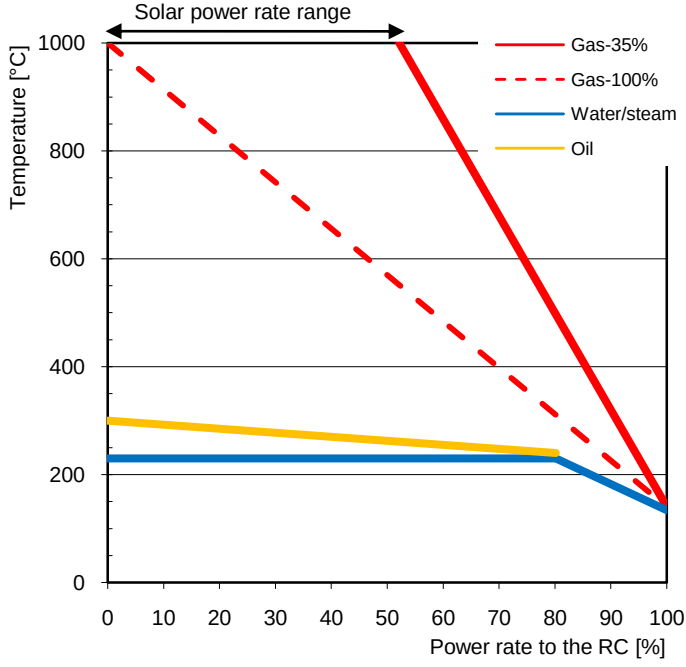

Figure 40: Heat exchanges graph.

The heat exchanges graph is shown in Figure 40. The exhaust gas, diathermic oil and water-steam fluids are represented relating the reached temperatures with the Rankine cycle exchanged power rate. In particular

for the exhaust gas two lines are plotted, one (Gas-35%) for the design condition with the biomass furnace working at 35% duty rate, and one (Gas-100%) for the fully biomass duty condition during the solar contribution lacks. The two extreme gas lines detect the range of the solar contribution to the heat exchanges and to the rate of power supply to the Rankine cycle, and thus the biomass energy contribution.

An important characteristic of the applied power cycle is that the steam sent to the expander is saturated steam and not superheated steam. This choice avoids the need of extremely high temperatures of the heat transfer fluid, from the solar field and biomass furnace, allowing the plants to be smaller.

It is worth remembering that the design data are determined under the hypothesis of a global renewable power supply on the diathermic oil side of 930 kW to the Rankine cycle. This hypothesis permits to reach the constant power outputs goal of the base-line plant. The imposed biomass system design is to supply the 25% of the renewable energy input, i.e. 35%, while the remaining 604,5 kW are directly supplied by the solar field, assisted by the thermal energy storage.

3.6.1 Evaporator

The evaporator, Figure 41, is used to turn the preheated water into saturated steam. For the proposed plant the hot fluid which exchanges thermal energy with water is diathermic oil from the solar and biomass circuits.

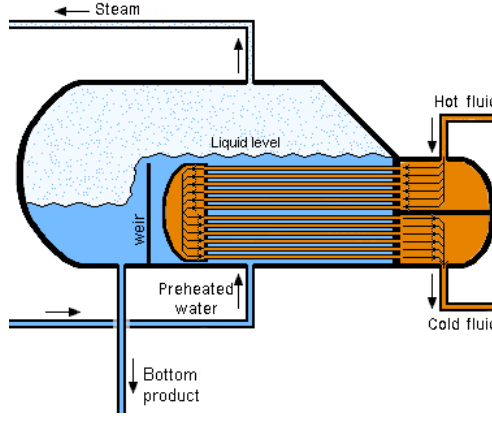

Figure 41: Evaporator scheme.

3.6.1.1 Thermodynamic parameters calculations

Water/steam side

The available heat from the diathermic oil at the evaporator is:

$$\dot{Q}_o = 930\ kW$$

The evaporation steam enthalpy drop is given by the difference between the steam enthalpy input and output values at the evaporator, Table 21, thus:

$$\Delta h_{\mathrm{w,ev}} = h_{out} - h_{in} = 2{\cdot}804{,}11 - 990{,}78 = 1{\cdot}813{,}33\ \frac{kJ}{kg}$$

At this standpoint, supposing an evaporator efficiency of $\eta_{ev} = 0{,}85$, it is possible to determine the steam power:

$$\dot{Q}_{ev} = \dot{Q}_o \cdot \eta_{ev} = 930 \cdot 0{,}85 = 790{,}50\ kW$$

and the steam flow rate:

$$\dot{m}_w = \frac{\dot{Q}_{ev}}{\Delta h_{w,ev}} = \frac{790{,}50}{1{\cdot}813{,}33} = 0{,}46\ \frac{kg}{s}$$

Table 21: Evaporator water/steam thermodynamic parameters.

Water/steam	Input	Output
T [K]	503,29	503,29
P [bar]	28,00	28,00
ρ [kg/m³]	827,10	13,99
u [kJ/kg]	987,39	2604,02
h [kJ/kg]	990,78	2804,11
s [kJ/kg K]	2,61	6,21
x	0,0	1,0

Oil side

Looking at the diathermic oil side, it enters the evaporator at 573,15 K and exits at 513,15 K. The corresponding specific heats, [96], are showed in Table 22.

Table 22: Evaporator input and output oil characteristics.

Oil	Input	Output
T [K]	573,15	513,15
c_p [kJ/kg K]	2,28	2,19

The specific heat at the average temperature of 543,15 K is 2,273 kJ/kg K [92]:

The oil enthalpy drop at the evaporator is then calculated as:

$$\Delta h_{o,ev} = \overline{c_p} \cdot (T_{o,in} - T_{o,out}) = 2{,}235 \cdot (573{,}15 - 513{,}15) = 136{,}38 \ \frac{\text{kJ}}{\text{kg}}$$

In conclusion, recurring to the energy conservation principle, the diathermic oil flow rate is:

$$\dot{m}_o = \frac{\dot{Q}_o}{\Delta h_{\text{o,ev}}} = \frac{930}{134{,}10} = 6{,}82 \ \frac{kg}{s}$$

3.6.1.2 Overall heat transfer factor

The thermal performance of a heat exchanger is expressed in terms of the effectiveness of the component. Heat exchanger effectiveness is defined as the actual heat transfer realized between streams over the maximum heat transfer possible for the given streams:

$$\varepsilon = \frac{\dot{Q}_{ev}}{\dot{Q}_{max}}$$

The capacitance rate of each stream is the product of its mass flow rate and specific heat:

$$C_C = \dot{m}_w \frac{\Delta h_{w,ev}}{\Delta T_{w,ev}}$$

$$C_H = \dot{m}_o \cdot C_o$$

The minimum and maximum heat capacitance rates of the two streams are identified, and the capacitance rate ratio is calculated:

$$C_{min} = MIN\ (C_C, C_H)$$

$$C_{max} = MAX\ (C_C, C_H)$$

The capacitance rate ratio of the fluid streams is the ratio of the smaller total heat capacitance of the two streams to the larger heat capacitance of the streams:

$$C_r = \frac{C_{min}}{C_{max}}$$

The maximum heat transfer possible between streams will equal the smaller total heat capacitance of the two fluid streams, multiplied by the difference in inlet temperatures between the streams.

$$\dot{Q}_{max} = C_{min}(T_{o,in} - T_{w,in})$$

For counter-flow sensible heat exchangers, the following relationship determines heat exchanger effectiveness as a function of capacitance ratio and the number of transfer units (*NTU*) [99]:

$$\varepsilon = \frac{1 - \exp\left[-NTU \cdot (1 - C_r)\right]}{1 - C_r \cdot \exp\left[-NTU \cdot (1 - C_r)\right]}$$

Alternatively the NTU can be determined from the graph for counter-flow heat exchangers, Figure 42, through ε and C_{min}/C_{max}. we obtain the value of *NTU* from which the value of UA_w can be determined.

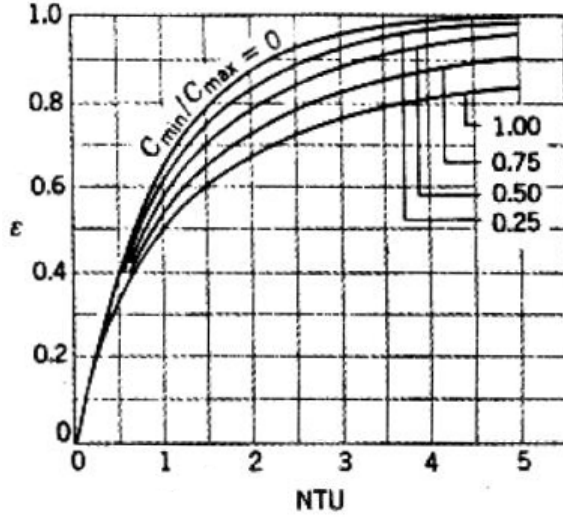

Figure 42: Effectiveness for cross-flow heat exchangers [99].

The ratio of the *NTU* to the heat capacitance of the feed water equals the reference *UA* of the heat exchanger:

$$NTU = \frac{UA}{C_{min}}$$

To calculate C_c, the specific heat of the boiling steam is assumed to be infinite. Furthermore, for heat exchangers in which one fluid undergoes a phase change, the effectiveness is related to *NTU*. Therefore, effectiveness for the steam generator is calculated according the equation:

$$\varepsilon_w = 1 - \exp\left(-NTU_w\right)$$

In the evaporator case HTF is diathermic oil. The calculations are:

$$\dot{Q}_{ev} = 790{,}50\ kW$$

$$\dot{m}_o = 6{,}82\ \frac{kg}{s}$$

$$C_C \rightarrow \infty$$

$$C_H = \dot{m}_o \cdot C_o = 6{,}94 \cdot 2{,}273 = 15{,}50\ \frac{kW}{K}$$

$$C_{min} = MIN(C_C, C_H) = C_H = 15{,}50 \frac{kW}{K}$$

$$\dot{Q}_{max} = C_{min}\left(T_{o,in} - T_{w,in}\right) = 15{,}51\ (573{,}15 - 503{,}29) = 1{\cdot}082{,}83\ kW$$

$$\varepsilon_w = \frac{\dot{Q}_{ev}}{\dot{Q}_{max}} = \frac{790{,}50}{1{\cdot}083{,}53} = 0{,}73$$

$$C_r = \frac{C_{min}}{C_{max}} = \frac{15{,}50}{\infty} = 0$$

$$NTU = -\ln(1 - \varepsilon_w) = -\ln(1 - 0{,}73) = 1{,}31$$

$$UA = NTU \cdot C_{min} = 1{,}31 \cdot 15{,}50 = 20{,}31\ \frac{kW}{K} = 73{\cdot}116\ \frac{kJ}{h\ K}$$

Table 23: Evaporator data summary.

Oil side		
Yielded heat	Q_o	930,00 kW
Inlet temperature	$T_{o,in}$	573,15 K
Outlet temperature	$T_{o,out}$	513,15 K
Mass flow rate	m_o	6,82 kg/s
Steam side		
Acquired heat	Q_{ev}	790,50 kW
Inlet enthalpy	$h_{w,in}$	990,78 kJ/kg
Outlet enthalpy	$h_{w,out}$	2˙804,11 kJ/kg
Mass flow rate	m_o	0,46 kg/s
Heat exchanger system		
Heat transfer efficiency		85%
Overall heat transfer factor	*UA*	20,31 kW/K

3.6.2 Economizer

The role of the economizer, Figure 43, is to pre-heat the water, shell fluid, fed to the evaporator. The tube fluid which supplies heat to the economizer is the exhaust gas from the biomass furnace. After passing the economizer the exhaust gas is sent to the filters and chimney plant section.

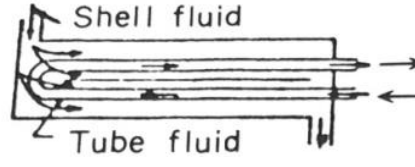

Figure 43: Economizer scheme.

3.6.2.1 Thermodynamic parameters calculations

Water/steam side

As calculated in the evaporator section, the water/steam flow rate amounts to m_w= 0,46 kg/s, and the economizer enthalpy drop is $\Delta h_{w,eco}$=425,72 kJ/kg. With these values, the heat at the economizer is:

$$\dot{Q}_{eco} = \dot{m}_w \cdot \Delta h_{w,eco} = 195{,}83\ kW$$

Table 24: Economizer water/steam thermodynamic parameters.

Water/steam	Input	Output
T [K]	407,15	503,29
P [bar]	28,00	28,00
ρ [kg/m^3]	932,75	827,10
u [kJ/kg]	562,06	987,39
h [kJ/kg]	565,06	990,78
s [kJ/kg K]	1,67	2,61
x	0,0	0,0

Gas side

As the economizer heat is provided by the biomass furnace exhaust gas, in the hypothesis of an 85% efficiency of the heat exchanger, the needed heat from the exhaust gas is:

$$\dot{Q}_{eg,eco} = 230{,}39\ kW$$

The exhaust gas mass flow rate has already been estimated as 0,66 kg/s and the gas outlet temperature has been fixed at 413,15 K.

3.6.2.2 Overall heat transfer factor

As previously done for the evaporator, the overall heat transfer factor for the economizer is calculated.

$$C_C = \dot{m}_w \frac{\Delta h_{w,eco}}{\Delta T_{w,eco}} = \ 0{,}46 \cdot \frac{425{,}72}{310{,}83} = 2{,}037\ \frac{kJ}{s\ K}$$

$$C_H = \dot{m}_{eg} \cdot c_{p,eg} = 0{,}66 \cdot 1{,}121 = 0{,}741\ \frac{kJ}{s\ K}$$

$$C_{min} = MIN\ (C_C, C_H) = \ 0{,}741\ \frac{kJ}{s\ K}$$

$$C_{max} = MAX\ (C_C, C_H) = 2{,}037\ \frac{kJ}{s\ K}$$

$$C_r = \frac{C_{min}}{C_{max}} = \frac{0{,}741}{2{,}037} = 0{,}364$$

$$\dot{Q}_{max} = \ C_{min}(T_{eg,in} - T_{w,in)} = 0{,}741 \cdot (723{,}98 - 407{,}15) = 234{,}84\ \ kW$$

$$\varepsilon = \frac{\dot{Q}_{eco}}{\dot{Q}_{max}} = \frac{195{,}83}{234{,}84} = 0{,}8339$$

$$NTU = 2{,}2536$$

$$UA = 1{,}67\ \frac{kW}{K} = 6{\cdot}013\ \frac{kJ}{h\ K}$$

Table 25: Economizer data summary.

Exhaust gas side		
Yielded heat	$Q_{eg,eco}$	230,39 kW
Inlet temperature	$T_{eg,eco.in}$	723,98 K
Outlet temperature	$T_{eg,eco.out}$	413,15 K
Mass flow rate	m_{eg}	0,66 kg/s
Steam side		
Acquired heat	Q_{eco}	195,83 kW
Inlet temperature	$T_{w,in}$	407,15 K
Outlet temperature	$T_{w,out}$	503,29 K
Mass flow rate	m_w	0,46 kg/s
Heat exchanger system		
Heat transfer efficiency		85%
Overall heat transfer factor	*UA*	1,67 kW/K

3.6.3 Steam engine

When looking to the steam expanders, steam turbines are more efficient than steam engines. Nevertheless, there are some remarkable limitations that have brought to choose a steam engine for this work. The most negative influence is represented by the turbines inability to maintain high efficiency when pressure or flow rate are reduced, which condition is a forecast for the proposed plant in the load tracking configuration, resulting in small turndown ratios. Other steam turbine inadequacies are: slow start-up times, large capital costs and lingering economies of scale and high costs for out-of-service time. Moreover for both DG and CHP applications, when steam is involved, turbines become questionable when the power output is below about 1 MW [84].

To the contrary, steam engines have several beneficial aspects that suit to the present plant [84]:

- **Fuel flexibility**: allows for a portfolio fuel approach. This includes thermal solar with very attractive installation costs since the rest of the system already exists. One must recognize that with many biomass and other waste fuels, there may be more

emissions concerns with sulphur, mercury and other non-standard pollutants.

- **Sensitivity to load**: System efficiency is insensitive to load and can respond to rapid changes in steam conditions.
- **Low pressure combustion**: combined with no preheating allows for modest combustion temperatures and very little problem with NO_x. Some new designs include coating the steam generator surfaces with an oxidation catalytic layer so that other emissions such as CO and unburned hydrocarbons can be reduced in a cost effective way.
- **Modest speeds, pressures and temperatures**: are all in ranges which allow for safe and flexible operations Wear, noise, and maintenance are all improved because of low piston speeds.
- **Out-of-service and Startup**: startup is fast and steam engines can be out-of-service for long periods of time.
- **Water Issues**: very modest water quality issues which results in reduced feed-water treatment costs. Also, the ability to handle wet steam in the pistons (even helping with lubrication) allows easy use of saturated steam.

Furthermore steam engines, Figure 44, are long life devices, i.e. 20-30 years, and moderate maintenance, resulting in a fast costs amortization, e.g. 3-4 years in Germany, [100].

Figure 44: Section of a Spilling steam engine.

3.6.3.1 Thermodynamic parameters calculations

Water/steam side

Referring to the thermodynamic parameters in Table 26, the enthalpy drop in the steam engine amounts to Δh_{se}=294,31 kJ/kg. This datum, with the steam mass flow rate of 0,46 kg/s gives the device power:

$$\dot{Q}_{se} = \dot{m}_w \cdot \Delta h_{se} = 135{,}38\ kW$$

Table 26: Steam engine steam thermodynamic parameters.

Water/Steam	Input	Output
T [K]	503,29	407,15
P [bar]	28,00	3,04
ρ [kg/m^3]	13,99	1,85
u [kJ/kg]	2˙604,02	2˙345,94
h [kJ/kg]	2˙804,11	2˙509,69
s [kJ/kg K]	6,21	6,46
x	1,0	0,9

3.6.3.2 Engine characteristics

With the presented data, the limit average pressure (p_{ml}) is calculated as [101]:

$$p_{ml}=p_{in}\cdot e-p_{out}\cdot(1-\gamma)+\frac{1}{k-1}\left\{p_{in}\frac{1+k}{\varepsilon v}\left(1-\varepsilon v^{1-k}\right)-p_{out}(\gamma+\mu)\left[\left(1+\frac{\gamma}{\mu}\right)^{k-1}\right]\right\}$$

The result value is p_{ml}=1˙447 kPa = 14,47 bar with,

- steam admission degree e = 0,25 [85],
- run fraction dedicated to the compression γ=0,3 [101],
- adiabatic exponent k = 1,135 [101],
- volume expansion ratio εv = 3,5 [101]
- dead space volume μ = 0,05 [101].

The capacity has been determined by the following relation [101],

$$P_{ltot} = p_{ml} \cdot V(2-\zeta)\frac{n}{60}$$

by substituting the total limit power (P_{ltot}) with the indicated power (P_i) and the limit average pressure (p_{ml}) with the indicated average pressure (p_{mi}), thus

$$V = \frac{P_i}{p_{mi}} \frac{60}{n(2-\zeta)}$$

Assuming the two cylinders are in phase, with an equal admission degree, r=4, it is possible to determine the indicated average pressure value of p_{mi}=13,71 bar as [102]:

$$p_{mi} = \frac{p_{in}(1+\ln(r))}{r} - p_{out}$$

For what concerns the indicated power P_i , it is coincident with the previously calculated device power Q_{se}=135,38 kW.

The considered values are:

n=1000 rpm, rotational frequency [85];

$\zeta = 0{,}15$, fraction accounting for the pistons shaft encumbrance [101].

The result is a total capacity of V = 0,0032 m^3.

3.6.4 Condenser

The condenser, Figure 45, is needed to return the water/steam discharged from the steam engine to the initial cycle conditions, exchanging heat with a cooling water flux.

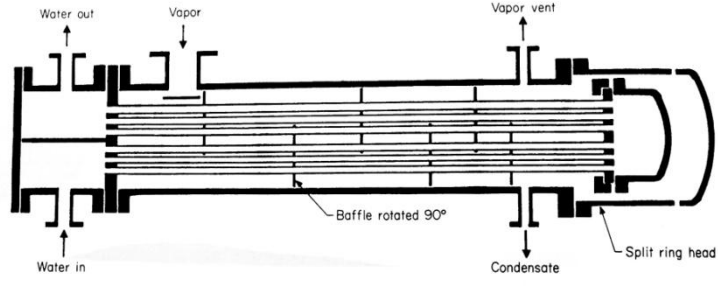

Figure 45: Condenser scheme.

3.6.4.1 Thermodynamic parameters calculations

Water/steam side

At the condenser the enthalpy drop is Δh_c=1˙947,40 kJ/kg, leading to a power of:

$$\dot{Q}_c = \dot{m}_w \cdot \Delta h_c = 895{,}80\ kW$$

Table 27: Condenser water/steam thermodynamic parameters.

Water/steam	Input	Output
T [K]	407,15	406,73
P [bar]	3,04	3,00
ρ [kg/m³]	1,85	931,78
u [kJ/kg]	2˙345,94	561,27
h [kJ/kg]	2˙509,69	561,60
s [kJ/kg K]	6,46	1,67
x	0,9	0,0

Cooling water side

For what concerns the condenser cooling water, the hypothesis is that the inlet temperature is of 323,15 K. In the hypothesis of a 85% efficiency, the released heat is

$$\dot{Q}_{cool} = 730{,}83\ kW$$

Considering the waters specific heat as $c_{p,cool}$ = 4,186 kJ/kg K and a temperature increase of ΔT_{cool} = 303,15 K, the cooling water mass flow rate is:

$$\dot{m}_{cool} = \frac{\dot{Q}_{cool}}{c_{p,cool} \cdot \Delta T_{cool}} = 5{,}43\ \frac{kg}{s}$$

3.7 End users

Electric and thermal energy may be used directly for energy scopes, e.g. lighting, space heating and cooling, transportation, or indirectly to obtain non-energetic products, e.g. hydrogen and desalted water. In this study both options are analyzed defining a CHP configuration and a

desalination configuration. In the following paragraphs both the options characteristics are explained.

3.7.1 CHP configuration

In combining a CHP plant energy production to a direct end user, it is fundamental to make a distinction between grid connected plant and stand alone plant.

When the plant configuration hypothesis is grid connected, the behaviour of the power output rates are not much troublesome, especially if they are constant. On the contrary, in a stand-alone plant hypothesis end user characteristic cannot be neglected. In this case it is essential to look for the end user which most fits the output power characteristics, in order to lower as much as possible electric and thermal energy dumps.

In this study, both stand alone and grid-connected configurations are evaluated. In particular, as the thermal power output is expected to be higher than the electric power one, the most suitable end users for the stand-alone configuration must have a thermal load higher than the electric one. Furthermore, it will be elemental to assure a thermal load even in the summer period, during the solar field peak power production.

The end user choice is the tertiary sector, even if it is possible to apply a CHP system to any end-user. As a matter of fact, it is not uncommon to consider the use of combined heat and power (CHP) schemes in commercial applications. With the Kyoto agreement, there has been a greater emphasis on reducing energy use and on considering energy efficient systems such as CHP. As a result, the installation of new CHP systems to displace less efficient means of power generation is now an important part of the strategy to reduce greenhouse gas emissions in nations like the United Kingdom. More specifically, CHP has been applied to two supermarket applications in the UK. Sainsbury's used CHP at their Greenwich store to produce electricity locally on site and to provide hot water for heating and toilet/canteen facilities. Safeway employed an ''Air CHP'' package at their Milton Keynes store. This used heat generated by the engine to warm air directly within an air handling unit [42] [43].

3.7.1.1 End users selection

For this study, the end users data have been chosen among several tertiary sector end-users, i.e. a shopping centre, a hospital, a hotel, a sporting centre and a bureaus building, Table 28.

Table 28: Nominee end-users [103].

	Shopping centre	Hospital	Hotel	Sporting centre	Bureaus building
Volume [m^3]	100˙000	42˙000	43˙000	9˙000	15˙000
Number of sleeping accommodations	-	140	350		
Heat load [GJ/y]	7˙820	7˙890	8˙640	4˙320	2˙030
Electric load [GJ/y]	28˙510	2˙880	1˙656	1˙140	1˙330
Cooling load [GJ/y]	6˙890	2˙178	2˙580	450	750
Heat/electric consumption ratio [GJ_{th}/GJ_{el}]	0,27	2,75	5,23	3,8	1,51
Installed electric power [kW_e]	1˙400	190	105	100	97

Looking at the shopping centre case, the electric energy load is remarkably higher than the thermal load, leading to an extremely low thermal/heat consumption ratio. Furthermore, the electric peak power is at least seven times greater than the electric peak power of the other cases and it is much greater than the selected size for the steam engine output selected for the designed plant.

The higher thermal/electric consumption ratio is showed by the hotel, with a value of 5,23, that is typical of European hotelier end-use figure, in contrast to the standard North-American hotel energy profile [104]. The other relevant consumption ratio are those of the sporting centre and the hospital. For what concerns the bureau building, the low thermal/electric consumption ratio is due to the extensive utilization of electrical devices, e.g. computers, printers copying machines, and to the lighting and elevators.

For an improved comparison of the users loads, it is worthy referring to the equivalent thermal load (obtained by the addition of the actual thermal load and the thermal load resulting if fulfilling the cooling load with a absorption chiller with a 0,7 COP.

Analyzing Figure 46 data, it is evident that in many case the ratio is greater than the one that can be obtained from an efficient cogeneration plant, conducing to two possible solutions:

- undersize the plant supplying the lack thermal and cooling load with auxiliary devices;
- sell the surplus electric energy to the grid, producing the right thermal energy.

In the cases of higher electric load, i.e. bureau building and shopping centre, a cogeneration plant if sized on the thermal energy is not able to do produce the whole electric energy request, which must be bought from the grid [103].

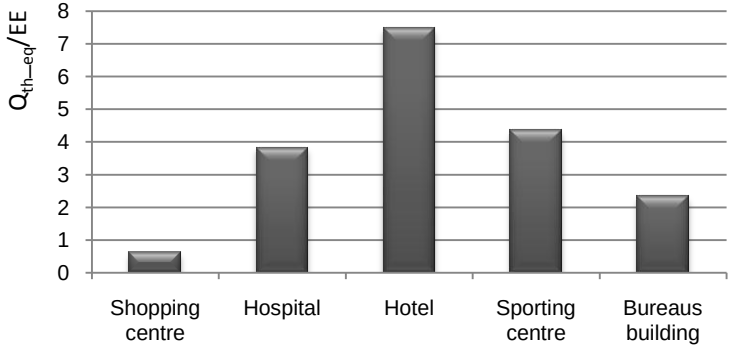

Figure 46: Consumption ratio between equivalent thermal and electric energy [103].

In reason of their low thermal/electric consumption ratio, the shopping centre and the bureaus building are excluded for the application to the studied plant. Furthermore, also looking to the electric and thermal consumptions the choice hospital and hotel users have been selected for their higher values.

3.7.1.2 End users load profiling

Looking at the hospital consumption characteristics, the monthly electric energy request, Figure 47, is almost constant during the whole year, while the thermal load is lower in the summer period, as expected even if it is not completely absent. The recur to the cooling devices is limited to the hottest summer months, from June to September, with an

average value of 540 GJ, although when considering the equivalent heat the values reach the 1000 GJ in those months.

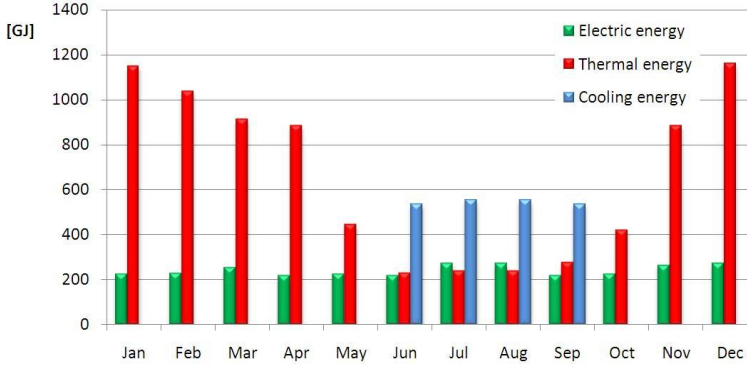

Figure 47: Hospital monthly consumption characteristics [103].

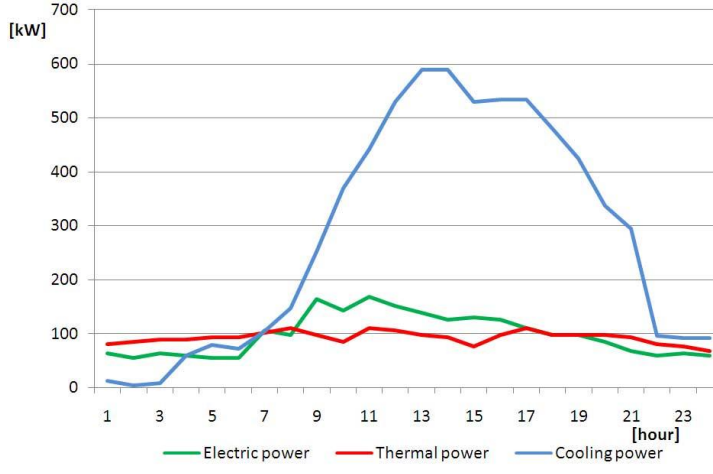

Figure 48: Hospital summer day power load [103].

In Figure 48 and Figure 49 the summer and winter typical daily power load are showed. By their comparison, it can be seen that the electric load shape is the same both in summer and in winter with a power range of 50-180 kW and lightly higher values in winter. The thermal power has

almost a constant behaviour during both days, while the cooling load presents a minimum of 500 kW power request difference between the night and day hours.

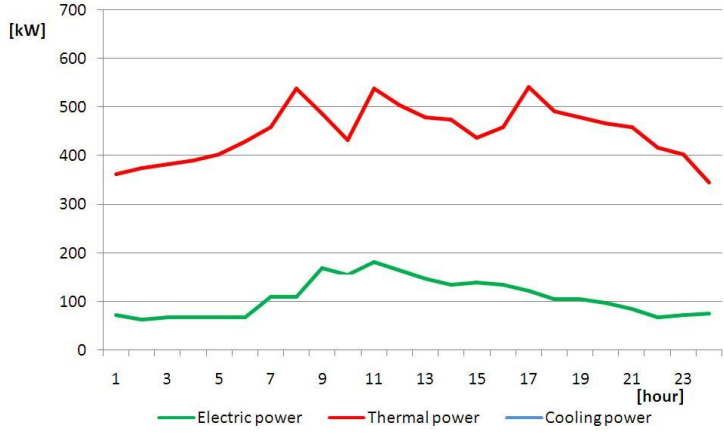

Figure 49: Hospital winter day power load [103].

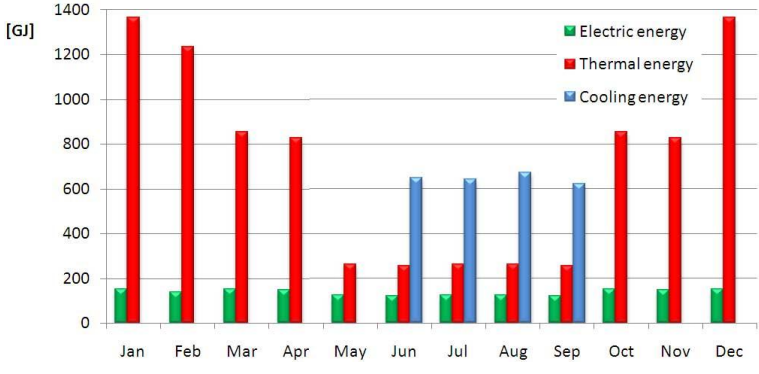

Figure 50: Hotel monthly consumption characteristics [103].

For what concerns the hotel monthly consumption characteristic, Figure 50, the general behaviour is equal to the hospital one, with nearly constant electric energy consumption and a seasonal connotation of the thermal and cooling energy request. Nevertheless, with respect to the hospital data, the electric energy values are lower, the thermal energy data

are higher and the cooling data are nearly the same. Moreover, when computing the equivalent heat it reaches values of about 1200 GJ, that is alike the winter thermal energy load.

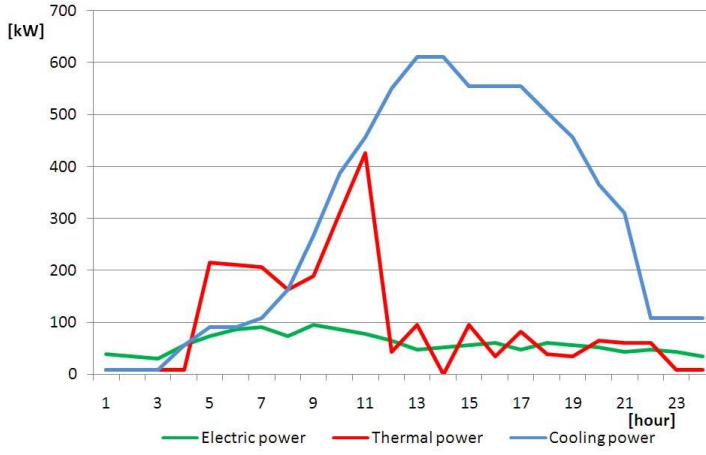

Figure 51: Hotel summer day power load [103].

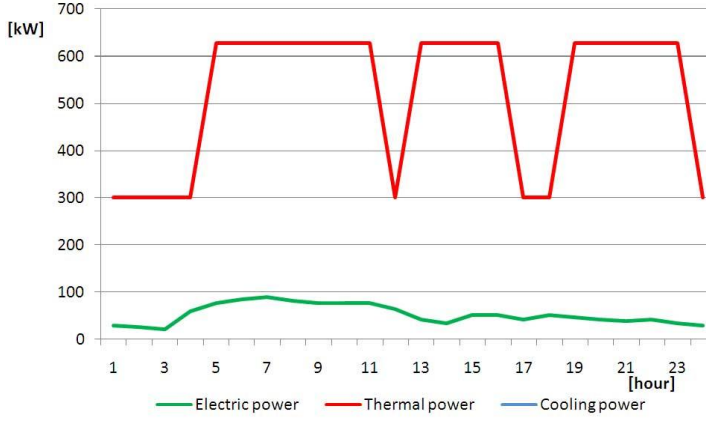

Figure 52: Hotel winter day power load [103].

Even in this case, referring to the typical the summer and winter daily power load, Figure 51 and Figure 52, the electric power shapes are alike.

The summer day thermal power although the average value of 99 kW has a power peak period from 5.00 a.m. until 11:00 a.m. with values over 210 kW, mainly related to the mornings need of hot sanitary water. In the winter period the thermal power request shows an extremely regular pattern with a minimum power of 300 kW and three peak periods at over 600 kW, due to the adopted space heating logic.

Using the monthly and daily load data, the annual load curves based on a hourly time step have been built for both the selected end-users. Furthermore, as the cooling load is evidently an important factor on the global energy request and has seasonal and daily shapes concordant to those of the solar energy availability, in this study the cooling energy will be added to the thermal one, considering the resulting equivalent heat.

3.7.1.3 End users annual hourly load curves

The annual load curves, based on a hourly step have been built starting from the summer and winter daily load data and from the monthly load data. In particular, month from May to October are considered as summer period, while the rest of the month are considered as winter period. The following procedure has been applied separately to the electric, thermal and cooling data. For each month, its total energy request is divided by the correspondent typical daily total load, obtaining an adaption factor, which interrelate the only daily load data with the several monthly load data. Hence, the adaption factor is applied to the typical daily load data, obtaining the daily load data corresponding to each month. Finally, the annual load curve has been built by adding for each month as many correspondent daily load curves as the number of days of the month itself. Obviously, the adopted procedure does not take into consideration different loads behaviours which may occur during week-ends or holidays periods. Nevertheless, as it is based on real data [103], the gap between real and derived load curve is supposed to be negligible for the goals of this study, the interest of which is to analyze the behaviour of the system under hourly variable loads and meteorological conditions.

Moreover, as already stated, the cooling load was added to the thermal one after being divided by an equivalence factor which takes into account the thermal energy losses related to the conversion in cooling energy. The result is an equivalent thermal load curve which, from this point will be named as thermal load.

Figure 53 and Figure 54 show the electric and thermal annual load behaviour of the hotel and hospital. In particular, the average daily energy demand (dot sign) is presented in relationship with the daily average power demand (ex sign) and the power demand excursion (bar).

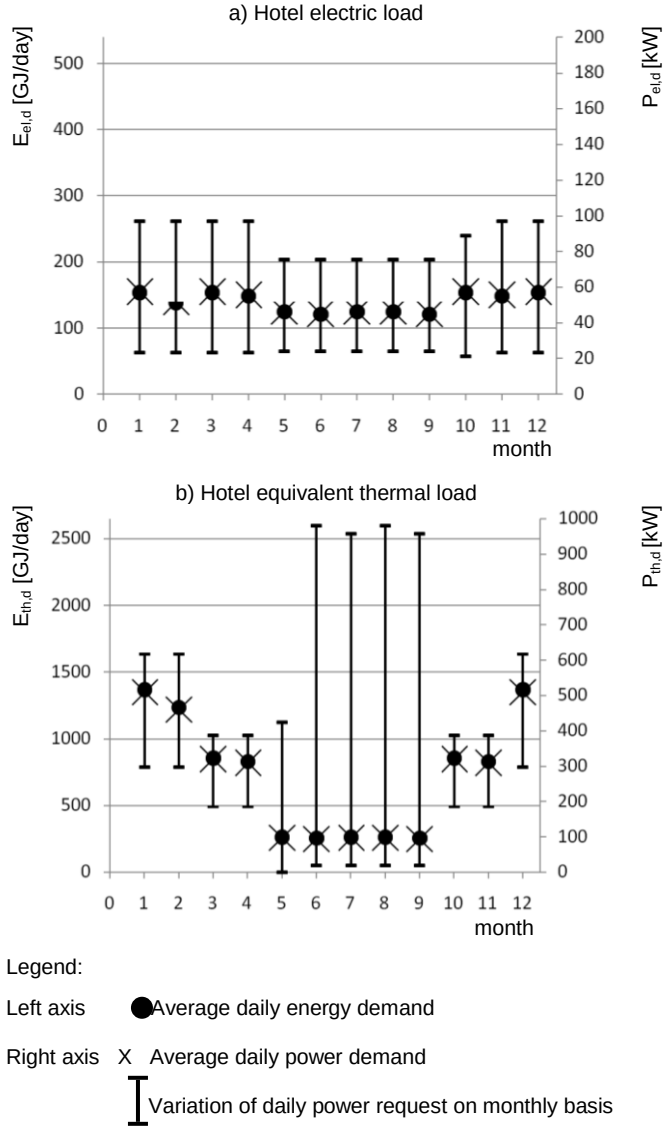

Figure 53: Hotel electric and thermal load yearly behaviour.

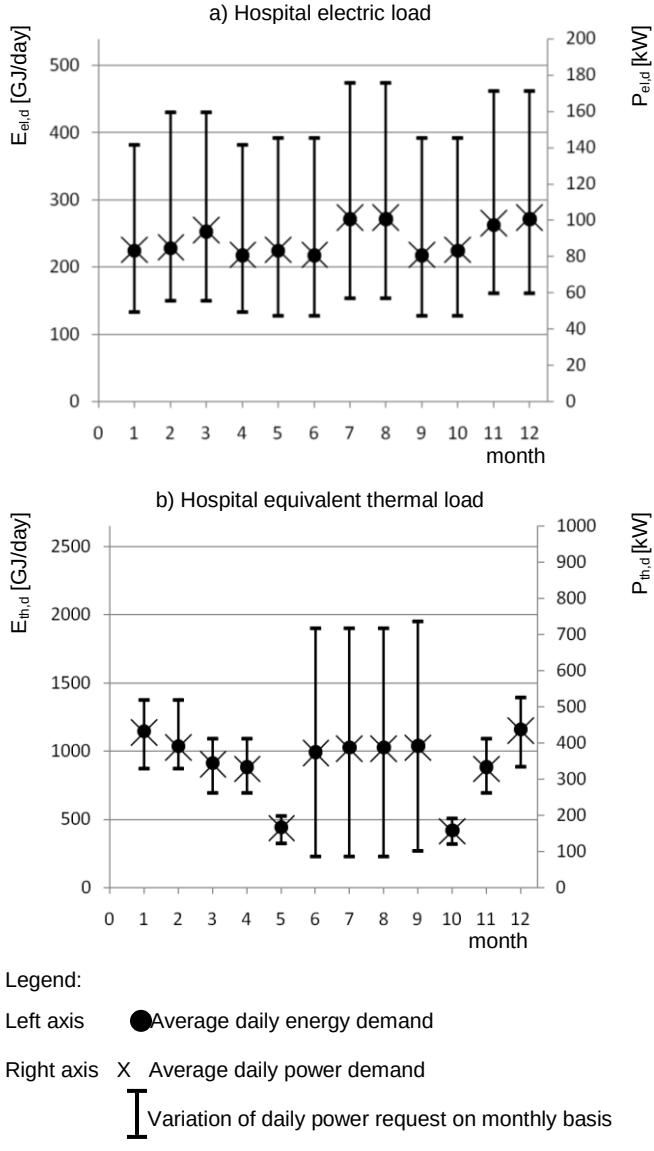

Figure 54: Hotel electric and thermal load yearly behaviour.

It is worth noting generally the average power demand is positioned on the lower part of the power demand excursion bars, indicating that the energy demand is composed by frequent low power demand values and

rare high power values. This behaviour is highlighted in the summer equivalent thermal load curves (from June to September) of both the end users, when during the day high peaks of cooling energy are requests, as already shown in Figure 48 and Figure 51.

3.7.2 Desalt units configuration

In the present work desalted water is considered as a by-product of the generating process, produced by using thermal energy resulting from the electric tracking of the hotel end user, chosen as more realistic to be in proximity of the sea. Thermal desalination has been chosen in reason of its remarkable availability in the developed system. Moreover, from a global perspective considering the pre and post-treatment of the feed water in a membrane layout, a distillation process is simpler and entails less operation and maintenance costs.

Table 29 provides a brief summary of the most common design operating parameters for the two most diffused thermal desalination processes. As evident, MED systems do not have a lower limit for the production capacity, in fact these systems are limited to smaller capacities with respect to MSF devices [75]. Furthermore, MED entails a lower electric power consumption.

Table 29: Most common design operating parameters of commercial thermal desalination systems [75].

Common design parameters	
Intake seawater temperature	5-35 °C
Intake seawater salinity	36˙000-45˙000 ppm
Brine blow down temperature	5-10 °C higher than intake seawater temperature
MSF design parameters	
Number of flashing states	20-24
Production capacity	5˙000-75˙000 m^3/day
Top brine temperature	90-110 °C
Gain output ratio	8-10 $kg_{distillate}/kg_{motive\ steam}$
Electrical power consumption	3-4 kWh/m^3
Brine blow down salinity	40˙000-70˙000 ppm
MED design parameters	
Number of evaporation effects	2-12
Production capacity	up to 30˙000 m^3/day
Top brine temperature	70 °C
Gain output ratio	8-16 $kg_{distillate}/kg_{motive\ steam}$
Electrical power consumption	1,2-2 kWh/m^3
Brine blow down salinity	65˙000 ppm

In order to produce as much water as possible reducing thermal energy dumps, the chosen desalting unit is a small capacity one and the system is composed of several units with a connection–disconnection strategy to match the variable energy supply.

The selected desalination system is a distillation device designed for diesel driven ships, which usually uses jacket cooling water from diesel engines to produce distilled water by evaporating sea water under a high vacuum (low temperature) condition [105]. The distiller working scheme is represented in Figure 55. The evaporator chamber is kept under vacuum by a water ejector. The seawater supplied by the ejector pump drives the water ejector and enters into the condenser tubes as a cooling medium before being discharged. Part of the jacket cooling water (fresh water) circulates to the outside of the heater tubes, giving up some of its heat to the sea water, which flows inside the tubes. The heated sweater (feed water) evaporates as it enters the main chamber due to the vacuum condition. Water droplets are removed from the vapour by the deflector and the mesh separator. The separated droplets fall back into the brine, which is extracted from the chamber and discharged. The vapour passes to the condenser tube bundle which is cooled by seawater flowing inside the tubes. The condensed vapour is collected and pumped to a fresh water tank by the distillate pump. Part of the seawater preheated in the condenser is used as the feed water to the distiller. The salinity of the distillate is monitored by a conductivity detector. If the salinity exceeds the design level, the solenoid valve in the discharge line of the distillate pump is automatically activated and the faulty distillate is returned to the brine side of the evaporator chamber.

Table 30: Desalting unit technical specifications [105]

	Capacity	3 t/24 h
	Distillate salinity	< 10 ppm
	Heat consumption	85 kW
Cooling seawater	Temperature	32 °C
Jacket cooling water	Quantity	6,4 t/h
	Inlet temperature	80,0 °C
	Outlet temperature	68,7 °C
Distillate pump	Capacity	0,3 m^3/h
	Speed	3450 rpm
	Power	0,4 kW
Ejector pump	Capacity	10 m^3/h
	Speed	3450 rpm
	Power	3,7 kW

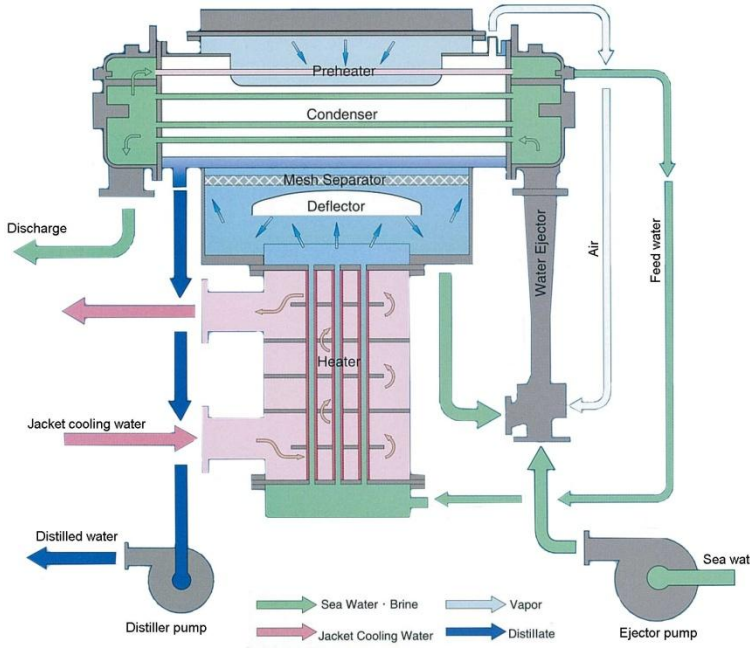

Figure 55: Sea water distillation device [105].

In the present work the jacket cooling water function is held by the Rankine cycle condensing cooling water, which is available at 353,15 K. To guarantee the distiller a proper working condition its technical specifications, Table 30, are maintained, while the input temperature of the cooling water at the condenser is changed from the previous value of 323,15 K to the present jacket cooling water outlet temperature from the distiller of 341,85 K. The effect of this choice is a higher cooling water flow rate at the Rankine cycle condenser.

Chapter 4
Analyses of hybrid system process

4.1 Control logic

A fundamental aspect of a power plant is the control logic, in order to keep the system work as much as possible closer to the design to obtain the prefixed goals. This is much true and harder to reach when the system entails a renewable, thus highly non-deterministic, energy input, like the sun.

As already introduced, the conceived hybrid plant has been analyzed under three configurations:

- constant power output configuration, i.e. that will be considered the base-line duty point;
- a configuration with electric or thermal load tracking; and
- a configuration where the hybrid plant is coupled to a desalt unit.

4.1.1 Baseline configuration

In the baseline configuration, the objective is to obtain a certain electric and thermal power output, without any load tracking, despite the meteorological data variability. The plant flow chart, Figure 56, highlights the renewable energy and the Rankine cycle subsystems component.

In the baseline configuration the subsets are linked and managed using the logical structure described by the flow diagram in Figure 57.

The adopted control logic aims to convert the maximum available solar energy contribution (P_{CSP}) either by sending it to the RC sub-system or by storing it in case of instantaneous surplus (P_{TESc}). To avoid power output deficits and furnace start-up problems, in conjunction with sun intensity off-hand variations, the biomass furnace is constantly on duty at a minimum power level of 35% of its maximum power (i.e. 407 kW) ($P_{b,35}$). The control system matches the target power demand (P_d) against the actual solar and the biomass thermal power input. In case of a thermal surplus ($P_{CSP} > P_d-P_{b,35}$), the exceeding fraction of solar power is sent to the thermal storage (P_{TESc}). In case of thermal deficit ($P_{CSP} < P_d-P_{b,35}$), the implemented logic first checks for the stored thermal energy (P_{TESd}) and if not sufficient ($P_{TESd}+P_{CSP}+P_{b,35}<P_d$) modules the biomass furnace duty point (P_{b+}). The result is a constant electric (P_{el}) and thermal (P_{th}) power output.

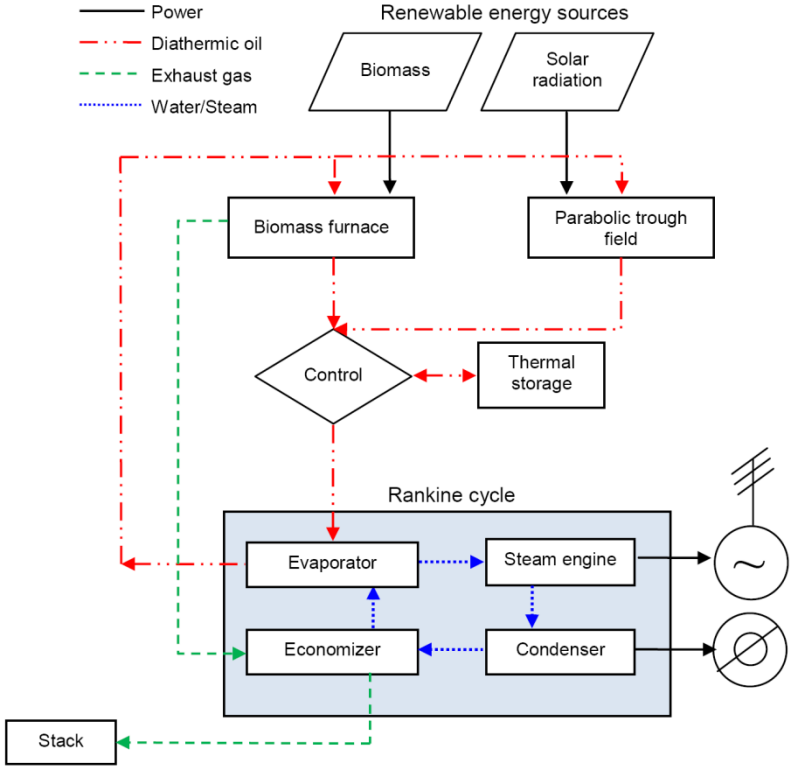

Figure 56: Base line plant flow chart.

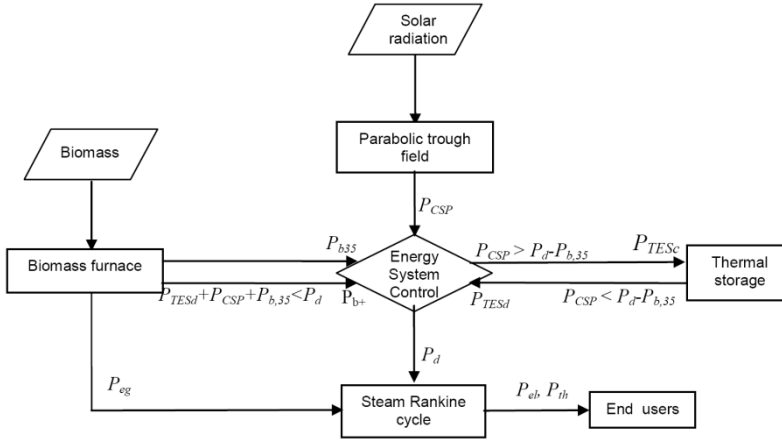

Figure 57: Base line plant control system flow diagram.

4.1.2 Load tracking configuration

In the load tracking configuration, the objective is to satisfy the load power request, either electric or thermal. The plant flow chart, Figure 58, demonstrates that the used devices are the same of the base line plant, with the exception of the end users power request, which influences the exploitation of the renewable energy sources.

The base-line control logic could be tailored to either the tracking of heat or power demands. The development of the load tracking strategy has been based on the definition of algebraic correlations between the HTF flow rate ($\dot{m}_F$), directly related to the RES power input, and the system thermal power output (P_{th}) or the system electric output (P_{el}), respectively. The HTF flow rate was selected as the reference parameter because it governs the actual power outputs from the Rankine cycle according to the instantaneous renewable energy availability. To obtain the HTF- flow/power-output correlations sensitivity analysis were carried out on the power system configuration.

The HTF flow rate is the sensitivity parameter. Figure 59 shows the values obtained with the sensitivity analysis (grey lines) and the corresponding trend lines (black lines) and equations. The HTF control equations, accordingly derived, read as:

$$\dot{m}_F = 2 \cdot 10^{-6} \cdot {P_{th}}^{3.289},$$

$$\dot{m}_F = 3.6 \cdot 10^{-2} \cdot {P_{el}}^{2.713}.$$

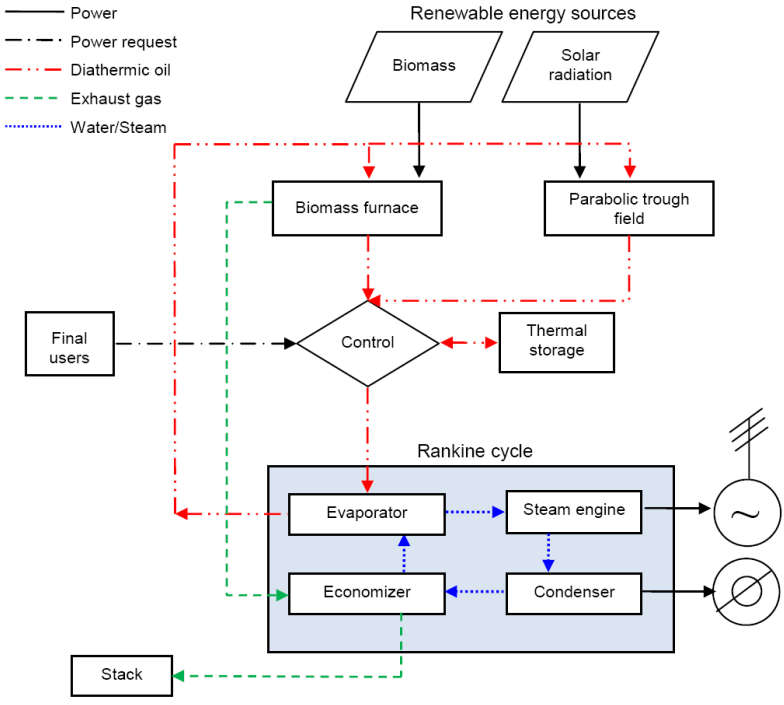

Figure 58: Load tracking configuration plant flow chart.

In the thermal power case, Figure 59 a, the HTF flowrate has been varied in the 200-23˙000 kg/h range, maintaining the thermal power output in the 455-1100 kW. The thermal power range minimum is settled by the system duty characteristics; in fact, although the minimum end user load is about 9 kW (corresponding to the hotel thermal summer behaviour during night hours, when thermal and cooling loads are lower) the 35% minimum power duty of the biomass furnace in the tracking configuration fixes the minimum thermal power output to 455 kW. Instead the upper limit of 1100 kW is higher than the maximum thermal load power of 980 kW (corresponding to the hotel thermal summer behaviour during daytime hours when the cooling load request is higher) in order to extend the data check.

In the electric power case, Figure 59 b, the HTF flowrate is varied in the range 200-31˙000 kg/h with the upper flow rate limit fixed by the imposed maximum diathermic oil flowrate in the system itself. The electric power limits are 55 kW and 150 kW. The lower and upper limits

in the electric case can be ascribed to the same observations done for the thermal one.

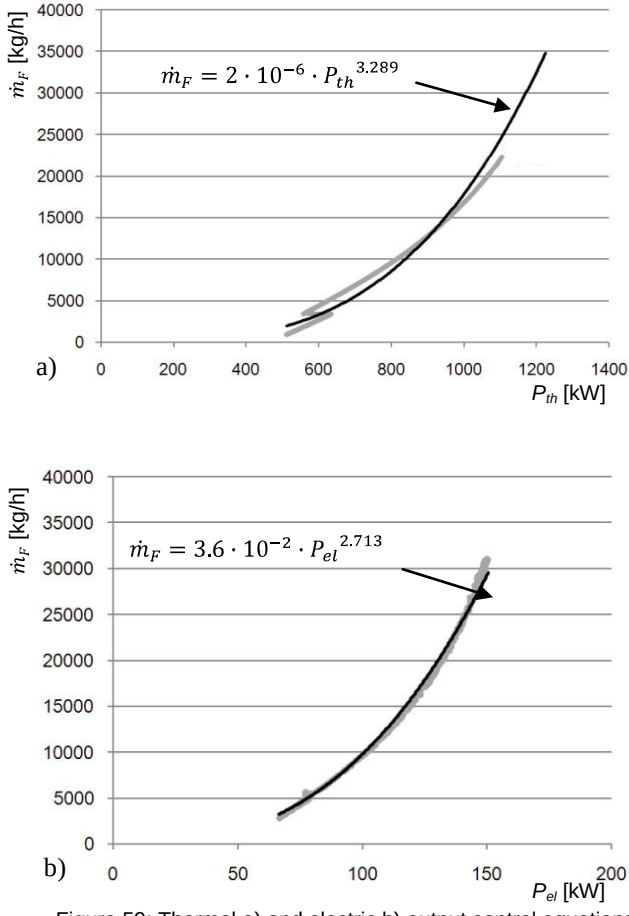

Figure 59: Thermal a) and electric b) output control equations.

Focusing on the thermal case, Figure 59 a, the trend line (black line) is lightly shifted from the distribution of the data (grey line). This means that, in this case, for thermal power loads higher than 900 kW the correspondent flowrate will be higher than the effective need, leading to an energy surplus. *Vice versa*, in most of the cases with thermal power load lower than 900 kW the corresponding flowrate will be lower than the need, leading to energy deficits. Similar findings could be drawn by

looking at the electric load tracking (Figure 59 b) but of reduced magnitude and with an opposite behaviour.

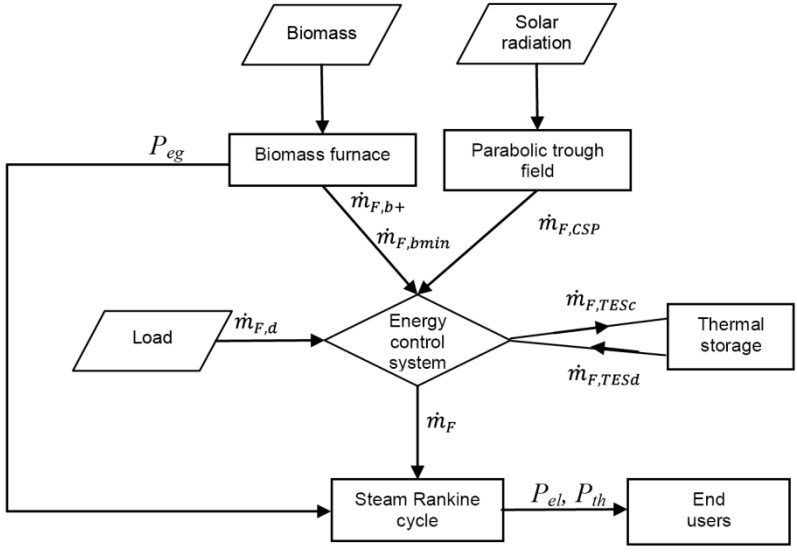

Figure 60: Tracking configuration control system flow diagram.

The control logic was described by the flow diagram in Figure 60. Notably this implementation was motivated by the goal of monitoring the requested HTF flow rate target ($\dot{m}_{F,d}$) with the actual power demand according to the adopted load tracking law. Hence, the HTF flow rate target tracks the load evolution following hierarchical control strategy in which the solar section has the energy delivery priority. In particular, the control acquires the load data ($\dot{m}_{F,d}$) and compares the HTF flow rate target with the actual HTF flow rate achievable from the solar field (flow rate $\dot{m}_{F,b+}$) and the minimum biomass furnace rate ($\dot{m}_{F,bmin}$) giving rise to three possible situations:

- direct CSP contribution surplus, the exceeding HTF flow rate will be sent to the thermal energy storage;
- direct CSP contribution deficit, the missing heat flux will be first requested to the TES (flow rate $\dot{m}_{F,TESd}$); and

- in case of insufficient flux from the solar section and minimum biomass contributions, an additional heat flux is requested to the biomass furnace (flow rate $\dot{m}_{F,b+}$).

4.1.3 Desalt configuration

In the desalt configuration the seawater distillation system is used as the heat source at the Rankine Cycle.

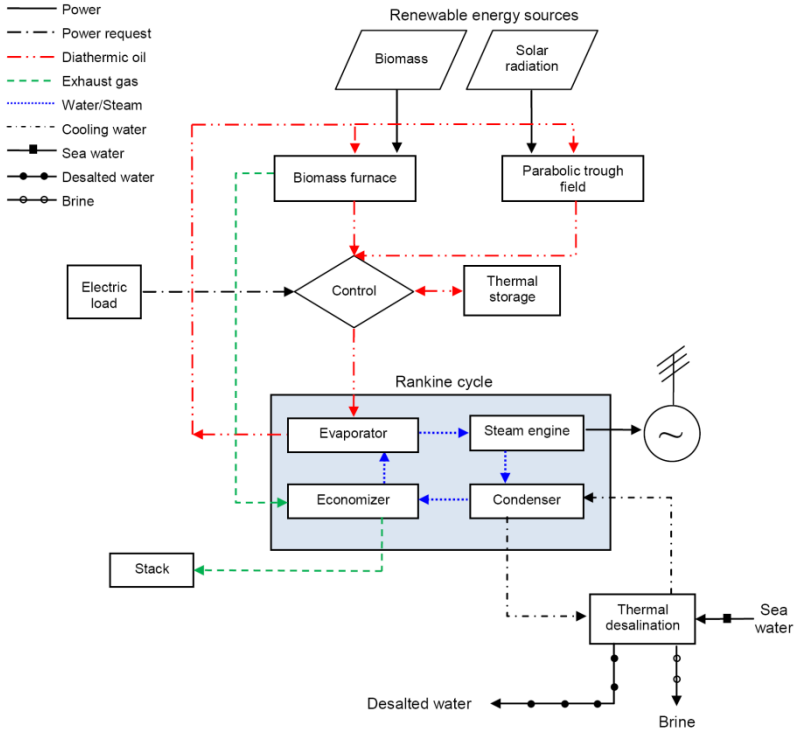

Figure 61: Desalt configuration plant flow chart.

Figure 61 and Figure 62 show respectively the desalt configuration plant flow chart and control logic flow diagram. In particular the electric load tracking is applied, in order to reserve the thermal energy for the desalination process. Moreover, in order to produce as much water as possible reducing thermal energy dumps, the desalting system is

composed of several small capacity units with a connection–disconnection strategy to match the variable energy supply. The desalination control system compares the available thermal power to the thermal power request for a single distillation unit to be on duty and determines the number of units to be turned on. Obviously the power datum and the number of on-duty units are strictly related to the amount of generated fresh water.

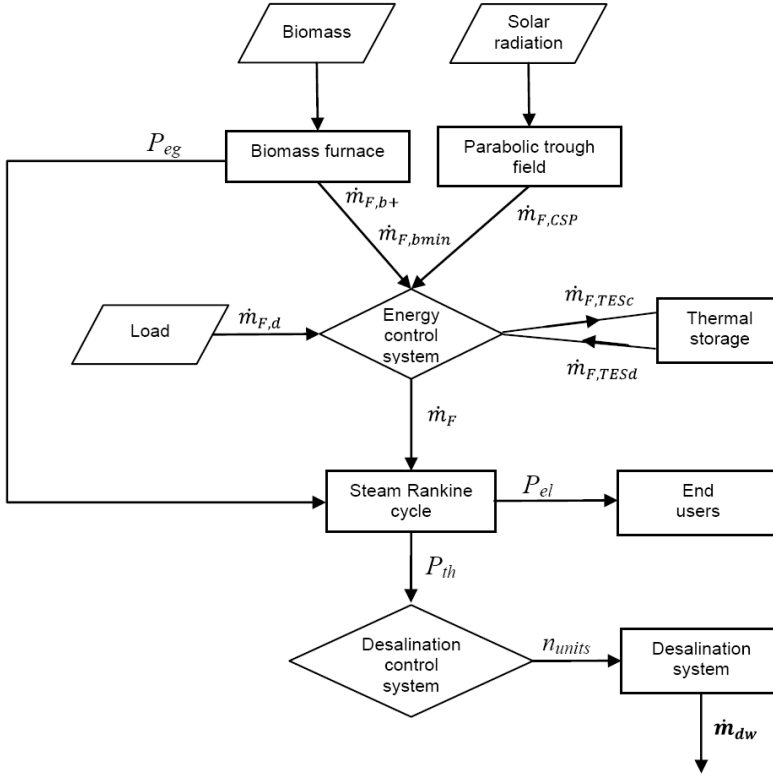

Figure 62: Desalt configuration control system flow diagram.

4.2 Investigation methodology

The will to deeply analyze a RES-based power plant behaviour entails the need to taking in account the sudden power intensity variations of the renewable source itself. For this reason, global energy data are insufficient, especially when trying to match load which has a different variation occurrence. In this scenario annual, monthly and daily data are inadequate and the minimum acceptable time step is the hourly one. Moreover the best situation is represented by the possibility to perform the hourly analysis on an entire year, that is $8 \cdot 760$ hours. As evident, it will take a long time to make all the calculations without the assistance of a software which can solve all the plant system equations in less time. In the present study the TRNSYS software is used.

TRNSYS is a TRaNsient SYstems Simulation program with a modular structure. It recognizes a system description language in which the user specifies the components that constitute the system and the manner in which they are connected. The TRNSYS library includes many of the components commonly found in thermal and electrical energy systems, as well as component routines to handle input of weather data or other time-dependent forcing functions and output of simulation results. The modular nature of TRNSYS gives the program tremendous flexibility, and facilitates the addition to the program of mathematical models not included in the standard TRNSYS library. TRNSYS is well suited to detailed analyses of any system whose behaviour is dependent on the passage of time. TRNSYS has become reference software for researchers and engineers around the world. Main applications include: solar systems (solar thermal and photovoltaic systems), low energy buildings and HVAC systems, renewable energy systems, cogeneration, fuel cells [106].

Few studies have appeared to date in the open literature, that propose the use of TRNSYS-framed models for complex energy systems. Some of the exceptions deal with studies on RES penetration in small-islands stand alone power systems [107], [20], SEGS-like CSP simulation [108], the analysis of storage systems behaviour for solar trough plants [109] and the investigation of DSG systems [110].

For the present work the TRNSYS 15 version environment [111] is used with the standard library and the Solar Thermal Energy Components (STEC) library [94]. In particular, the employed standard and in-house components are listed in Table 31. The working parameters for each type are displayed in Appendix B. Concerning the in-house made types, the subroutines are specified in Appendix A.

The simulation are made adopting a time-step of 1 hour. In order to analyze fully periodic behaviour, the simulations have been ran for two years, but only the second year data have been analyzed. The data analyzed and shown refer to a year with starting at 1.00 a.m. of January 1st and lasting on December 31th at 12.00 p.m.

Table 31: List of the TRNSYS types employed.

Standard TRNSYS types	
Type 9	Free formatted files data reader
Type 11d	Flow mixer
Type 11f	Flow diverter
Type 16	Solar Radiation Processor
Type 25	Output data printer
Type 89	Typical Meteorological Year (TMY) data reader
Type 115	Economizer for water/steam heated by one phase fluid
Type 116	Steam evaporator
Type 183	Condenser
Type 191	Converter from representation p,t,x to h,p for water steam (Steam properties)
Type 192	Conversion of water steam properties from h,p to t,x; (Steam properties 2)
Type 230	Concrete thermal storage for HTF(TES)
Type 231	Charge-discharge controller for concrete thermal storage system
Type 296	Parabolic Trough Field Model
In-house made TRNSYS types	
	Biomass furnace model
	Biomass furnace control
	Reciprocating steam engine model
	HTF flow request calculator

4.2.1 Developed types

4.2.1.1 Biomass furnace type

The created biomass furnace type has the aim to furnish the desired outlet temperature by modulating its generator rating power. Basically it calculates the oil and exhaust gas outlet flowrate and indicates the quantity of generated heat.

Obviously, the difference among the constant power output and the tracking configurations is in the HTF desired flowrate, which is constant in the first case and variable in the second one.

Table 33: Biomass furnace control type parameters, inputs and outputs.

Parameters		
Furnace minimum duty rate	γ_{SET}	
Inputs		
Solar HTF flowrate	$\dot{m}_{HTF,sol}$	kg/h
Desired HTF flowrate	$\dot{m}_{HTF}$	kg/h
Outputs		
Furnace duty rate	$\gamma(t)$	

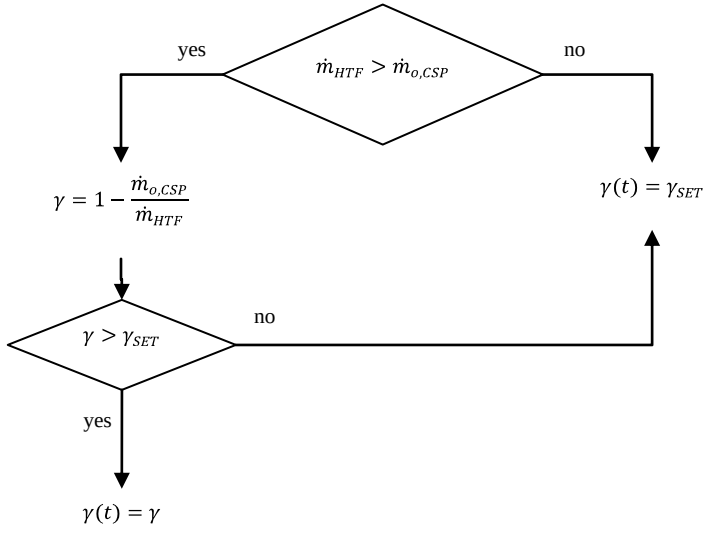

Figure 64: Biomass furnace control type flowchart.

4.2.1.3 Reciprocating steam engine type

The general type characteristics of the reciprocating steam engine are shown in Table 34. Figure 66 shows the steam engine type flowchart.

In particular, when the effect value (*ef*) is equal to zero, the engine mode is single effect; otherwise the mode is double effect. The following conditions, checking for the steam flowrate and the pressure admission

The parameters, inputs and outputs of the type are showed in Table 32, while the flowchart is showed in Figure 63.

The relations governing the furnace operation have been previously showed in §3.5. Furthermore, the oil input and output specific heat values ($c_{p\_o,in}$, $c_{p\text{-}o,out}$) are determined by a temperature dependent relation deduced by the diathermic oil properties found in [92] and shown in §3.3.2.

Table 32: Biomass furnace type parameters, inputs and outputs.

Parameters		
Furnace heat input	P_{nom}	kW
Generator rating	P_{gen}	kW
Desired oil output temperature	$T_{o,out}$	°C
Air excess	e	%
Biomass carbon rate	C	%
Biomass hydrogen rate	H	%
Biomass oxygen rate	O	%
Biomass sulphur rate	S	%
Biomass low heating value	H_i	kJ/kg.K
Furnace minimum duty rate	γ_{SET}	%
Inputs		
Oil input temperature	T_{o_in}	°C
Furnace needed duty rate	$\gamma(t)$	%
Outputs		
Air mass	Am	kg/kg
Gas mass	Gm	kg/kg
Exhaust gas flowrate	$\dot{m}_{eg}$	Kg/h
Biomass flowrate	$\dot{m}_b$	Kg/h
Oil outlet temperature	$T_{o,out}$	°C
Oil outlet flowrate	$\dot{m}_o$	Kg/h
Generated heat	Q_{out}	kW

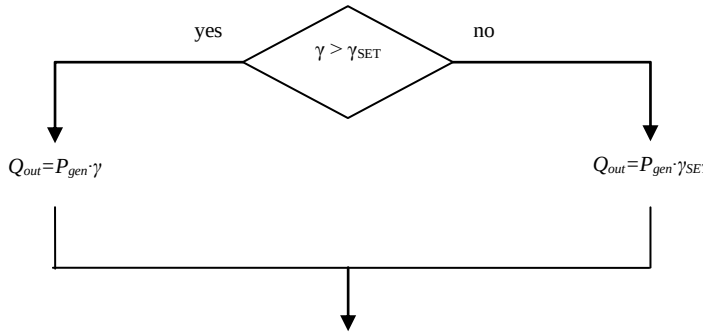

$$c_{p\_io} = 0.0028 \cdot T_{o,in} + 1.5162$$

$$c_{p\_oo} = 0.0028 \cdot T_{o,out} + 1.5162$$

$$c_p = (c_{p\text{-}o,in} + c_{p\text{-}o,oou})/2$$

$$\Delta T = T_{o,out} - T_{o,in}$$

$$\dot{m}_o = Q_{out} \cdot 3600/c_p \cdot \Delta T$$

$$Atm = 0.11484 \cdot C + 0{,}34204 \cdot H + 0{,}4302 \cdot S - 0{,}0431 \cdot O$$

$$n = e/100 + 1$$

$$Am = Atm \cdot n$$

$$Gm = Am + 1$$

$$\dot{m}_{eg} = \frac{\dot{m}_w \cdot c_{p,w} \cdot \Delta T_{w,eco}/0{,}85}{c_{p,eg} \cdot \Delta T_{eg,eco}}$$

$$\dot{m}_b = \dot{m}_{eg} \cdot G_m$$

Figure 63: Biomass furnace type flow chart.

4.2.1.2 Biomass furnace control

The biomass furnace control is based on the matching between the desired hot thermal fluid flowrate (m_o) and the hot thermal fluid flowrate deriving from the solar section ($m_{o,CSP}$), i.e. the direct contribution of the solar field and the eventual contribution of the thermal energy storage. At this standpoint, the needed biomass furnace duty set point to reach the desired flowrate can be determined.

The biomass furnace control type parameters, inputs and outputs are summarized in Table 33; the flowchart is shown in Figure 64.

ratio ranges are based on the values deduced by the Spilling engines characteristics in Figure 67 [100]. The angular coefficients (*c*) for the two sheaves of straight lines in Figure 67 have been determined on dependency of the pressure admission ratio (*z*), given as the ratio between the input (*pa*) and output (*ps*) pressure of the steam engine (*z=pa/ps*), in order to obtain the electric power output when the steam mass flowrate is known. In particular the angular coefficient (*m*) for each line in Figure 67 has been determined. Hence each angular coefficient has been bonded to the respective pressure admission ratio, separating the single and double effect working modes, obtaining the points drawn in Figure 65. The points have been interpolated with a second degree polynomial line (grey line) obtaining the equations of the angular coefficient (*c*) of the sheaves of straight lines of Figure 66.

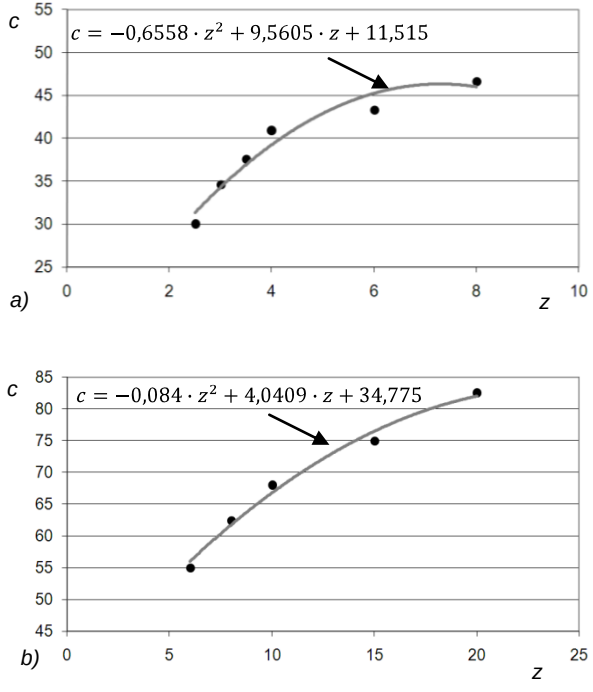

Figure 65: Angular coefficient (*c*) distribution for single a) and double b) effect engine.

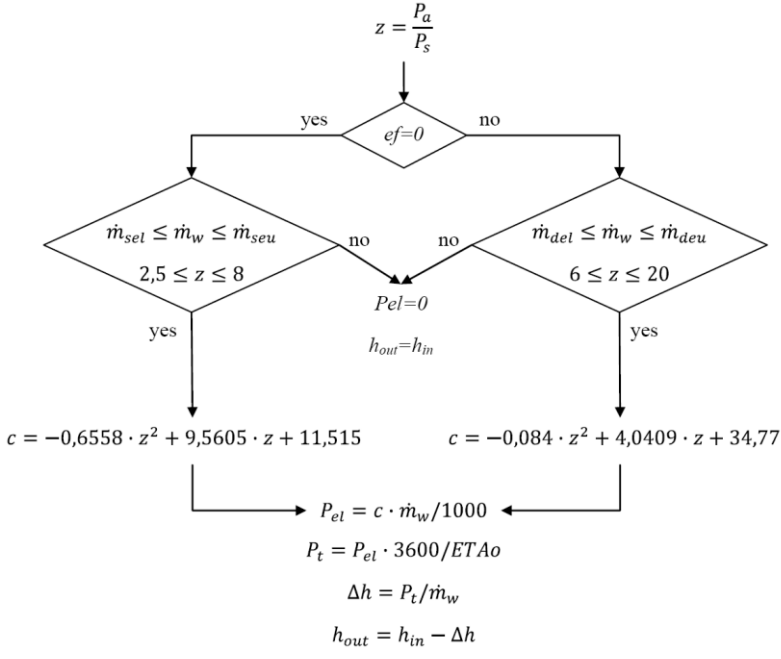

Figure 66: Steam engine type flowchart.

Table 34: Reciprocating steam engine parameters, inputs and outputs.

Parameters		
Effect mode, single or double	*ef*	
Flowrate single effect lower limit	$\dot{m}_{sel}$	kg/h
Flowrate single effect upper limit	$\dot{m}_{seu}$	kg/h
Flowrate double effect lower limit	$\dot{m}_{del}$	kg/h
Flowrate double effect upper limit	$\dot{m}_{deu}$	kg/h
Outlet pressure	P_s	bar
Steam admission degrees	*r*	-
Rotation frequency	*n*	-
Expansion chamber volume	*V*	m^3
Capacity reduction rate	*XSI*	-
Operational efficiency	*ETAo*	-
Inputs		
Steam flowrate	$\dot{m}_w$	kg/h
Admission pressure	P_a	bar
Input enthalpy	h_{in}	kJ/kg
Outputs		
Electric power output	P_{el}	kW
Admission ratio	*z*	-
Output enthalpy	h_{out}	kJ/kg

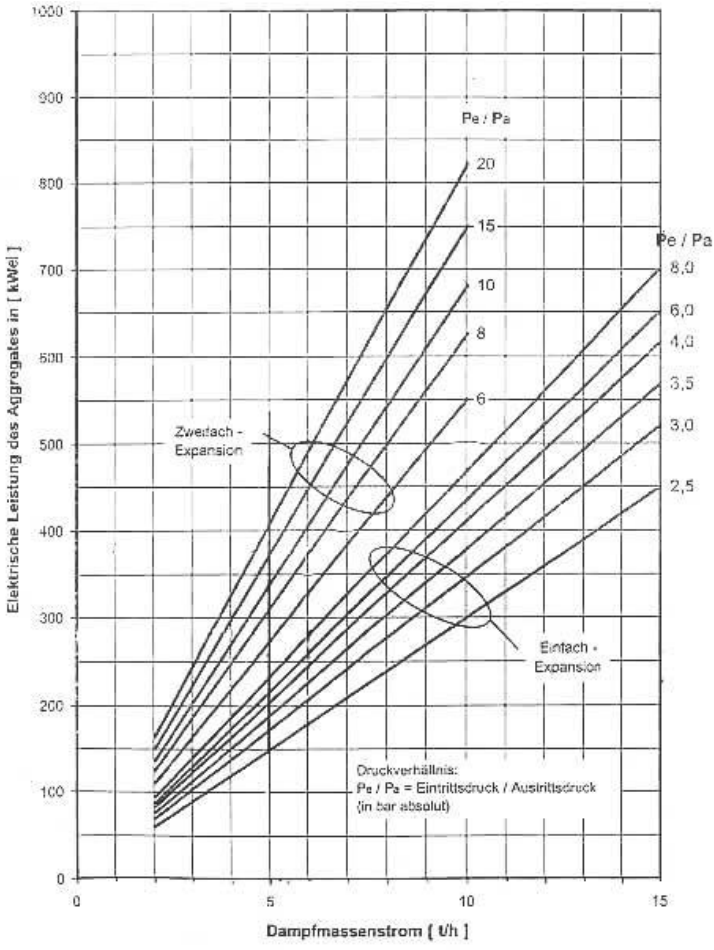

Figure 67: Approximation values curves for saturated steam engine [100].

4.2.1.4 HTF flow request calculator

The HTF flow request calculator type returns the corresponding diathermic oil flow rate needed to supply the electric or thermal load power request in the tracking configuration. It is based on the relations explained in § 4.1.2, and has only inputs and outputs, Table 35, as it exclusively executes the assigned equations, Figure 68.

Table 35: Biomass furnace control type parameters, inputs and outputs.

Parameters		
-		
Inputs		
Electric load power	P_{el}	kW
Thermal load power	P_{th}	kW
Outputs		
Needed oil flow rate for electric tracking	$\dot{m}_{o,el}(t)$	Kg/h
Needed flow rate for thermal tracking	$\dot{m}_{o,th}(t) =$	Kg/h

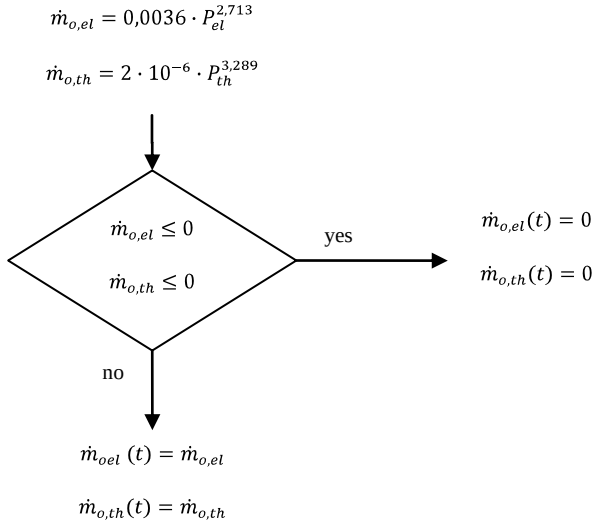

Figure 68: HTF flow request calculator type flowchart.

4.2.2 Hybrid CSP-biomass transient models

4.2.2.1 Baseline configuration

The TRNSYS model scheme for the baseline configuration is shown in

The information about the diathermic oil temperature and flow rate are then supplied from the CSP field to the CSP control, which, in function of the design oil flowrate requested at the RC settles on the oil flow rates to or from the TES and communicates to the biomass furnace control the amount of diathermic oil flow-rate deriving from the solar section.

The biomass furnace control sets the furnace duty rate needed to reach the design power of the system.

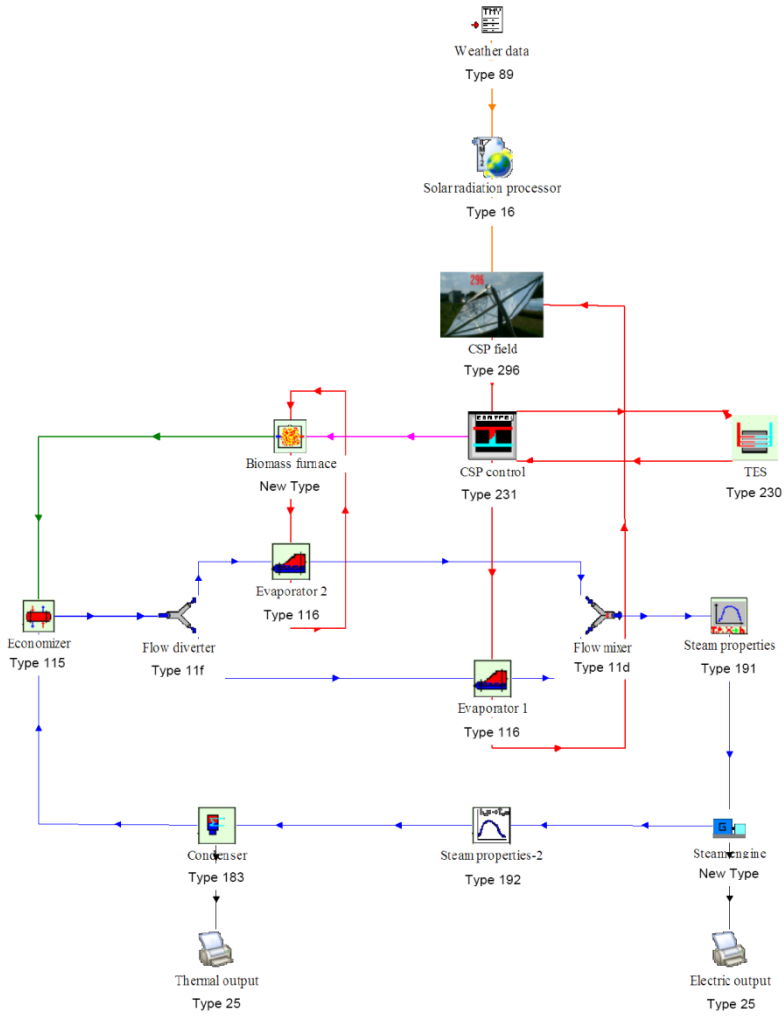

Figure 69 and, as evident, it overlaps with the scheme in Figure 56, letting identify the RES and RC subsystems. In particular, the weather data is sent to the solar radiation processor, which gives back the solar azimuth and zenith angle in function of the imposed latitude. Hence, the sun position and energy information are supplied to the CSP field.

Information about the diathermic oil temperature and flow rate are then supplied from the CSP field to the CSP control, which, in function of the design oil flowrate requested at the RC settles on the oil flow rates to or from the TES and communicates to the biomass furnace control the amount of diathermic oil flow-rate deriving from the solar section. The biomass furnace control sets the furnace duty rate needed to reach the design power of the system.

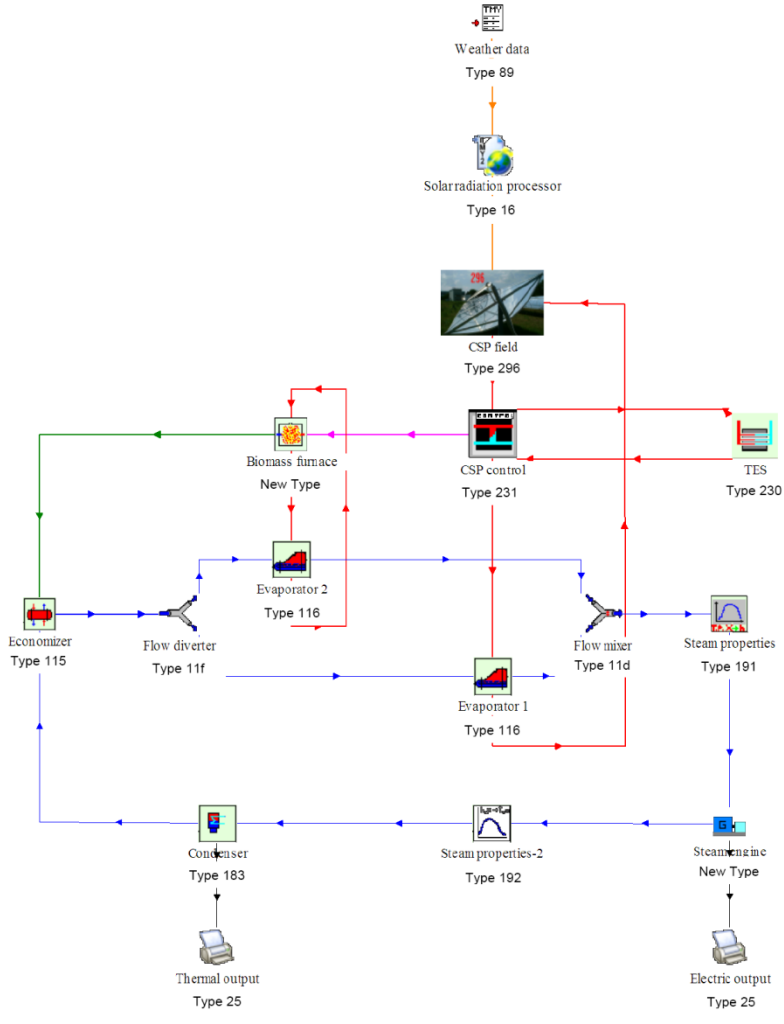

Figure 69: Baseline configuration TRNSYS model flowsheet.

When comparing Figure 69 to Figure 56, it is evident the difference in the oil circuit and its interlacement with the Rankine cycle. In fact, in the TRNSYS model the evaporator is subdivided in two different units, disconnecting the biomass and solar oil circuits. This choice helps to distinguish the solar and biomass contributions to the steam production, thus to the power output. Furthermore, the system is run under the hypothesis of the presence of an oil vessel on the return of the oil, to support the changes in the oil flow, due to the different meteorological conditions.

The biomass furnace exhaust gas is sent to the economizer, and the preheated water is supplied to the two evaporators, via a flow diverter, in function of the flowrate demanded from the evaporators themselves. Hence the produced steam from the two evaporators is mixed and sent to the steam engine by passing through two steam properties types to determine steam enthalpy from its temperature, pressure and flowrate, before and after the steam expansion. Finally the steam passes through the condenser and returns to the economizer. In conclusion the thermal end electric hourly output power results are collected in two files *via* two on-line printers.

4.2.2.2 Tracking configuration

The tracking configuration, Figure 70, differs from the baseline in the up-stream section, where starting from the electric or thermal power data, the hot thermal fluid flowrate is calculated *via* a in-house made type based on the relations described in §4.1.2. The HTF flow request calculator communicates the needed flow rate to the CSP field and to the furnace control. The furnace control receives the information about the solar flow supply from the CSP field and the TES, and consequently sets the furnace duty rate in order to face the solar deficits. From this point the tracking model perfectly overlaps the base line model.

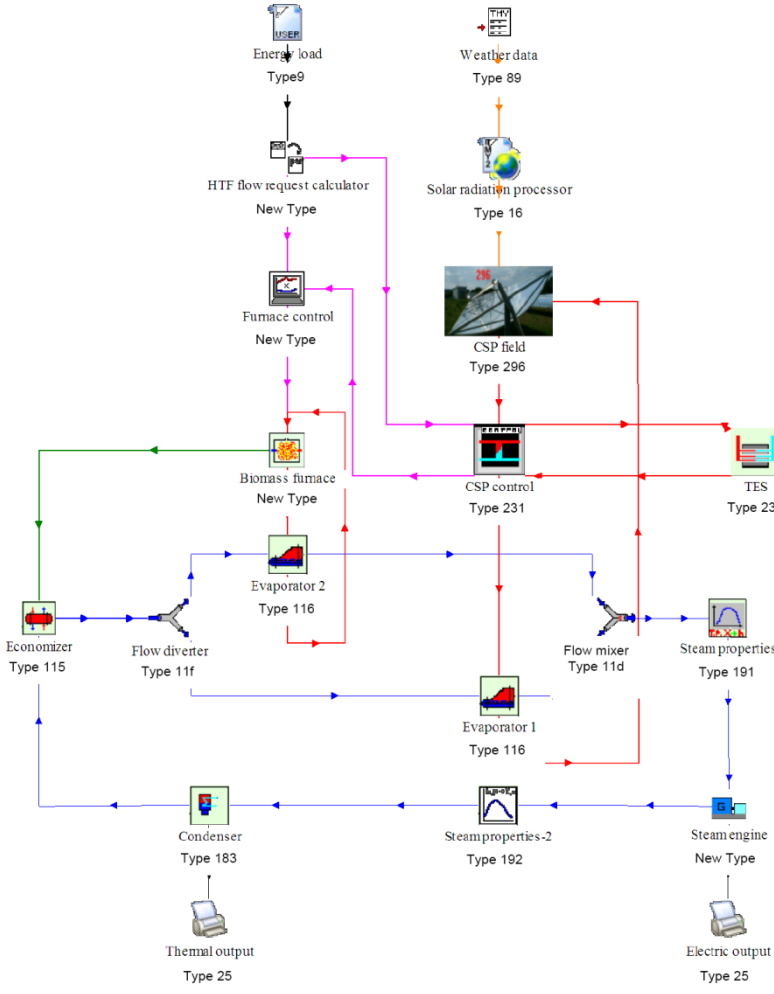

Figure 70: Load tracking configuration TRNSYS model flowsheet.

4.3 Desalt configuration

In the desalt configuration, Figure 71, a desalination system is applied to the load tracking configuration, which is in the electric tracking mode. The desalting system is positioned downstream the condenser, in place of

the thermal circuit to the end user load, in order to employ the available thermal energy to produce fresh water.

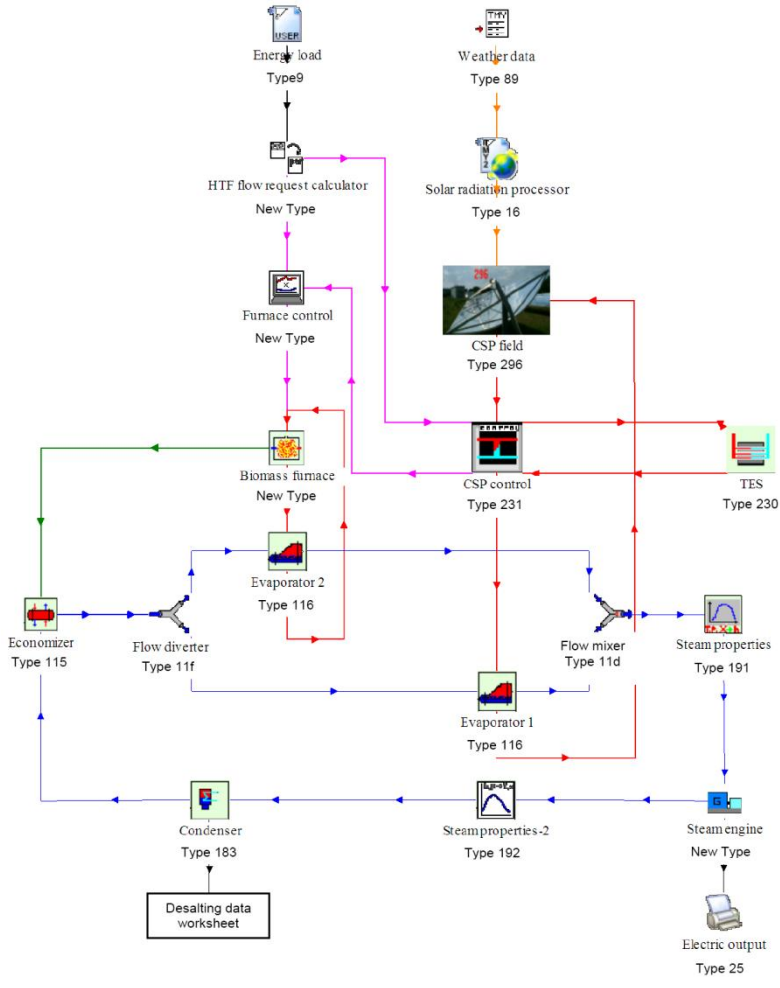

Figure 71: Desalting configuration TRNSYS model flowsheet.

As, to the best of the author knowledge, there are no thermal desalination system types modelled in TRNSYS, and in reason of the complexity in modelling a distillation device under variable work conditions, simulations have been performed by running the electric tracking configuration, recording hourly values of the available thermal energy. Hence, those data have been processed in a Microsoft Excel

worksheet. The number of running units can be determined by the ratio between the effective cooling water flowrate at the condenser and the quantity of jacket cooling water for a single on duty desalting unit. In this way the hourly number of on-duty devices has been determined and the correspondent seawater, fresh water and brine fluxes have been calculated besides the thermal and electric power consumption.

Chapter 5

Time-dependent simulations of hybrid system operations

5.1 Design data check

The first analyses of the base line configuration regard the thermodynamic data, in order to check if the results are fit together with the design data. To this Table 36 and Figure 72 provide a summary of the design parameters of the system.

The design data check is based on the performance of the system in a typical hour of the year. In particular, the reference hour is the 5009^{th} , corresponding to 5 p.m. of the 28^{th} of October, selected as the solar direct normal radiation is high enough to assure the requested diathermic oil flow rate from the solar field, i.e. DNI equal to 2˙899 kJ/h m^2.

Table 37 provides the performance data for the design check. It is worth noting that, as the results of Table 37 are outcomes of a transient simulation, also the charge and discharge data are taken into account, as the solar field is not able to work at a fixed point.

Figure 73 represents the distribution of the surplus and deficit values of the solar field hot thermal fluid flowrate with respect to the design value of 15˙948 kg/h taken as zero. The graph does not take into account the 6˙739 hours of field inactivity in which the direct flowrate from the solar troughs is void. It is evident that the exceeding values are mostly concentrated in the spring/summer period, while the deficit values are distributed all over the simulated year. Nevertheless the surplus and

deficit cases are nearly balanced, with 937 exceeding events and 1˙084 debit episodes.

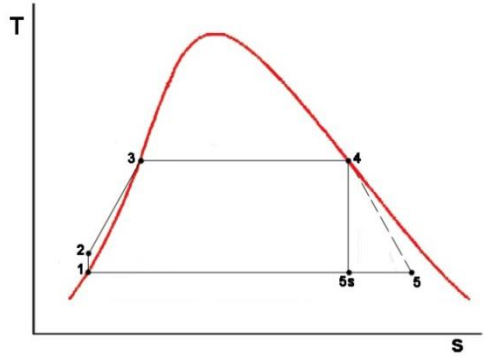

	1	2	3	4	5
T [K]	406,73	407,15	503,29	503,29	407,15
P [bar]	3,00	28,00	28,00	28,00	3,04
ρ [kg/m^3]	931,78	932,75	827,10	13,99	1,85
u [kJ/kg]	561,27	562,06	987,39	2604,02	2345,94
h [kJ/kg]	561,60	565,06	990,78	2804,11	2509,69
s [kJ/kg K]	1,67	1,67	2,61	6,21	6,46
x	0,0	0,0	0,0	1,0	0,9

Figure 72: Temperature-Entropy diagram of the Rankine power cycle at reference state.

By comparing Table 36 and Table 37, it is evident that all the resulting temperatures are extremely close to the design ones with the exception for the gases output at the economizer and the diathermic oil output at the biomass related evaporator. In both cases, the reason of such behaviour is due to the overall heat transfer factor applied in the TRNSYS model. In fact, the model differs from the design just for its transient feature, thus to obtain an optimum result for different duty states the overall heat transfer factor value is changed with respect to the design one, as already shown in §4.2.2.1. In particular, in the economizer case the output temperature of the gases is about 137°C higher than the expected value, while the diathermic oil outlet temperature at furnace evaporator is about 10 °C smaller than the design one.

	Solar field	Biomass furnace	Economizer	Evaporator 1	Evaporator 2	Steam engine	Condenser
Mass flows [kg/h							
Diathermic oil	15˙948	8˙604		15˙948	8˙604		
Gases		2˙376	2˙376				
Water/steam			1˙656	1˙076	580	1˙656	1˙656
Cooling water							19˙548
Temperatures [°C]							
Diathermic oil output	300,00	300,00		240,00	240,00		
Gases output		450,83	140,00				
Water/steam output			134.00	230.14	230.14	134,00	133,5
Cooling water output							80,00
Cooling water input							50,00
Power [kW]	604,5	325,50	195.83	513,83	276,67	135,38	895,90

Table 36: Design thermodynamic and power data summary of the system.

Table 37: Thermodynamic and power data results at design duty conditions.

	CSP field	TES charge	TES disch.	Solar system supply to RC	Biomass furnace	Econ.	Evap. (solar)	Evap. (biomass)	Steam engine	Cond.
Mass flows [kg/h]										
Diathermic oil	18˙759	2˙811	0	15˙948	8˙602		15˙948	8˙602		
Gases					2˙761	2˙761				
Water/steam						2˙030	1˙320	711	2˙030	2˙030
Cooling water										31˙817
Temperatures [°C]										
Diathermic oil output	300	300		300	300		239,76	229,7		
Gases output					494,81	277,16				
Water/steam output						229,55	229,55	229,55	133,54	133,58
Cooling water output										80
Cooling water input										50
Exchanged powers [kW]	713,48	110,38	0	603,1	325,91	275,55	606,56	381,82	132,31	1˙108,29

The effects of these variations are a higher temperature to clear in the flue gas stream ending stack, while the smaller temperature of the output diathermic oil, considering the low flowrate with respect to the full duty state and the high solar oil flowrate, is negligible.

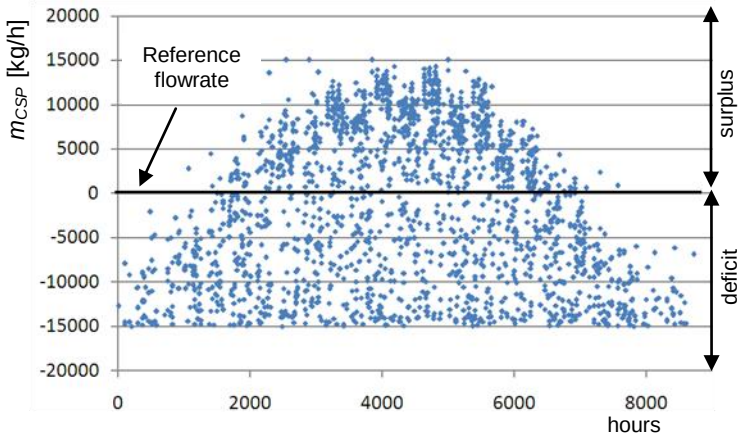

Figure 73: Solar field HTF flowrate surplus and deficit values yearly distribution.

Concerning the flow rates, the solar field is able to furnish an oil flowrate 17,6% greater than the design rate, thus the 2˙810 kg/h surplus flow is sent to the thermal energy storage, while the design rate is sent to the Rankine cycle.

As evident, the water/steam flow in the Rankine cycle is 374 kg/h higher than the design value, in reason of the different modelled overall heat transfer factor, as already explained which elevates the water/steam flow rate at low diathermic oil flow conditions. The higher water/steam flowrate at the economizer obviously rebounds on the evaporators flows, nevertheless, as expected, the solar evaporator processes the 65% of the steam and the biomass evaporator supplies the remaining 35%, with a total steam production of about 2˙030 kg/h.

Concerning the steam engine, the resulting power is the 97,73% of the one indicated in the design specification, thus less than the expected value, although the higher flow availability. This result is consistent with the Spilling engine characteristics [100] on which the TRNSYS engine type is based. In fact, referring to the graph in Figure 67 §4, the Spilling

resulting power for the obtained flowrate of 2˙030 kg/h is about 130 kW, while the power for the design flowrate of 1˙656 kg/h is 108 kW.

At last, as the condenser receives a higher flowrate than the design rate, also the exchanged power is higher than the expected one, resulting in 1˙108 kW in place of 896 kW.

5.2 Base line configuration performance

5.2.1 Power and energy results

It is worth remembering that the present configuration logic is driven to work at constant power outputs.

The first analysis concerns the renewable energy exploitation. The HTF receives a gross thermal energy input of about 4˙280 GJ/y from the solar source and 35˙900 GJ/y from the biomass source, including both the biomass energy released to the diathermic oil in the furnace and the energy released to the water/steam in the economizer.

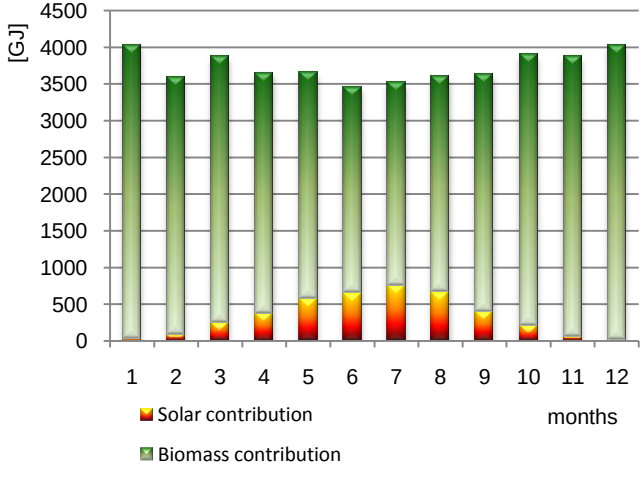

Figure 74: Available solar and biomass energy share distribution

The total amount of available energy for the power block is of 40˙000 GJ/y. The monthly available energy share from solar trough field and biomass furnace is shown in Figure 74 and Table 38. As can be seen the solar contribution is nearly absent in winter, with a minimum share of 0.5% in December, while in July it reaches a peak contribution of about 21%. The evident biomass contribution preponderance is exclusively due to the selected plant design.

Table 38: Monthly available energy, solar and biomass share.

Month	Total available energy [MJ]	Solar Share [%]	Biomass share [%]
Jan	3˙560,42	0,84	99,16
Feb	3˙175,73	2,96	97,04
Mar	3˙440,69	7,13	92,87
Apr	3˙263,08	11,71	88,29
May	3˙292,77	17,36	82,64
Jun	3˙124,59	21,00	79,00
Jul	3˙196,92	23,69	76,31
Aug	3˙248,31	20,59	79,41
Sep	3˙257,13	12,33	87,67
Oct	3˙464,63	6,07	93,93
Nov	3˙423,98	1,76	98,24
Dec	3˙556,33	0,56	99,44

Table 39: RES technologies power performance.

RES	Total energy [GJ/y]	Power setting [-]	Duty time [h/y]
Solar field	4˙278	43,43% of peak power	2˙021
Biomass furnace	35˙907	85,97% of nominal power	8˙760
		100% of nominal power	6˙315
		less than 50%of nominal power	1˙604
		35% of nominal power	1˙436

Table 39 shows the global RES technologies performance. The solar field contribution is available for 2021 h/y, i.e. 23,00% of the annual duty

period and the 43,72 of the annual hours with a DNI higher than 0 kJ/h m^2.

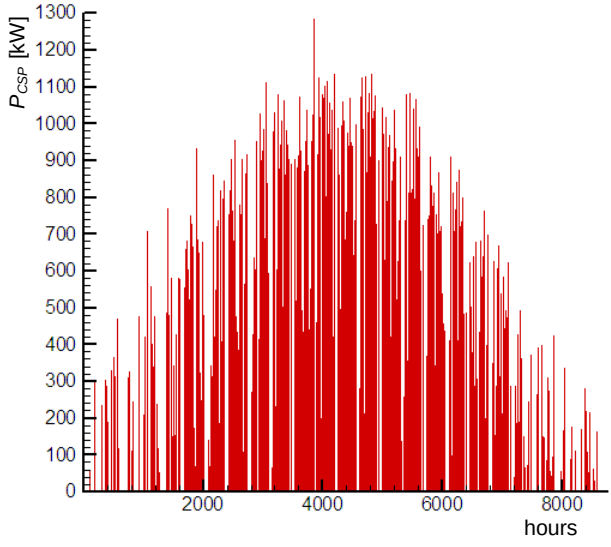

Figure 75: CSP field annual hourly power contribution.

In particular, looking at the CSP available power, Figure 75, it reaches the maximum value of 1˙283 kW on middle June. On the average, the CSP field works at about 43% of its nominal power, i.e. 1˙294 kW_p, for all its duty period. Its contribution permits the biomass furnace to be on maximum duty for only 6˙315 h/y, that is 72,01% of the annual duty period. For the 65,48% of the remaining 2˙445 duty hours the biomass furnace is at a duty lower less than 50% of its maximum generating power. In particular the furnace is allowed to be on minimum duty for 1˙436 h/y. On the average, the furnace works at about 86% of its nominal power for all its duty period, consuming 1˙962 ton/y of biomass. Finally, the solar fraction of supply, calculated as the percentage ratio between the solar system energy supply, comprising the TES contribution, and the global energy input to the Rankine cycle, is equal to 10,04%.

The previous data refer to the RES direct availability, nevertheless, for what concerns the solar contribution, it is not always entirely sent to the power conversion subsystem. In fact, reckon with the permanent biomass minimum contribution, solar power surpluses or deficits may occur with

respect to the power targets. As the biomass furnace is taken in account as a complementary source, only the solar field is assisted by the thermal energy storage unit, which shifts the excess solar energy to periods of deficit. The performance of the thermal energy storage system is first described by means of the annual hourly power charge-discharge cycle, shown in Figure 76.

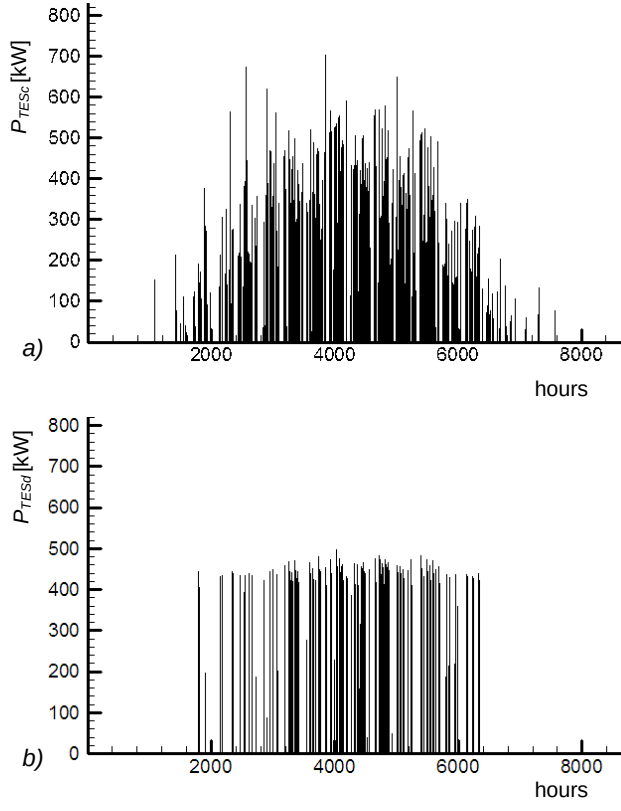

Figure 76. TES annual performance, a) charge cycle (P_{TESc}) and b) discharge cycle (P_{TESd}).

As illustrated in Figure 76a, the charge period is concentrated in the period of the year with a solar DNI above the threshold value of 14,4 MJ/m^2 d. The overall stored energy surplus from the CSP field is 1˙162,45 GJ which is charged in 917 h. A remarkable time shifting in the

discharge of thermal energy to the HTF is also evident, Figure 76b, confirming the effectiveness of TES in supporting CHP plant operation. The discharge cycle returns 890,42 GJ in 498 hours.

Figure 77 shows the hourly performance of the stored energy during the reference year. As the system is calibrated in order to use almost the whole available solar energy to obtain a high electric and thermal power output, there remains not much solar energy to completely fill the storage and maintain it full. Furthermore, it is evident again that the storage is on duty mainly in the central part of the year, during the summer period, with sudden alternation of charge and discharge duty cycles.

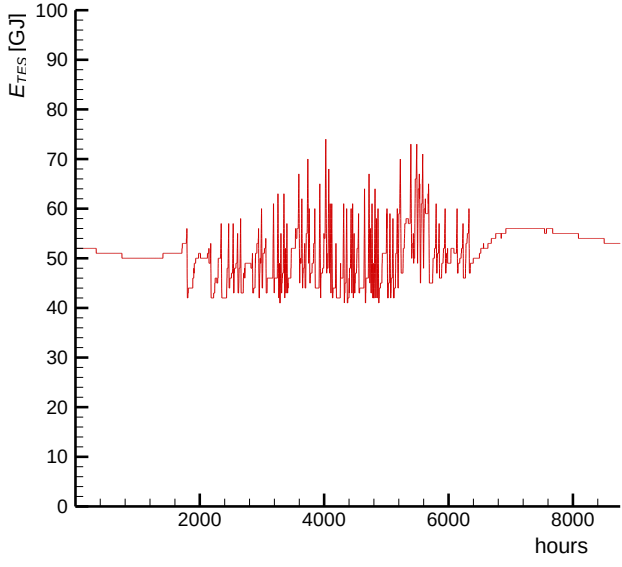

Figure 77: Hourly energy storage performance during the reference year.

When looking at the TES temperatures distribution, Figure 78, is evident that the storage never reaches the maximum temperature of 300 °C at the top of the concrete, due to the continuous discharge cycles that soak up the previously stored temperature. Furthermore, the middle and bottom temperature are almost identical, with a mean value of about 255 °C. This temperature difference is useful for the storage to be discharged more frequently.

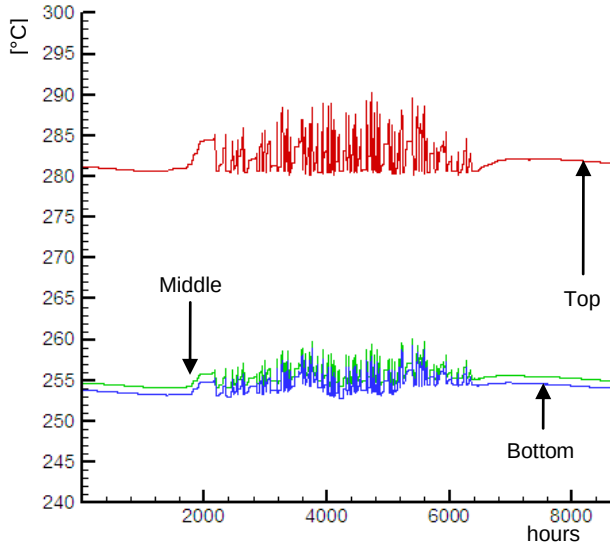

Figure 78: Storage concrete top, middle and bottom node temperature.

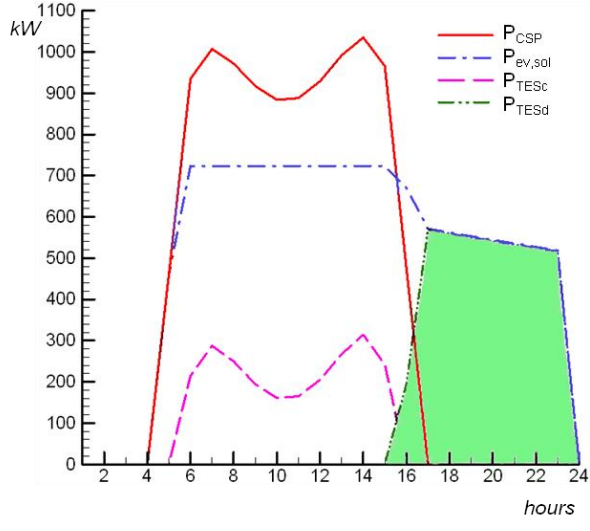

Figure 79. Storage charge-discharge behaviour on typical summer day time

In order to provide additional hints about the storage performance, Figure 79 shows the charge-discharge transient behaviour on a typical summer day-time, i.e. 5 August. When the power from the CSP (P_{CSP}) attains the design power input to the evaporator ($P_{ev,sol}$), the surplus heat (P_{TESc})is stored during a charging sub-cycle that lasts about 10 hours. When the DNI decrease, the TES discharge cycle is switched on. The cycle takes place over a time interval of 8 hours, beginning at 3 p.m., when the DNI undergoes the value of 3˙000 kJ/m^2. The behaviour of the power input from TES (P_{TESd}) is shown in Figure 79 by the green area. It is remarkable that the TES is able to establish a buffer of the solar thermal input. It is also worth noting that P_{TESd} doesn't reach the $P_{ev,sol}$ value, because the minimum HTF output temperature allowed from the concrete storage is 280 °C instead of 300 °C as required by the solar field.

Table 40. Baseline configuration annual performance data summary.

RES system	Solar field energy [GJ/y]	4˙277,53
	Effective solar energy supply [GJ/y]	4˙005,50
	Biomass supplied energy [GJ/y]	35˙906,69
	Solar fraction [%]	10,04
	Biomass consumption [ton/y]	1˙962
	Global effective energy input E_g [GJ/y]	39˙912,16
	Plant electric energy output E_{el} [GJ/y]	3˙654,22
	Plant thermal energy supply E_{th}[GJ/y]	30˙608,36
RC system	Net electric efficiency = E_{el}/E_g [%]	9,16 %
	Net thermal efficiency = Eth/Eg [%]	76,69 %
	Electric index = E_{el}/E_{th} [-]	11,94 %
	Primary energy ratio= $(E_{el}/\eta_{el}+E_{th}/\eta_{th})/E_g$ [-][8]	1,20

For what concerns the power block, the Rankine cycle system provides 15˙574,75 ton/y of saturated steam, at 230 °C and 2˙800 kPa. The steam is produced by the contribution of the exhaust gas in the economizer and the solar and biomass HTF in the evaporator. The reciprocating steam engine returns 3˙654,22 GJ/y of electric energy, with the available electric power ranging from 108,4 kW to 118,4 kW. Despite the constant power output target, the light power variations are related

[8] For the primary energy ratio evaluation, the values for the reference electric and thermal efficiencies are η_{el} = 0.38 and η_{th} = 0.8

differences in the steam characteristics caused by mall variations of the oil's temperature and flowrate.

At the RC condenser, which is operated at 134 °C and 300 kPa, an overall thermal energy of 30˙608,36 GJ/y is recovered which is able to produce 244˙085,58 ton/y of hot water at 80 °C available to district heating.

The standard CHP efficiency indices computed on the investigated daily period are compared in Table 40. As expected, in view of the power technology and the RC limits, the net electric efficiency stays about 9% and the net thermal efficiency is of 76,69%. The system electric index is 11,94%. Furthermore, the value of 1,20 for the primary energy ratio, which indicates whether a cogeneration system allows a primary energy saving or not with respect to a conventional power plant, demonstrates that the presented solar-biomass Rankine cycle systems, in this configuration, allow the saving of a small quantity of conventional primary energy sources.

5.2.2 Base-line power plant performance assessment

In order to validate the proposed solar-biomass powered CHP plant, its annual performance are compared respectively with those of solar-powered and biomass-powered plants. The comparison criterion has been based on the requirement of identical power outputs for the three different systems. Under this working hypothesis the ensuing modifications to the solar-powered scheme have been considered. First, the solar field is to be extended by a factor 8,5:1, corresponding to a parabolic trough field of 22˙000 m^2. Furthermore, it is worth noting that in the solar-alone plant, due to the biomass furnace absence, the economizer is no more fed by the exhaust gases, but directly by the evaporator HTF flow output, leading to lower oil input temperatures in the solar field.

For the biomass-powered plant, i) the furnace size of the biomass-powered plant is kept constant and rated at 95% of its maximum power, moreover, according to the changeless duty condition, ii) the TES is not used.

The energy performance of the CHP schemes under exam are summarised in Table 41, in terms of power output to the users and inputs from the renewable energy sources. The only remarkable difference is the evidence of a reduction of 11,1% of the biomass consumption in the solar-biomass powered plant.

Table 41. Combined CHP, solar-alone and biomass-alone plants performance comparison

Plant	E_{el} [GJ/y]	E_{th} [GJ/y]	Bc [ton/y]
solar-biomass CHP plant	3˙654,22	30˙608,36	1˙962
solar-alone plant	3˙628,16	30˙517,29	-
biomass-alone plant	3˙656,00	30˙623,92	2˙207

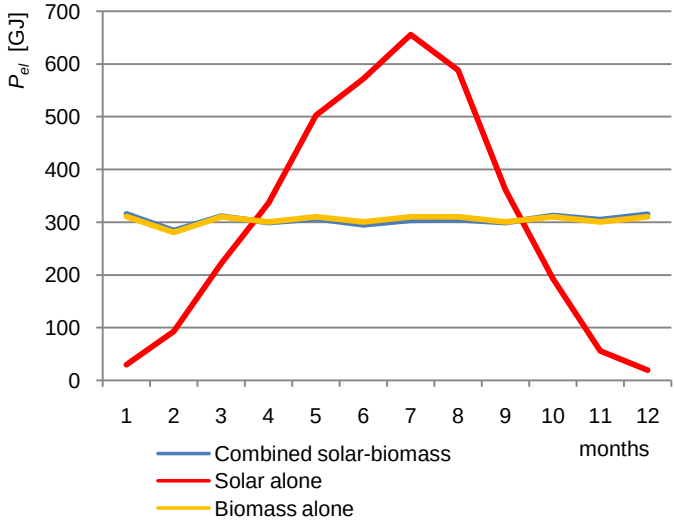

Figure 80: Electric power output (P_{el}) comparison.

Figure 80 compares the electric energy output monthly behaviour. The combined CHP and the biomass-alone plants feature coincident trends with a mean value of about 304 GJ/month, matching with the established operating conditions. When looking at the solar-alone plant performance, even if the annual energy target is gained and, although the TES, the lack of any support from RES switching leads to seasonal dependent energy output ranging from a peak production of about 660 GJ in July to a minimum value of about 19 GJ in December. Similar oscillations are registered at the condenser in terms of thermal energy output from the RC.

The underlined differences demonstrate that the combination of RES power inputs in the proposed combined CHP plant effectively permits to control the unpredictability of solar radiation exploiting a fossil-fuel-free energy generating process more network-friendly.

5.3 Load tracking configurations

5.3.1 Energy performance

The overall performance for the two selected end users under the electric and thermal tracking hypothesis are shown in Table 42. As can be seen, the available energy from the solar field is the same in each configuration, nevertheless, due to the different energy request and the presence of the thermal energy storage, it is useful to look at the effective solar energy supply, which is a balance between the available solar field energy, and the charged-discharged rates. It can be seen that the effective solar energy supply values are very similar in each case, and are in the 4˙030-4˙170 GJ/y range. It is worth noting that in some cases the effective solar energy supply exceeds the solar field energy. This result is due to the TES capacity to shift the energy distribution in a full performance situation, in this case represented by a multy-year simulation, i.e. two years hourly-step simulations. For what concerns the biomass furnace energy, it shows higher values in the electric tracking configurations and the higher biomass consumption, i.e. 1˙481 ton/y, is related to the hospital electric tracking scenario, as it is the scenario with the higher global energy input request. The solar fraction, calculated as the percentage of the effective solar energy with respect to the sum of the effective solar energy and the biomass furnace energy, varies in the 12,94-19,66 range.

Looking at the RC system performance in Table 42, the value recurrent value of 1.2 for the primary energy ratio demonstrates that the presented solar-biomass Rankine cycle systems can effectively allow the saving of conventional primary energy sources in each presented scenario.

As far as the tracking behaviour is concerned, it is worth noting that the hotel has an electric load 1,7 times greater than the hotel one and a thermal load which is 0,9 times the hotel one. Looking at the electric output, globally, with the exception of the hospital thermal tracking case, the system produces more electric energy than the need with a peak production/request ratio of 124% for the hotel eclectic tracking. Nevertheless, the global data in a RES based plant are not indicative of the effective load covering.

Table 42: Overall performance comparison.

		Hotel		Hospital	
		Electric Tracking	Thermal Tracking	Electric Tracking	Thermal Tracking
RES system	Solar energy [GJ/y]	4˙277,53	4˙277,53	4˙277,53	4˙277,53
	Effective solar energy supply [GJ/y]	4˙172,09	4˙092,72	4˙027,85	4˙092,96
	Biomass energy [GJ/y]	18˙132,39	17˙221,31	27˙103,92	16˙725,59
	Solar fraction	18,71	19,20	12,94	19,66
	Biomass consumption [ton/y]	990,84	941,06	1481,09	913,97
	Global effective energy input E_g [GJ/y]	22˙304,48	21˙314,03	31˙131,77	20˙818,55
Electric output	Plant electric energy output E_{el} [GJ/y]	2˙064,37	2˙017,10	2˙956,18	1˙931,52
	$E_{el,d}$ [GJ/y]	**1˙664,68**	1˙664,46	**2˙886,42**	2˙886,42
	$E_{el}/E_{el,d}$ [%]	**124,01**	121,19	**102,42**	66,92
	Surplus [%]	**19,80**	25,80	**5,18**	2,66
	Deficit [%]	**0,44**	8,32	**2,82**	52,09
Thermal output	Plant thermal energy supply E_{th}[GJ/y]	17˙291,93	16˙895,49	24˙761,79	16˙179,00
	$E_{th,d}$ [GJ/y]	11˙656,13	**11˙653,99**	10˙668,96	**10˙668,96**
	$E_{th}/E_{th,d}$ [%]	148,35	**144,98**	232,09	**151,65**
	Surplus [%]	40,09	**33,27**	56,91	**34,95**
	Deficit [%]	7,49	**2,26**	0,00	**0,89**
RC system	Net electric efficiency = E_{el}/E_g [%]	9,26	9,46	9,50	9,28
	Net thermal efficiency = E_{th}/E_g [%]	77,53	79,27	79,54	77,71
	Electric index = E_{el}/E_{th} [-]	11,94	11,94	11,94	11,94
	Primary energy ratio = $(E_{el}/\eta_{el}+E_{th}/\eta_{th})/E_g$ [-][9]	1,21	1,24	1,24	1,22

As a matter of fact, analyzing the hourly behaviour of the systems, there are both surplus and deficit situations. In particular looking at the electric tracking performances, the hotel case presents the lower deficit value even if in the hospital one there is a better balance between surplus and deficit. Looking at the thermal tracking performance the hotel and hospital scenarios are similar. It is worth noting that the hospital electric tracking scenario offers a completely absence of thermal supply deficits, but showing a 132% of thermal energy surplus. Considering that the electric source is easier to manage than the thermal one, as it can be sold

[9] For the primary energy ratio evaluation, the values for the reference electric and thermal efficiencies are $\eta_{el} = 0.38$ and $\eta_{th} = 0.8$.

or bought from the grid, the most suitable configuration appears to be the hotel thermal tracking one.

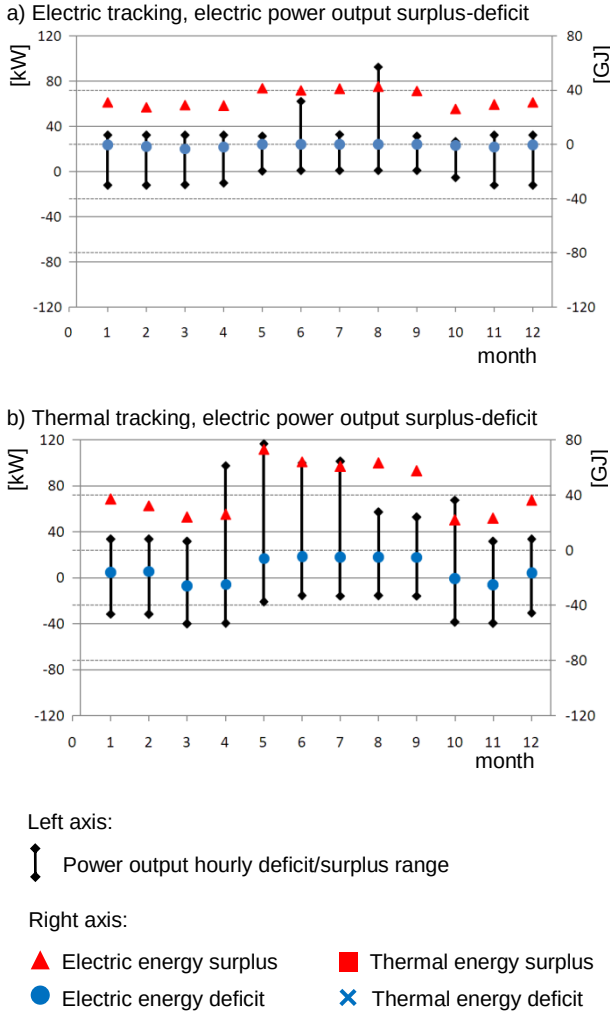

Figure 81 a) and b): Hotel electric and thermal power surplus/deficit behaviour during a one year period under electric and thermal load tracking conditions.

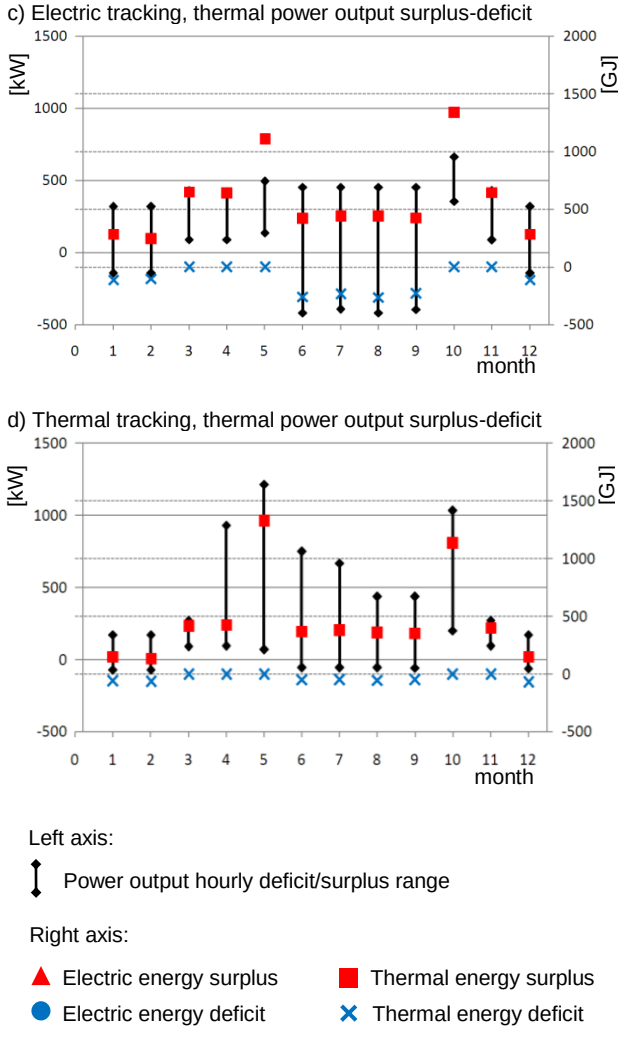

Figure 81 c) and d): Hotel electric and thermal power surplus/deficit behaviour during a one year period under electric and thermal load tracking conditions.

Figure 81 and Figure 82 show the surplus (values higher than zero) and deficits (values lower than zero) behaviour of the electric and thermal power supply for both the electric and thermal tracking scenario, respectively for the hotel and the hospital end user. The graphs, presented on a monthly basis, are based on hourly data, and show, on the left axis, the minimum and maximum difference registered in the month between

the load and the supplied power. On the right axis the cumulative surplus and deficit energy is shown for each month.

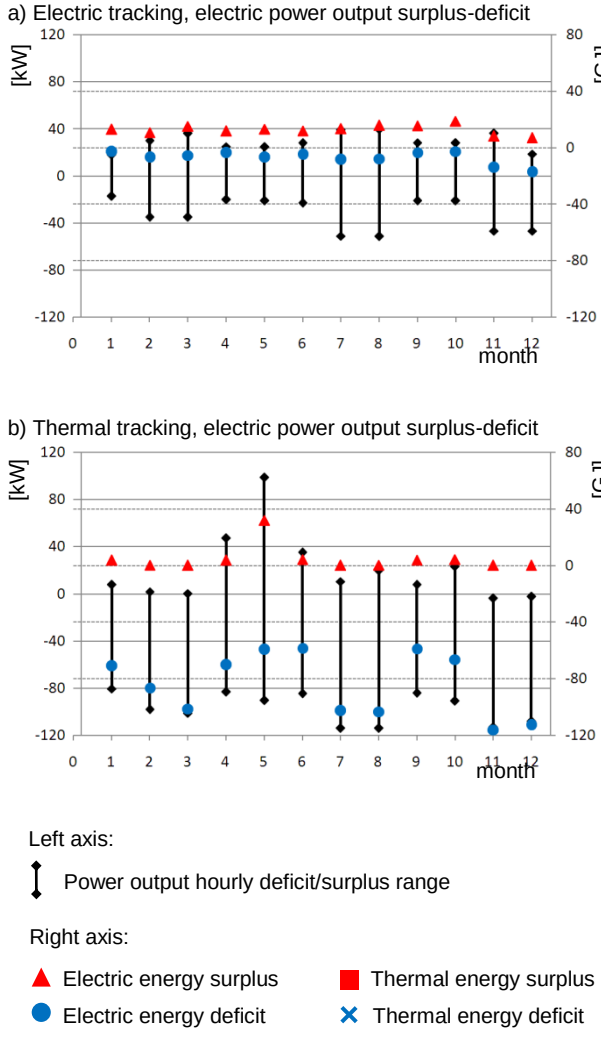

Figure 82 a) and b): Hospital electric and thermal power surplus-deficit behaviour during a one year period under electric and thermal load tracking conditions.

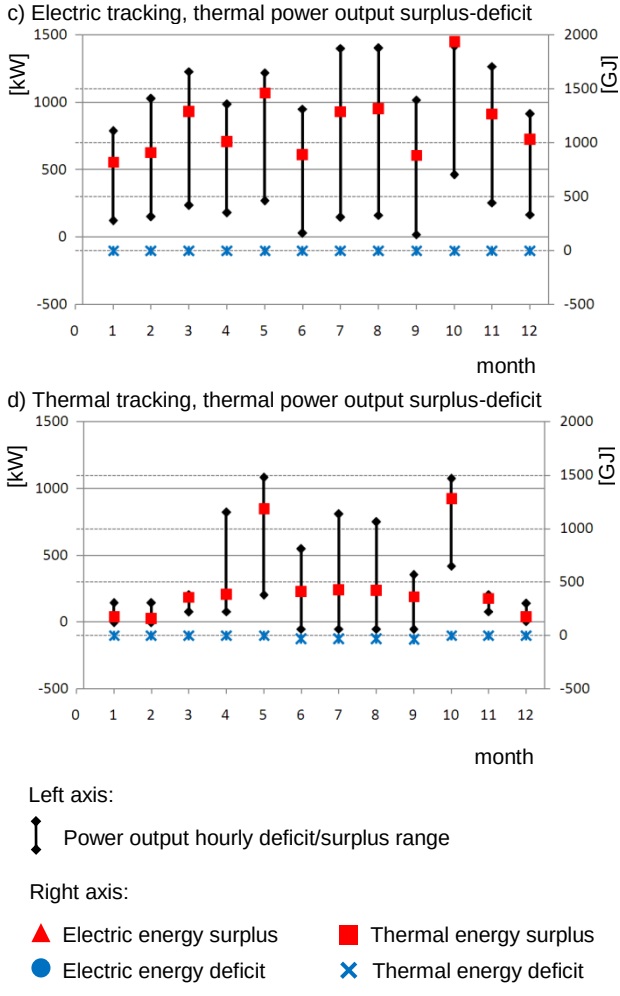

Figure 82 c) and d): Hospital electric and thermal power surplus-deficit behaviour during a one year period under electric and thermal load tracking conditions.

Concerning the hotel, Figure 81 confirms that in each case the surplus rate is higher than the deficit. Moreover, the electric output of the electric tracking configuration, Figure 81 a, shows the smaller values variation. Nevertheless, as this good result corresponds to the electric behaviour on the electric tracking configuration, the thermal behaviour is worst, with a high rate of surplus distributed all over the reference year and a deficit

peak during the summer period, as the electric energy request is not sufficiently high to let the system to produce the requested thermal energy too.

Considering the hospital surplus/deficit behaviour, Figure 82, the deficit event in the thermal supply are minimal in the thermal tracking configuration and totally absent in the electric tracking one. Nevertheless, surplus events are remarkably higher than those registered in the hotel case. When looking at the electric output, in the electric tracking configuration the surplus and deficit values are distributed all over the reference year. In the thermal tracking case the deficits are noteworthy frequent and of high value.

The deficit and surplus events have a quadruple explanation. The first one is that in half the showed cases are non tracked results, e.g. when discussing the electric tracking configuration, the thermal output does not follow any production law, but is dependent from the electric production trend, without any correlation to the thermal load. Secondly, in most of the occasions the gaps with the requested load are entailed to the used correlation among load energy and hot thermal fluid flowrate, already commented in §4.1.2, which do not perfectly fit the sensitivity analysis data, conducing to gaps between the desired output and the obtained one. Nevertheless, those gaps are not particularly remarkable. The third reason, instead, explains the high surplus peaks that occur, by observing that sometimes there are contemporarily an elevated available solar supply and full thermal energy storage. In those cases the system, which has to deliver the collected heat, sends all the hot flowrate directly to the Rankine cycle. The last reason, is that the biomass furnace is always on duty, even if on a minimum rate, supplying energy also in extremely low energy request.

The presence of instantaneous power surplus and deficits affects the load energy matching. Figure 83 and Figure 84 show, monthly, the comparison between the load energy ($P_{el,d}$, $P_{th,d}$) the total supplied energy (P_{el}, P_{th}) and the load effectively covered by the supply ($P_{el,d,c}$, $P_{th,d,c}$), respectively for the hotel and the hospital end users.

In the hotel case, it is evident how the best results are the tracked ones, i.e. the electric output for the electric tracking configuration and the thermal output for the thermal tracking configuration, with the load and effective contribution curves nearly superimposed, despite the little deficit already declared in Table 42 and Figure 81.

The global electric energy deficit in the electric tracking configuration, Figure 83 a, is of 9 GJ, whit a deficit peak of 2,9 GJ in March, and does not interest the month between May and September. The

global thermal deficit on the thermal tracking configuration, Figure 83 d, is of about 380 GJ with the peak of 68 GJ in December, and is not present in the months of March, April, May, October and November. In the non related tracking energy output cases, Figure 83 b and c, the energy supply rarely overlaps the requested load, despite the surplus output energy. For the hotel user the best tracking ode appears to be the electric one.

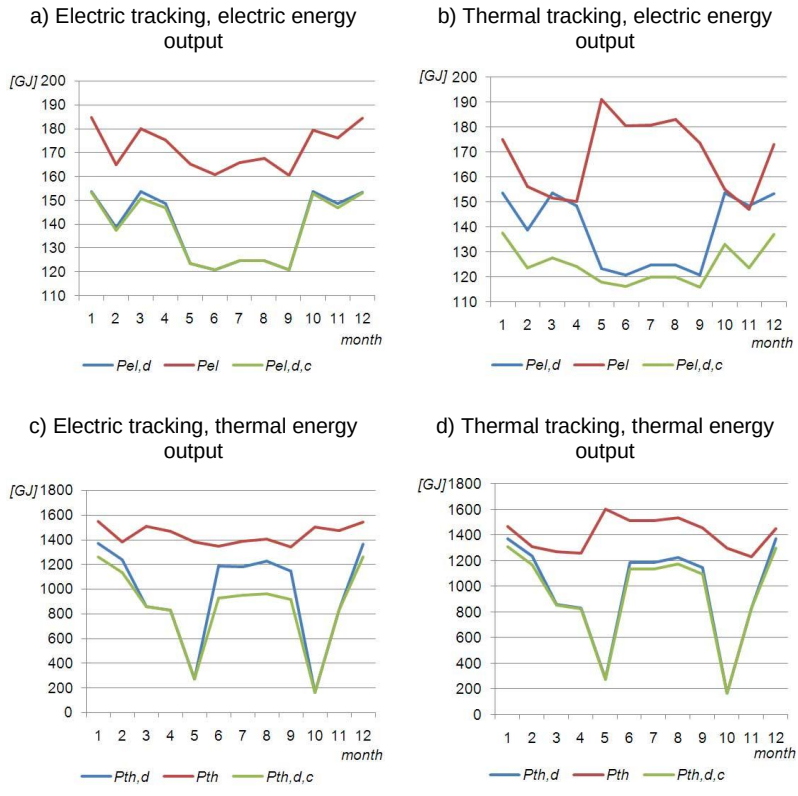

Figure 83: Monthly comparison of hotel user energy load ($P_{el,d}$ and $P_{th,d}$) with total energy supply (P_{el}, P_{th}) and effectively covered energy load ($P_{el,d,c}$ and $P_{th,d,c}$).

Looking at the hospital case, the electric output behaviour in the electric tracking configuration, Figure 84 a, in spite of its constant deficit in the effective load covering, has the best supply shape, as it strictly follows the load shape. Moreover, in this tracking configuration the thermal load, Figure 84 c, is completely satisfied, even if there is a huge

amount of surplus energy. When analyzing the thermal tracking behaviour, the thermal load, Figure 84 d, is almost fully satisfied on the contrary of the electric load case, Figure 84 b, in which neither the entire electric energy supply reaches the requested energy values.

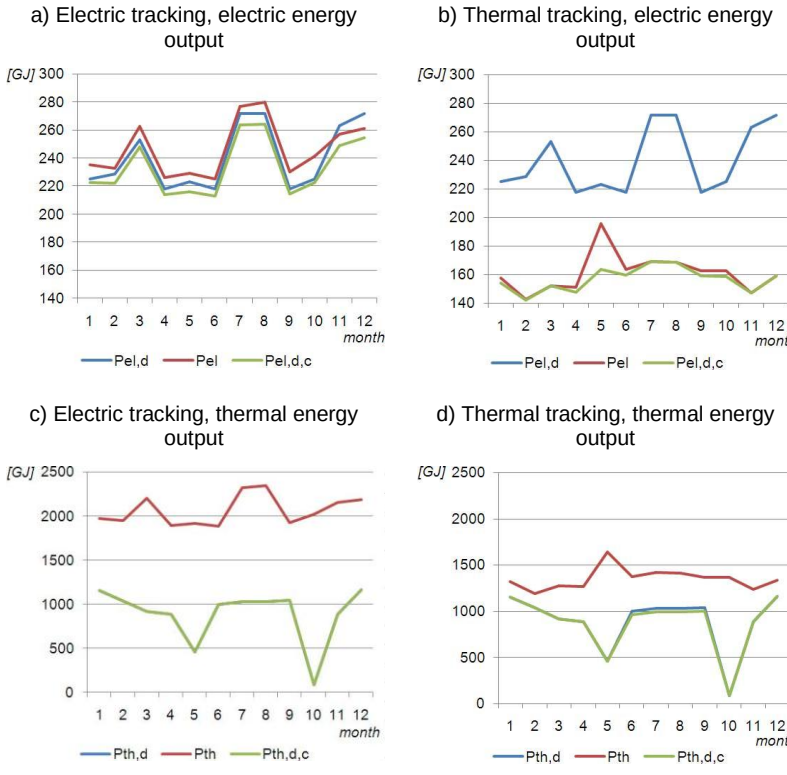

Figure 84: Monthly comparison of hospital user energy load (Pel,d and Pth,d) with total energy supply (Pel, Pth) and effectively covered energy load (Pel,d,c and Pth,d,c).

A fundamental element of the system is the thermal energy storage, which in the worst case is able to deliver about 680 GJ/y of energy, Table 43. The charge cycle duty time is always lower than the discharge cycle one, indicating that the instant charge energy rates are higher than the discharge rates. In fact, looking at the maximum power values in Table 43, those relative to the charge cycle are sensible higher than those related to the discharge cycle. The higher charge values, superior than 1000 kW,

are registered for the electric tracking configurations, as in general they require less power from the system. The maximum discharge value, about 772 kW, is registered in the hospital electric tracking configuration. It is worth remembering that the charge and discharge cycles are closely related to the requested power from the end user, thus their values depend on the residual solar power supply, despite the global available solar power.

Table 43: Charge and discharge cycles overall performance.

	End user	Hotel		Hospital	
	Tracking	Electric	Thermal	Electric	Thermal
Charge cycle	Duty time [h/y]	1824	1561	764	1530
	Charged energy [GJ/y]	1167,11	807,35	961,61	635,25
	Minimum power [kW]	0,04	0,22	5,62	0,17
	Maximum power[kW]	1109,19	768,40	1037,24	839,31
Discharge cycle	Duty time [h/y]	4633	4725	1382	6118
	Discharged energy [GJ/y]	1291,67	852,54	941,92	680,67
	Minimum power [kW]	1,19	0,05	3,06	0,18
	Maximum power[kW]	374,72	567,43	771,83	246,85

Figure 85 shows the hourly performance of the stored energy during the simulated year. It is evident that the maximum storage capacity is reached during the summer period, although there are continuous discharge-charge events. It is also evident that at the end of the year, when the solar DNI decreases, the stored energy drops down, returning to a minimum storage level of about 50 GJ. The exception to this behaviour is represented by the storage performance of the hospital electric tracking configuration, in which the system is not able to lead the storage to a complete charge due to the high power request from the load conducing to frequent high discharge powers, as demonstrated in Figure 88b.

Figure 86 shows the hourly thermal behaviour of the concrete energy storage during a one year period for each of the four tracking situations. It is evident as in the hospital electric tracking case, Figure 86 b, the TES maintains the same behaviour of the baseline configuration, with a marked temperature difference between the top, middle and bottom temperatures of the concrete. This bad storage performance is due to the high load power request, which does not leave energy for the storage, disabling it to work at proper conditions.

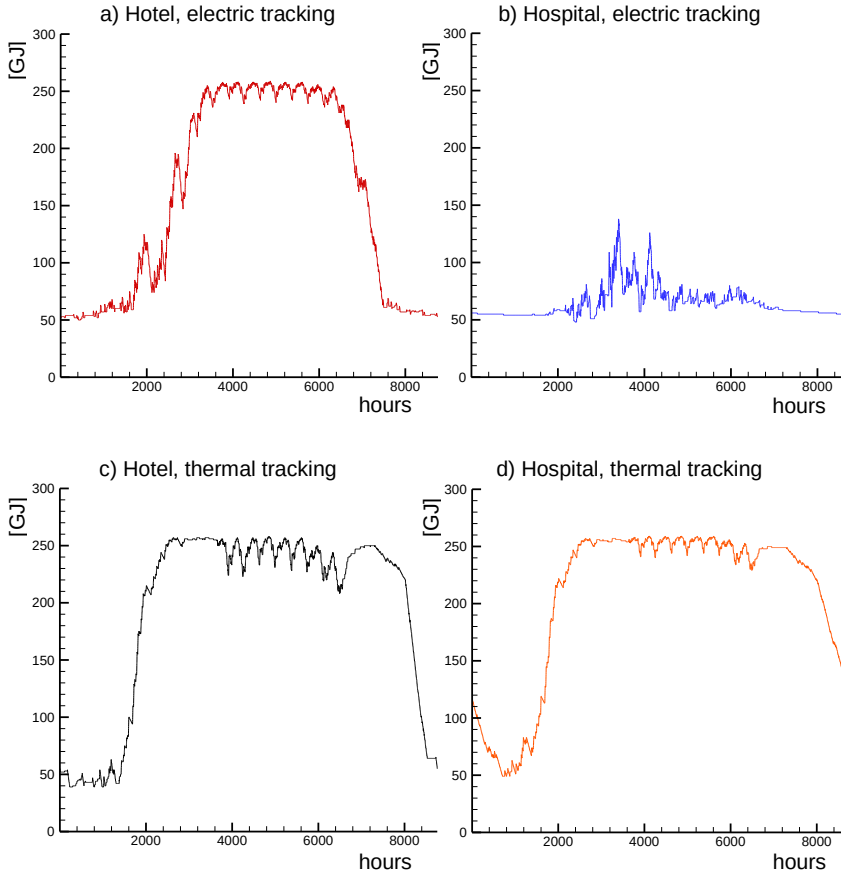

Figure 85: Hourly energy storage performance during the reference year.

Thermal tracking configurations, Figure 86 c and d, allow the TES to reach the maximum allowed temperature, i.e. 300 °C, earlier than in the electric case, and keep this high temperature for a longer time, due to the high surplus energy outputs from the system. Nevertheless, with the exception of the hospital electric tracking case, in the summer period the middle concrete is at the same temperature concrete on the top of the storage and in some cases also the bottom temperature reach values close to the maximum, entailing the TES fullness.

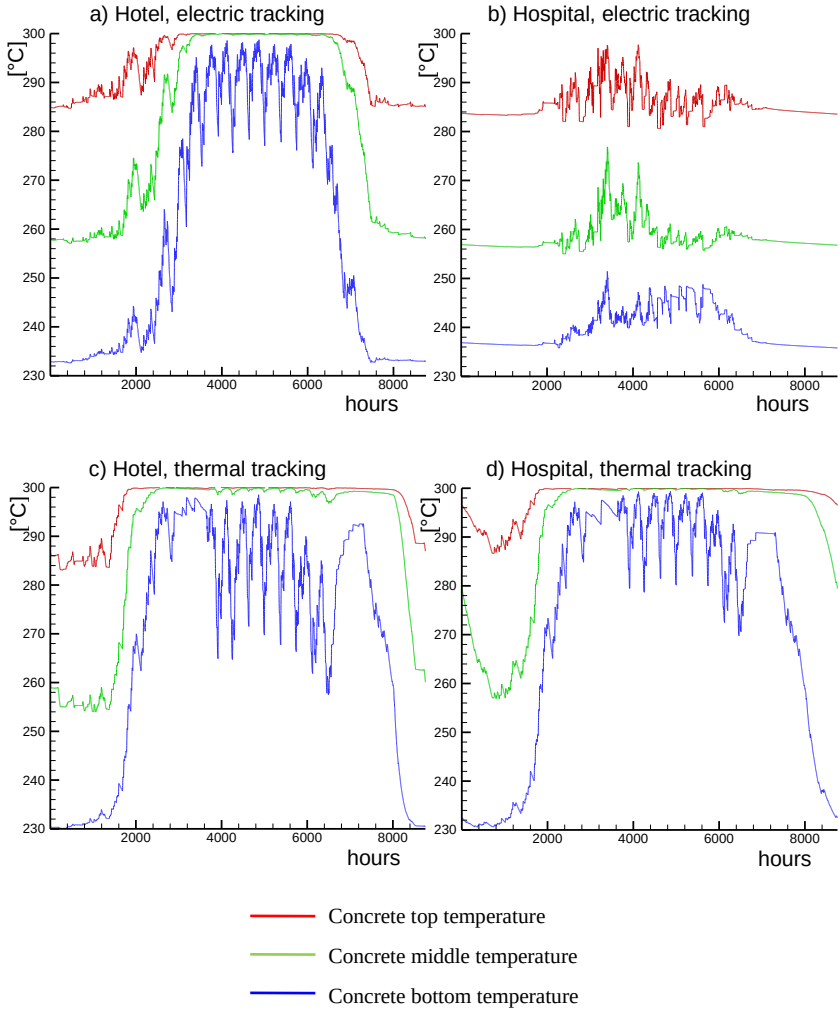

Figure 86: Storage concrete top, middle and bottom node temperature.

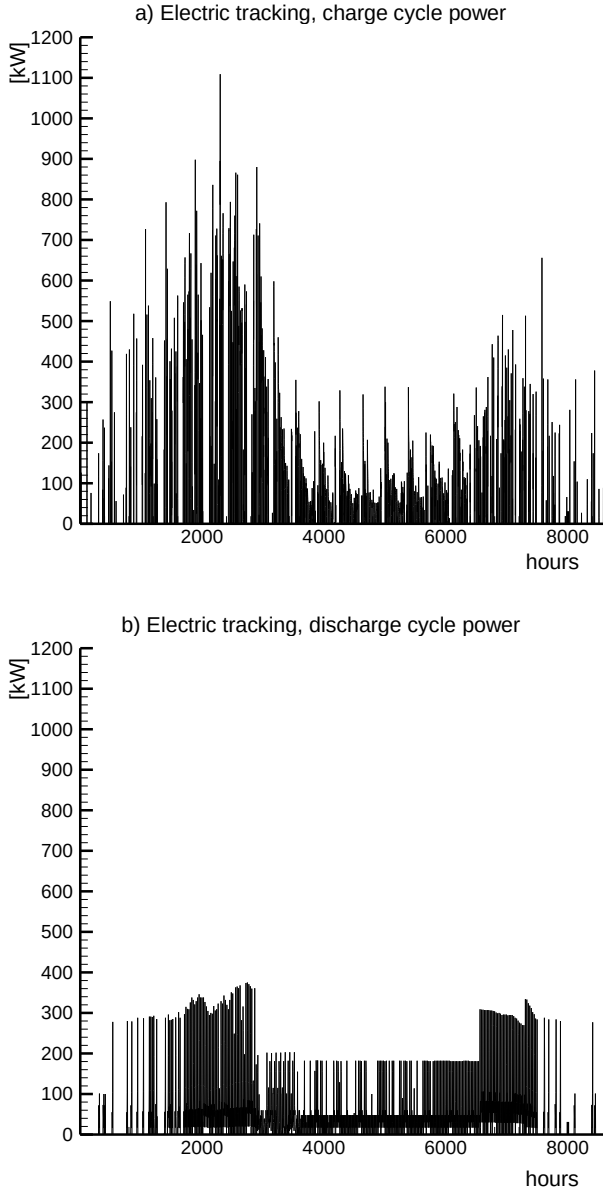

Figure 87 a) and b): Hotel charge discharge cycles power in electric and thermal tracking.

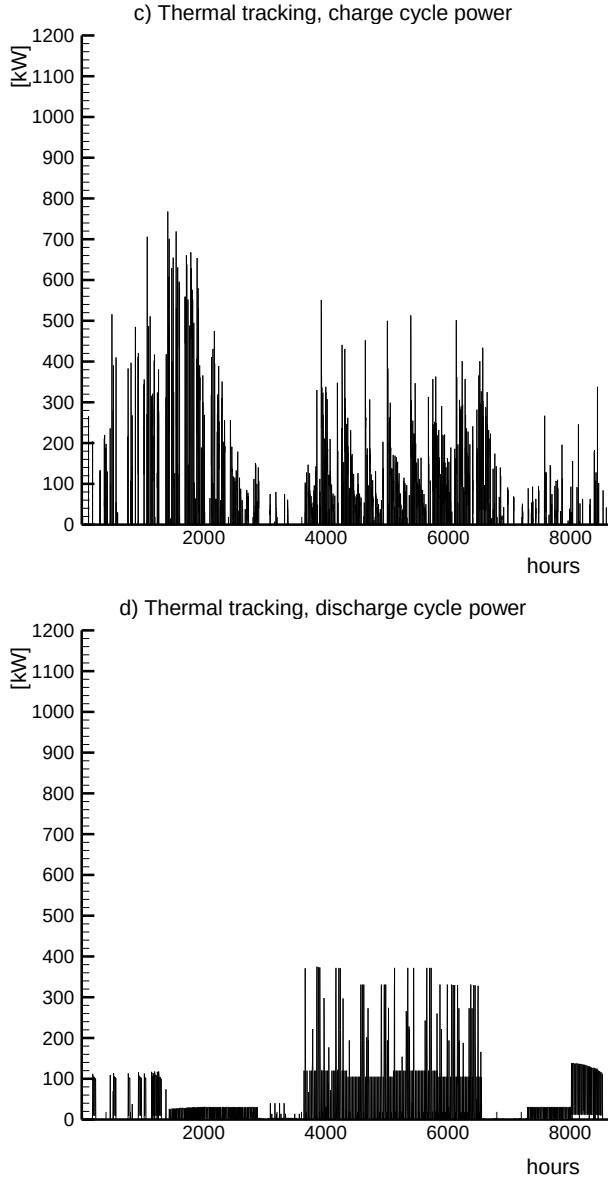

Figure 87 c) and d): Hotel charge discharge cycles power in electric and thermal tracking.

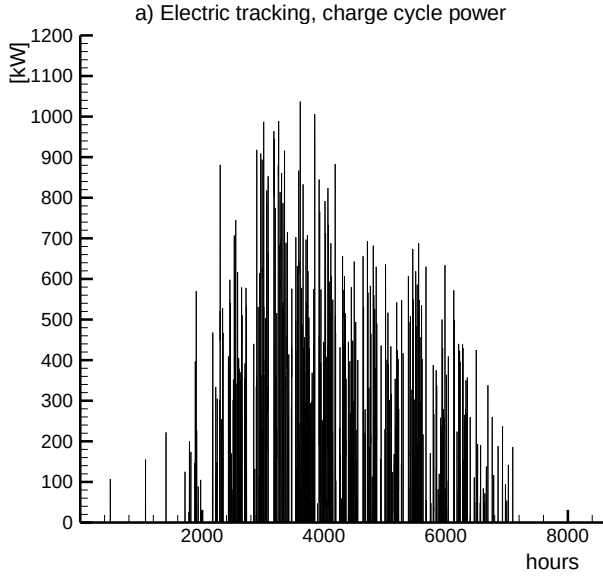

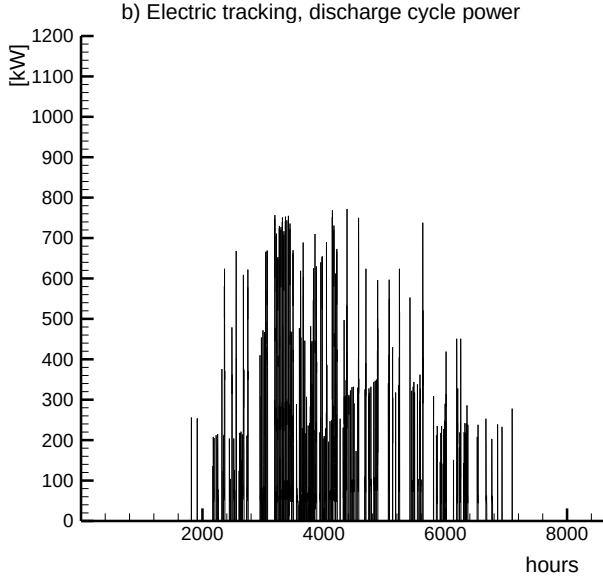

Figure 88 a) and b): Hospital charge discharge cycles power in electric and thermal tracking.

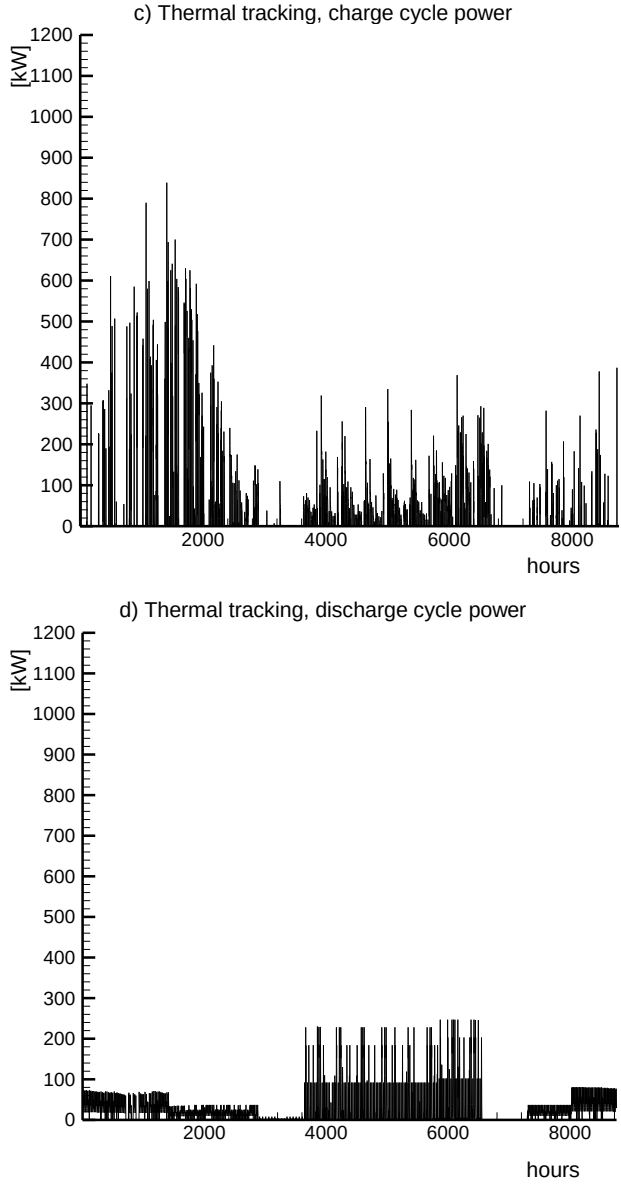

Figure 88 c) and d): Hospital charge discharge cycles power in electric and thermal tracking.

Figure 87 and Figure 88 show the charge discharge cycles power in electric and thermal tracking, respectively for the hotel and hospital end users.

For both the end users, the charge and discharge cycles during thermal tracking have almost the same behaviour, despite the higher discharge values for the hotel case. It is worth noting that the charge cycle is distributed all over the year, with higher and more frequently events during the spring period, while the discharge is mostly concentrated during the summer period. For what the electric tracking is concerned, the charge discharge cycles in the hotel case share a similar shape with peaks during spring and fall seasons, while for the hospital scenario, the cycles are most elevated in the summer period.

5.4 Hybrid system desalt performance

The desalting configuration uses the available thermal energy to drive a certain number of desalting devices. This configuration is based on the hotel electric tracking; for this reason, with the exception of the electric and thermal power outputs, Figure 89, the energy output aspects are not further analyzed and the attention is entirely dedicated to the water production performance.

In Figure 89 the electric and thermal power outputs for the desalting configuration are shown. The electric power output, which follows the hotel electric load, reaches values of 97 kW with a minimum basis of 55 kW. Moreover, there are some power output spikes, given by the necessity of the RES system to deliver the captured solar power. The yearly behaviour is a seasonal type, with higher values during the winter/fall period. As strictly related, the thermal power output curve shape overlaps the electric power one, even if it has usual values ranging from 462 kW to 812 kW.

Table 44: Single desalting unit technical specifications [105]

Distillate capacity	125 kg/h
Distiller heat consumption	85 kW
Distillate pump power	0,4 kW
Jacket cooling water flowrate	6,4 t/h
Ejector pump capacity	10 m^3/h
Ejector pump power	3,7 kW

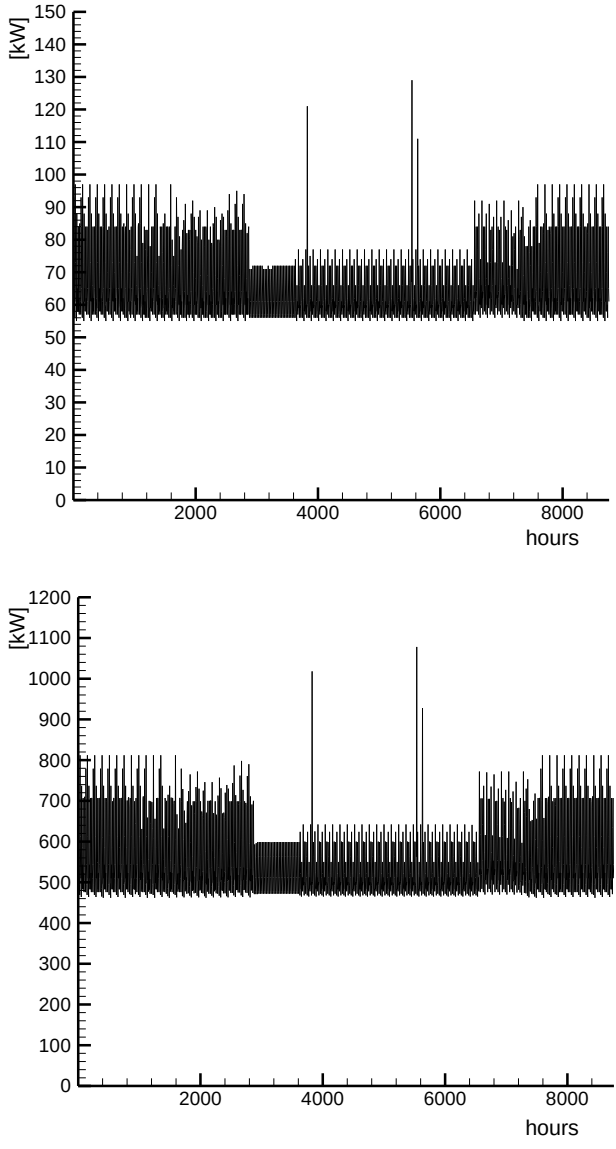

Figure 89: Yearly a) electric and b) thermal energy output.

Considering the performance data of a single desalting device, Table 44, and the hourly available thermal power, the number of on-duty units has been calculated, as shown in Table 45. The result show that five units

are constantly on duty all over the year. The maximum reachable on duty devices is thirteen, nevertheless, as the number of duty hours are negligible for units from ten to thirteen, the maximum number of units has been limited to nine, considering the remaining available heat as a dump.

Table 45: Desalting units' duty hours.

On duty units number	Duty hours
Up to 5	8760
6	4928
7	2265
8	1243
9	274
10	7
11	7
12	5
13	1

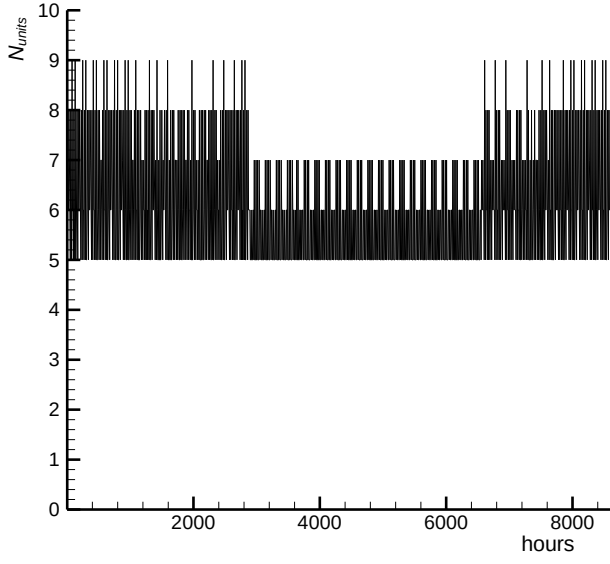

Figure 90: Number of desalting units on duty.

Looking at Figure 90 it clearly results the seasonal behaviour of the desalting plant, which, despite the constant contribution of five desalting units, reaches the full operation activity, with all the nine systems' units on duty, only during the winter/fall period, according to the electric load of the end user.

It is evident that each term of performance comparison is directly related to the number of on duty desalting units, so the graphs will be similar one to each other with the only difference of the scale values on the y-axis. For this reason, only the distillate output flow is shown,

Figure 91. The maximum hourly distillate output corresponds to 1˙125 kg/h of desalted water and, as previously highlighted, this value recurs only during the winter/fall period. In addition, the fresh water output is never lower than 625 kg/h.

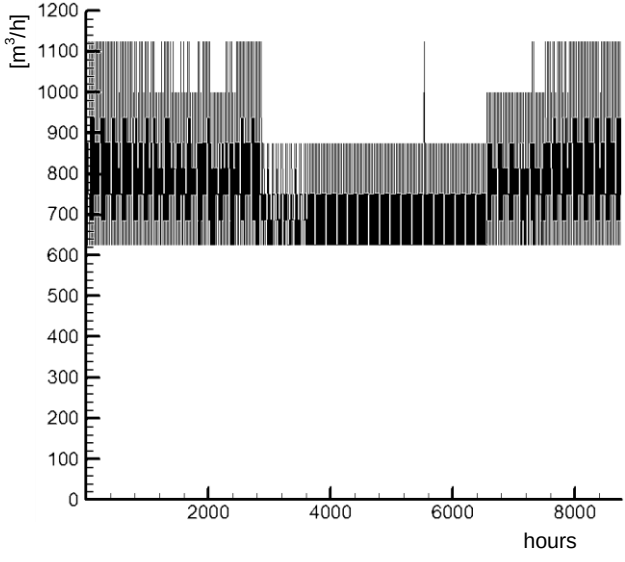

Figure 91: Distillate output flow rate.

As far as the dumped heat is concerned, Figure 92 demonstrates that its values are always below the threshold value of 85 kW, which is the thermal power needed from a single desalting unit to distillate water. The few exception to this assertion correspond to the already commented possibility to run a number of desalting units higher than the nine fixed in

this study and entail dump spikes with a maximum thermal power of 397 kW.

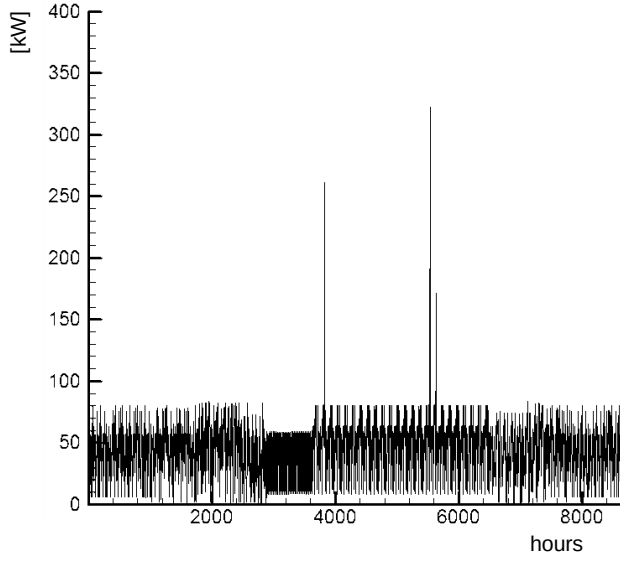

Figure 92: Dumped heat.

Table 46: Global desalination system performance.

Flow results	
Available cooling water [ton/year]	366˙091
Used cooling water [ton/year]	336˙064
Dumped cooling water [ton/year]	30˙027
Used seawater [m^3/year]	525˙100
Distillate output [ton/year]	6˙564
Power consumption	
Removed heat [GJ/year]	15˙911,64
Dumped heat [GJ/year]	1˙380,29
Distillate pump energy consumption [GJ/year]	75,6
Ejector pump energy consumption [GJ/year]	698,4

Looking at the global performance results of the desalination system, the annual distillate output amounts to about 6600 ton/year of water,

exploiting for this purpose about 525˙000 m^3/year of seawater. For what concerns the available cooling water deriving from the Rankine cycle condenser the 91,79% of the hot flow is used in the desalination process, removing 15˙912 GJ/year of heat. The remaining 395 MWh/year thermal power must be dumped and dissipated in other ways. Finally, the desalting system electric energy consumption globally amounts to 215 MWh/year.

Conclusions

In the present work a small scale hybrid concentrated solar power – biomass system for electric and thermal power has been analyzed. During the conception of the system, fundamental concepts as sustainability, innovation, renewable energy, distributed generation, integration and reproducibility have been taken into account. Particular attention has been paid to the challenge of conceiving a new operational systems using standard technologies instead of developing new technologies. To this end the novelty of the proposed energy plant is basically brought by the small scale of the concentrating solar field and the employment of a reciprocating steam engine.

Table 47: Power system main technologies.

Technology	Nominal power
Parabolic trough field	1˙294 kW
Concrete thermal storage	70˙000 kW
Biomass furnace	1˙163 kW
Steam engine	135 kW

The selected technologies, Table 47, were a 1˙294 kW_p parabolic trough concentrating solar power field equipped with a 70 MW concrete thermal energy storage, a 1˙163 kW_p biomass furnace for solar energy deficits compensation and a water/steam Rankine cycle with a 135 kW reciprocating steam engine. The plant has been managed in order to favour the solar energy exploitation with respect to the biomass source.

To assess the presented plant soundness yearly hour-based transient model simulations results for three different arrangements have been shown. The proposed configurations are:

- a baseline configuration, with constant power outputs;
- a load tracking configuration, which follows electric or thermal power demand of selected end-users, i.e. a hotel and a hospital;
- a desalting configuration, which besides the end-user electric tracking employs thermal energy to produce desalted water.

The end users main characteristics are summarized in Table 48. Concerning the hospital and hotel end users, it is worth remembering that the cooling load has been included in the heat load by means of an equivalence factor.

Table 48: End users characteristics.

	Hospital	Hotel	Desalination
Volume	42˙000 m^3	43˙000 m^3	
Number of sleeping accommodations	140 GJ/y	350 GJ/y	
Heat load	7˙890 GJ/y	8˙640 GJ/y	9x85 kW/h
Electric load	2˙880 GJ/y	1˙656 GJ/y	9x4,1 kW/h
Cooling load	2˙178 GJ/y	2˙580 GJ/y	
Heat/electric consumption ratio [GJ_{th}/GJ_{el}]	2,75	5,23	
Distillate capacity			125 kg/h

Table 49 summarizes the performance results for the three studied configurations. Obviously the solar field collected energy is equal for each simulated scenario. Nevertheless, as each scenario has different energy requirements, the thermal energy storage has different behaviours in each case. In particular, in some cases it results that the discharge energy is higher than the charged one, indicating that the system has used the energy stored during the previous simulation year. Moreover, the solar system energy supply, including both direct solar field and TES contributions, is quite similar in each configuration. To the contrary the biomass energy contribution shows remarkable variations, particularly evident in the step between the baseline and the tracking configurations, indicating that in the tracking and desalination scenarios the lower energy demand affects the recur to the biomass source, according to the initial power plant management hypothesis and the load energy. In fact, in the tracking and desalination configurations the electric and thermal energy

supply is, on the average, about 60% of the baseline energy supply. The result is significant when looking at the solar fraction supply, calculated as the percentage ratio between the solar system energy supply and the global energy input to the Rankine cycle, which passes from a value of 10% in the baseline scenarios to a 19% in the less energivorous tracking scenarios.

Table 49: Results summary for the simulated configurations[10].

		Baseline	Load tracking				Desalination
			Hotel.		Hospital		
			Electric.	Thermal	Electric	Thermal	
RES system	Solar field collected energy [GJ/y]	4'277,53	4'277,53	4'277,53	4'277,53	4'277,53	4'277,53
	TES charged energy [GJ/y]	1'162,45	1'397,11	1'037,35	1'191,61	865,25	1'397,11
	TES discharged energy [GJ/y]	890,42	1'291,67	852,54	941,92	680,67	1'291,67
	Solar system energy supply [GJ/y]	4'005,50	4'172,09	4'092,72	4'027,85	4'092,96	4'172,09
	Biomass energy supply [GJ/y]	35'906,69	18'132,39	17'221,31	27'103,92	16'725,59	18'132,39
	Global effective energy input E_g [GJ/y]	39'912,16	22'304,48	21'314,03	31'131,77	20'818,55	22'304,48
	Biomass consumption [ton/y]	1'962	990,84	941,06	1'481,09	913,97	990,84
	Solar fraction of supply	10,04	18,71	19,2	12,94	19,66	18,71
Electric output	Electric energy demand E_{el} [GJ/y]		1'664,68	1'664,68	2'886,42	2'886,42	1'664,68
	Electric energy supply E[GJ/y]	3'654,22	2'064,37	2'017,10	2'956,18	1'931,52	2'064,37
	Met electric load [%]		99,46	89,91	97,11	65,14	99,46
	Electric energy surplus [GJ/y]		408,7	520,33	153,14	51,31	408,7
	Electric l energy deficit [GJ/y]		9,01	167,91	83,38	1006,22	9,01
Thermal output	Thermal energy demand E_{th} [GJ/y]		11'656,13	11'656,13	10'668,96	10'668,96	
	Thermal energy supply [GJ/y]	30'608,36	17'291,93	16'895,49	24'761,79	16'179,00	17'291,93
	Met thermal load [%]		88,88	96,73	100	98,64	
	Thermal energy surplus [GJ/y]		6'931,48	5'620,89	14'092,83	5'654,64	
	Thermal energy deficit [GJ/y]		1'295,67	381,52	0	144,6	
Desalting system	Desalted water supply [ton/y]						6'564
	Employed heat [GJ/y]						15'911,64
	Dumped heat [GJ/y]						1'380,29
RC system	Net electric efficiency = E_{el}/E_g [%]	9,16	9,26	9,46	9,5	9,28	9,26
	Net thermal efficiency = E_{th}/E_g [%]	76,69	77,53	79,27	79,54	77,71	
	Electric index = E_{el}/Et_h [-]	11,94	11,94	11,94	11,94	11,94	
	Primary energy ratio= $(E_{el}/\eta_{el}+E_{th}/\eta_{th})/E_g$ [-][9]	1,2	1,21	1,24	1,24	1,22	

[10] For the primary energy ratio evaluation, the values for the reference electric and thermal efficiencies are $\eta_{el} = 0.38$ and $\eta_{th} = 0.8$.

It is worth noting that, concerning the thermal output, the desalination configuration has the higher utilization factor of the thermal energy supply, with a dump of only 1˙380 GJ/y, due to the cluster character of the desalination plant thermal request, with respect to the average 8˙075 GJ/y of the tracking scenarios.

The plant performance results demonstrate the versatility of the plant, capable to work either at full duty and on load tracking configurations, following hourly-based electric and thermal load. The nearly full met power load in the tracking configurations also makes obvious that, with some management adjustments, the system is capable to work in off-grid configurations. Moreover, also the capability to employ the produced power to obtain an alternative product, such as fresh desalted water, has been demonstrated, widening the possible applications of this energy system to different sites and with different end-uses. However it is worth reminding that the power plant output is about 11% electric and 89% thermal, thus to achieve the best power output utilization, the load must be compatible with such power output, presenting an adequate heat/electric consumption.

To evaluate the environmental impact of the studied plant, the related emission savings have been estimated, Table 51, by means of emission factors, Table 50, related to the Italian thermoelectric power stations at reference year 2003 [103]. As expected, the baseline configuration has the higher savings, corresponding to 9˙136 ton/y of carbon dioxide, 9,5 ton/y of sulphur oxides, 5,7 ton/y of nitrogen oxides and 0,4 ton/y of total suspended particulates, as it works with high constant power outputs in the hypothesis of complete employment of the supplied electric and thermal energy.

Table 50: Emissions factors [103].

CO_2	690 g/kWh
SO_x	1,0 g/kWh
NO_x	0,6 g/kWh
TSP[11]	0,04 g/kWh

The tracking and desalination configurations emissions savings are evaluated considering the entire electric energy supply, in the hypothesis of grid transfer of the surplus, and the fraction of thermal energy supplied to the end users, in the hypothesis of dump of the thermal energy surplus. Looking at the tracking configuration, the hospital electric tracking shows

[11] Total suspended particulates.

the higher emission savings, due to its higher electric energy load and supply. Nevertheless, the best environmental performance of the end users scenarios, i.e. tracking and desalination, is the desalination configuration which allows to avoid about 4˙794 ton/y of carbon dioxide. This primacy is related to its remarkable thermal energy employment.

Table 51: Configurations emission savings.

	Baseline	Tracking				Desalination
		Hotel		Hospital		
		Elec.	Therm.	Elec.	Therm.	
CO_2 [ton/y]	9˙136,69	2˙967,87	3˙442,71	3˙633,37	3˙283,01	4˙793,60
SO_x [ton/y]	9,52	3,09	3,59	3,78	3,42	4,99
NO_x [ton/y]	5,71	1,85	2,15	2,27	2,05	3,00
TSP [ton/y]	0,38	0,12	0,14	0,15	0,14	0,20

Table 52: Plant land use.

	Net land use
Solar field	6˙780 m^2
TES	570 m^2
Biomass furnace, filter and stack	700 m^2
Biomass storage	3˙000
Buildings (Rankine cycle elements, desalting units, offices)	2˙100
Total	**13˙150 m^2**

Another essential environmental aspect is the land use of the plant. Table 52 shows the estimated land use for the main plant technologies, which globally need a net area of 13˙150 m^2. The larger land use is requested from the solar field, as evident also in Figure 93. Considering security distances and the need of space for the power conversion block the needed surface rises to 31˙000 m^2. Comparing this surfaces with a standard FIFA soccer field, which measures 7˙140 m^2, the parabolic solar troughs need an area big as 4,34 soccer fields.

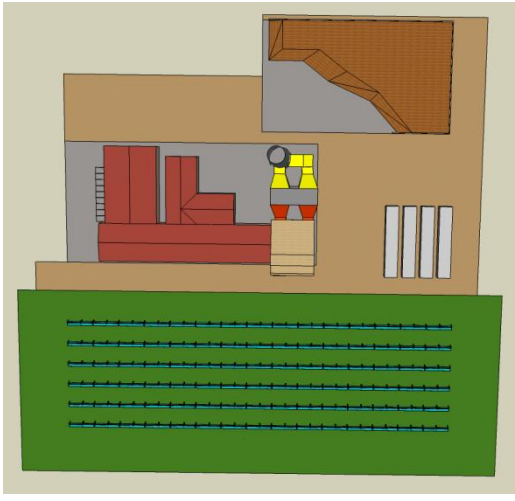

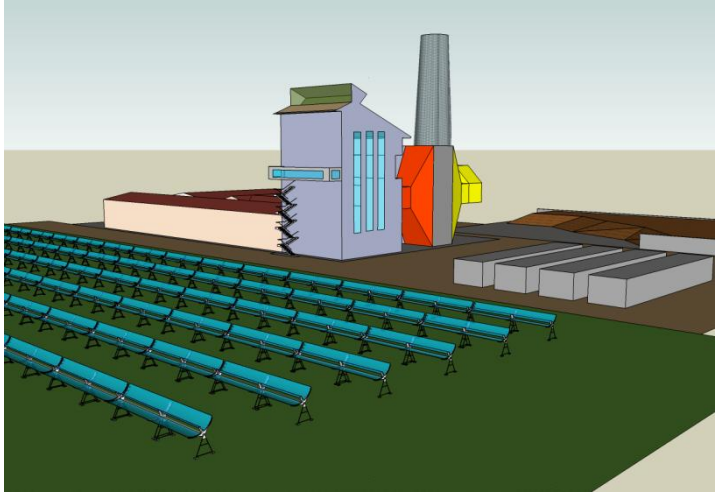

Figure 93: Rendering of the proposed power plant lay-out.

Concerning the plant costs, Table 53 indicates that the parabolic trough field with the thermal energy storage are the most expensive devices of the proposed system. In particular, the capital cost of a solar trough field with thermal storage has been evaluated in 4˙820 $/kW for the reference year 2006 [112], that is 6˙052 €/kW. It is worth noting that these data refer to large CSP technologies and must be considered only as a rough estimate of the present CSP device.

Referring to the other technologies, the capital costs have been obtained by private communications with producers. In the utilities heading, it entails costs for electric panels, electric and hydraulic connections, civil works &c.

Table 53: Plant estimated capital cost data.

Technology	Cost [€]
CSP field with TES	7˙870˙000
Biomass furnace	130˙000
Economizer	15˙000
Evaporator	45˙000
Steam engine	220˙000
Condenser	15˙000
Utilities	300˙000
Total	**8˙595˙000**
Desalting units	194˙000
Total	**8˙789˙000**

The plant potential and versatility have been analyzed, demonstrating the suitability of the plant itself to work either grid-connected, referring to the baseline configuration, and off-grid connected, referring to the electric and thermal power tracking and to the desalting configurations. Taking notice of the economic topic, is obvious that such high costs are constraining to the development of the proposed system when thinking to the standard fossil fuel based power technologies. Nevertheless, in a fossil fuel free power generation perspective, given from the exhaustion of fossil energy sources and from the need to pull down the fossil sources related emissions, the current high costs become a side issue in behalf of the sustainable development of the energy sector.

However, as the economy matter effectively drives the world, notwithstanding the efforts to let prevail the sustainability principles, it will be fundamental to reduce the plant costs, in order to become competitive towards the other commercial renewable-based power technologies. To this end, some development paths for the proposed system are suggested.

The first path is to substitute the parabolic trough technology with the compound parabolic concentrator (CPC). CPC technology is simpler than parabolic trough and do not need a constant sun tracking. The result of this choice may positively affect the plant costs, even if the economic benefits must be compared to a lower solar energy capture capacity.

Furthermore, CPC working fluid can be water. The use of water in place of diathermic oil will permit to lower the fluid temperatures and additionally lowering the costs, as water is cheaper than diathermic oil, besides being more safety.

The second development path is to convert the water/steam Rankine cycle in an organic fluid Rankine cycle (ORC). This choice allows to obtain identical results at lower working temperatures, making the water-CPC option completely available. Furthermore, this choice may lead to an additional solar field downscaling maintaining the same plant power, further lowering the capital costs.

Finally, as recently the interest in small scale CSP applications is rising, with systems supplying energy to remote off-grid areas [113] and buildings [52], it would be interesting and useful to outline the cost for downscaled CSP plants.

References

[1] United Nations, "Report of the World Commission on Environment and Development," in *United Nations 96th Plenary Meeting of the General Assembly*, New York, NY, 1987.

[2] Abu Dhabi Future Energy Company PJSC. (2010) Masdar City, Sustainability. http://www.masdarcity.ae

[3] European Commission. (2010) Environment, Sustainability. http://ec.europa.eu

[4] IEA. (2002) IEA Statement on Sustainable Development. http://www.iea.org

[5] Ram Nidumolu, C. K. Prahalad, and M. R. Rangaswami, "Why sustainability is the key driver of innovation," *Harvard Business Review On Point*, pp. 79-86, 2010.

[6] Energy Information Administration (EIA), "International Energy Outlook," Washington, D.C., 2008.

[7] OECD/IEA, "World Energy Outlook 2008 - Global Energy Trends to 2008," Paris, 2008.

[8] OECD/IEA, "World Energy Outlook 2007 - Global Energy Prospects - Impact of Developments in China and India," Paris, 2007.

[9] Nuobo Tanaka, "Our Global Energy Future - Looking beyond the economic crisis," in *Ministry of Economy*, Warsaw (PL), 2009.

[10] OECD/IEA, "Toward Solutions - Sustainable Development in the Energy Sector," Paris, 2002.

[11] William F. Pickard, Amy Q. Shen, and Nicholas J. Hansing, "Parking the power: Strategies and physical limitations for bulk energy storage in supply–demand matching on a grid whose input power is provided by intermittent sources," *Renewable and Sustainable Energy Reviews*, pp. 1934–1945, 2009.

[12] OECD/IEA, "Renewables in global energy supply. An IEA factsheet," Paris, 2007.

[13] Giovanni B. Zorzoli, "Il futuro energetico dell'Italia," in *Crisi energetica, cambiamenti climatici e città sostenibili: quale modello energetico per il futuro?*, Latina, 2010.

[14] OECD/IEA, "The impact of financial and economic crisis on global energy investment," IEA background paper for the G8 Energy Ministers' meeting - 24-25 May 2009.

[15] European Renewable Energy Council. (2010) Turnover. http://www.erec.org/

[16] PricewaterhouseCoopers LLP, "100% renewable electricity. A roadmap to 2050 for Europe and North Africa," London, U.K., 2010.

[17] Mark Z. Jacobson and Mark A: Delucchi, "Providing all global energy with wind, water and solar power, part I: technologies, energy rsources, quntities and areas of infrastructure, and materials.," *Energy Policy*, 2011.

[18] K. Fröhlke and O.J. Haidn, "Spinning reserve system based on H2/O2 combustion," *Energy Conversion, S0196-8904(1996)00128-8.*

[19] S. Kélouwani, K. Agbossou, and R. Chahine, "Model for energy conversion in renewable energy system with hydrogen storage," *Journal of Power Sources 140 (2005) 392-399.*

[20] Alessandro Corsini, Franco Rispoli, Mario Gamberale, and Eileen Tortora, "Assessment of H2- and H2O-based renewable energy-buffering systems in minor islands," *Renewable Energy 34 (2009) 279–288.*

[21] G. Sinden, "The practicalities of developing renewable energy stand-by capacity and intermittency," Oxford, Submission to The Science and Technology Select Committee of the House of Lords 2004.

[22] Edward Khan, "The reliability of distributed wind generators,"

Electric power systems research, pp. 1-14, 1979.

[23] Cristina L. Archer and Mark Z. Jacobson, "Spatial and temporal distributions of U.S. winds and wind power at 80 m derived from," *Journal of geophysical research*, 2003.

[24] Christina L. Archer and Mark Z. Jacobson, "Supplying baseload power and reducing transmission requirements by interconnecting wind," *Journal of applied meteorology and climatology*, 2007.

[25] R. Buck, O. Goebel, R. Koehne, R. Tanurie, and F. Trieb, "Advanced solar/fossil combined power plants.," in *Proceedings of The International Energy and Environment Conference*, Shanghai, 1998, pp. 423–34.

[26] G. J. Kolb, "Evaluation of power production from the solar electric generating system at Kramer junction 1988," in *Proceedings of ASME International Solar Energy Conference,* Hawai, 1997, pp. 499–504.

[27] Y. Allani and D. Favrat, "Concept Global d'une Nouvelle Centrale Solaire a` Cycle Combine´ Dual Fuel," *Entropie*, 1991.

[28] M. Kane and D. Favrat, "Approche de conception et d'optimisation de centrale solaire inte´gre´e a` cycle combine´ inspire´e," *International Journal on Thermal Science*, 1999.

[29] M. Kane, D. Favrat, K. Siegler, and Y. Allani, "Thermoeconomic analysis of advanced solar–fossil combined cycle power plants," *Internationa Journal on Applied Thermodynamics*, 2000.

[30] Pilkington Solar International GmbH, "Solar Thermal Power Plants," Koln, Germany, Status Report 1996.

[31] OY. Goswami, "Solar energy and the environment," in *ASME 1993 International Conference on*, Cracow, Poland, 1993, pp. 77–85.

[32] H. W. Price, D. D. Whitney, and H. I. Beebe, "SMUD Kokhala Power Tower Study," in *Proceedings of the 1996 international Solar Energy Conference*, San Antonio, Texas, USA, 1996, pp.

273–9.

[33] S. Ashok, "Optimised model for community-based hybrid energy system," *Renewable Energy, 32, 1155–1164, 2007.*

[34] O. Ekren and B.Y. Ekren, "Size optimization of a PV/wind hybrid energy conversion system with battery storage using response surface methodology," *Applied Energy, 85, 1086–1101, 2008*.

[35] J. Paska, P. Biczel, and M. M. Klos, "Hybrid power systems – An effective way of utilising primary energy sources," *Renewable Energy, 34, 2414–2421, 2009*.

[36] Graeme R.G. Hoste, Michael J. Dvorak, and Mark Z. Jacobson, "Matching Hourly and Peak Demand by Combining Different Renewable Energy Sources - A case study for California in 2020," Stanford University - Department of Civil and Environmental Engineering, Atmosphere/Energy Program 2005.

[37] Alessandro Corsini, Domenico Borello, Franco Rispoli, and Eileen Tortora, "A combined solar-biomass Rankine cycle concept for small-size cogeneration," in *Proceedings of ECOS 2009 Conference*, Foz do Iguaco, 2009.

[38] José M. Angulo and Santiago Arnaltes, "A modern day solution to LVRT: regulatory prescriptions and technological responses," *Renewable energy focus*, pp. 58-59, 2010.

[39] Peter Crossley and Agnes Beviz, "Smart Grids: Low carbon electricity for the future," *Renewable energy focus*, pp. 55-56, 2010.

[40] T. Ackermann, G. Andersson, and L. Soder, "Distributed generation: a definition," *Electric Power Systems Research 57, 195–204.*, 2001.

[41] Neil Strachan and Alexander Farrell, "Emissions from distributed vs. centralized generation: The importance of system performance," *Energy Policy 34 (2006) 2677–2689*.

[42] G.G. Maidment, X. Zhao, S.B. Riffat, and G. Prosser, "Application of combined heat-and-power and absorption

cooling in supermarkets," *Applied Energy 63 (1999) 169-190*.

[43] G.G. Maidment and R.M. Tozer, "Combined cooling and power in supermarkets," *Applied Therma Engineering 22 (2002) 653-665*, 2002.

[44] HyonUK Seo, Jinil Sung, Si-Doek Oh, and Ho-Young Kwak, "Economic optimization of a cogeneration system for apartments in Korea," in *ASME Internationl Mechanical Engineering Congress and Exposition*, Seattle, Washington, USA, 2007.

[45] Alessandro Corsini, Vincenzo Naso, and Paolo Venturini, "Biomass co-firing: analysis of the main technical problems in coal power plants," in *15th European Biomass Conference*, Berlin, Germany, 2007.

[46] Alessandro Corsini, Vincenzo Naso, G. Mattei, and Paolo Ventiruni, "Biomass co-firing: estimation of fuel requirements and land needed to feed some Italian coal power plants," in *15th European Biomass Conference*, Berlin, Germany, 2007.

[47] Asfaw Beyene and Benjamin Erpelding, "Sizing, part-load, and system performance of combined heat and power," in *ASME International Mechanical Engineering Congress and Exposition*, Seattle, Washington, USA, 2007.

[48] Mark W. Johnson and Josh Suskewicz, "How to jump-start the clean tech economy," *harvard business review on point*, pp. 89-96, 2010.

[49] William B. Stine and Michael Geyer, *Power from the sun*.: www.powerfromthesun.net, 2001.

[50] Green Peace International; International Solar PACES; European Solar Thermal Electricity Association, "Global Concetrating Solar Power Outlook. Why renewable energy is hot," 2009.

[51] IHS Emerging Energy Research. (2010) Research focus: solar. http://www.emerging-energy.com

[52] Ming Qu, Hongxi Yin, and David H. Archer, "A solar thermal cooling and heating system for a building: Experimental and model based performance analysis and design," *Solar Energy 84*,

pp. 166–182, 2010.

[53] M. Kane, D. Larrain, D. Favrat, and Y. Allani, "Small hybrid solar power system," *Energy 28*, pp. 1427–1443, 2003.

[54] FLABEG Holding GmbH. (2008) Track Record Solar Mirrors 1983–2010. http://www.flabeg.com

[55] M. Eck, E. Zarza, M. Eickhoff, J. Rheinlander, and L. Valenzuela, "Applied research concerning the direct steam generation in parabolic troughs," *Solar Energy 74*, pp. 341-351, 2003.

[56] M. Eck and E. Zarza, "Saturated steam process with direct steam generating parabolic troughs," *Solar Energy 80*, pp. 1424–1433, 2006.

[57] Peter Viebahn Viebahn, Stefan Kronshage, Franz Trieb Trieb, and Yolanda Lechon, "Final report on technical data, costs, and life cycle inventories of solar thermal power plants," 2008.

[58] P.G. Grodzka, *Solar Engineering Energy Technology Handbook*. New York, USA: Marcel Dekker Inc., 1980.

[59] N. Lineback et al., "Industrial greenhouse gas emissions: does CO 2 from combustion of biomass residue for energy really matter?," *Climate Res 13*, pp. 221-229, 1999.

[60] K. Bernotat and , T. Sandberg, "Biomass fired small-scale chp in sweden and the baltic states: a case study on the potential of clustered dwellings," *Biomass Bioenergy 27*, pp. 521–530, 2004.

[61] Talbott's Heating Ltd. (2005) Biomass Fuelled Indirect Fired Micro Turbine. http://www.dti.gov.uk

[62] World Resources Institute. (2007) Technology - Biomass. www.thegreenpowergroup.org

[63] International Energy Agency - Biomass. (2004) Technologies. www.aboutbioenergy.info

[64] European Biomass Industry Association (EUBIA). (2005) About biomass - Conversion routes. www.eubia.org

[65] Unites States Department of Energy Efficiency and Renewable Energy (EERE). (2005) Biomass. www.eere.energy.gov

[66] Leilei Dong, Hao Liu, and Saffa Riffat, "development of small-scale and micro-scale biomass-fuelled CHP systems. A literature review.," *Applied thermal engineering*, 2009.

[67] GSE, Italian Electric Service Manager, "Biomasse, Rapporto statistico," 2009.

[68] H. Kopetz. (2007) Present Development in Small Scale Combined Heat and Power. http://www.svebio.se

[69] International Water Managment Institute (IWMI). (2009) Startegic Plan 2009-2013, Water for a food-secure world. http://www.iwmi.cgiar.org/index.aspx

[70] European Commission. (2011, February) Water scarcity. http://ec.europa.eu/environment/water/quantity/scarcity_en.htm

[71] Eftihia Tzen et al., "Autonomous desalination units based on renewable energy systems," Work Package 2, Co-ordination action 2005.

[72] Franz Trieb et al., "Technologies for large scale seawater desalination using concentrated solar radiation," *Desalination 235 (2009) 33-43*.

[73] Artin Hatzikioseyian, Roza Vidali, and Pavlina Kousi, "Modelling and thermodybìnamic analysis of a multieffect distillation (MED) plant for seawater desalination," Almeria, Spain, Research results 2003.

[74] K. Sampathkumar, T.V. Arjunan, P. Pitchandi, and P. Senthilkumar, "Active solar distillation—A detailed review," *Renewable and Sustainable Energy Reviews 14 (2010) 1503–1526*.

[75] Andrea Cipollina, Giorgio Micale, and Lucio Rizzuti, *Sewater Desalination*. Berlin Heidelberg, Germany: Springer, 2009.

[76] Sargent & Lundy LLC Consulting Group, "Assessment of Parabolic Trough and Power Tower Solar Technology Cost and

Performance Forecasts," Chicago, Illinois, 2003.

[77] Green Peace International; International Solar PACES; European Solar Thermal Electricity Association, "Concentrating solar power: outlook 2009," 2009.

[78] Hans Muller-Steinhagen and Franz Trieb, "Cocnetrating sola power. A review of technology," Stuttgart, Germany, 2004.

[79] Thomas Nussbaumer, "Combustion and Co-combustion of Biomass: Fundamentals, Technologies, and Primary Measures for Emission Reduction," *Energy Fuels, 2003, 17 (6), pp 1510–1521*.

[80] Christina L. Archer and Mark Z. Jacobson, "upplying baseload power and reducing transmission requirements by interconnecting wind," *Journal of applied meteorology and climatology*, 2007.

[81] Doerte Laing, Wolf D. Steinmann, Rainer Tamme, and Christoph Richter, "Solid media thermal storage for parabolic trough power plants," *Solar Energy 80 (2006) 1283–1289.*

[82] H. Lund and A.N. Anderson, "Optimal designs of small CHP plants in a market with fluctuating electricity prices," *Energy Conversion and Management Vol 46: 893-904.*, 2005.

[83] A. Beyene and B. Erpelding, "Sizing, part-load operation, and system performance of combined heat and power," in *ASME International Mechanical Engineering Congress and Exposition 2007*, Seattle, Washington USA, 2007.

[84] M.R. Muller, "The Return of the Steam Engine," in *ACEEE Summer Study on Energy Efficiency in Industry*, 2005.

[85] G. Molinari and F. Bonfà, "Utilizzazione di biomasse per alimentazione di gruppi cogenerativi con motori a vapore alternativi per utenze piccole e medie," in *Conferenza Nazionale Politica Energetica in Italia*, Bologna, Italy, 2005.

[86] Solar Energy Laboratory, University of Wisconsin-Madison. (2003) Generated Hourly Weather Data.

http://sel.me.wisc.edu/trnsys/weather/generate.htm

[87] HelioClim. (2009) Kloben - Solar Evolution Cmpany. http://www.helioclim.net

[88] ENI, "Agip lubricants, technology comes alive," Products data sheets 2009.

[89] Exxon Mobil Corporation, "Essotherm 500," Product technical data 2001.

[90] Total Italia, "Jaritherm DBT," Product Technical data 2004.

[91] Solutia, "Therminol VP-1, Vapour phase liquid phase heat transfer fluid," Product thecnical data 2004.

[92] The Dow Chemical Company, "Dowtherm A heat transfer fluid," U.S.A., Product technical data 1997.

[93] Italian Ministry of the Economy Development and Ministry of Environment, D.M. 11 aprile 2008 - Criteri e modalita' per incentivare la produzione di energia elettrica da fonte solare mediante cicli termodinamici, 2008.

[94] P Schwarzbözl, U. Eiden, R. Pitz-Paal, and S. Jones, "A TRNSYS model library for solar thermal electric components (STEC).," Reference manual. Release 2.2. 2002.

[95] Changkook Ryu et al., "Effect of fuel properties on biomass combustion: Part I.," *Fuel 85 (2006) 1039–1046*, 2006.

[96] Ferroli, "DW FHF gm, Diathermic fluid heater for solid fuels," Technical data sheets 2008.

[97] AGICO Group, "AGICO Biomass Furnaces Brochure," Hong Kong (PRC), 2011.

[98] Donatello Annaratone, *Generatori di vapore*. Milano: Libreria Clup, Gennaio/Febbraio 1995.

[99] DeWitt, Bergam, Lavine Incropera, *Fundamentals of Heat and Mass Transfer*., 2004.

[100] Spilling Energie Systeme GmbH, Private comunications, 2008.

[101] Oreste Acton and Carmelo Caputo, *Macchine a fluido - Compressori ed espansori volumetrici*. Torino: UTET, 1992.

[102] Samule C: Mc Birnie and William J. Fox, *Marine steam engines and turbines*. London, UK: Newnes-Butterworth, 1970.

[103] E. Macchi, S. Campanari, and P. Silva, "La micocogenerazione a gas naturale," in *La micocogenerazione a gas naturale*. Milano: Polipress, Politecnico di Milano, 2005, pp. 229-244.

[104] United States Environmental Protection Agency, "National Action Plan for Energy Efficiency Sector Collaborative on Energy Efficiency, Hotel Energy Use Profile," EPA Summer Workshop Report 2007.

[105] Sasakura Engeneering CO., LTD, Fresh Water Generator, Series K - Private communication, January 2011.

[106] Solar Energy Laboratory, Univeristy of Wisconsin - Madison. (2010) About TRNSYS. http://sel.me.wisc.edu/trnsys/index.html

[107] Alessandro Corsini, Mario Gamberale, and Franco Rispoli, "Assessment of renewable energy solutions in an Italian small island energy system using a transient simulation model," *ASME Journal of Solar Energy Engineering*, 2006.

[108] S.A. Jones, R. Pitz-Paal, P. Schwarzboezl, N. Blair, and R. Cable, "TRNSYS modelling of the SEGS VI parabolic trough solar electric generating system," in *Solar Forum 2001 - Solar Energy: The Power to Choose*, Washington, USA, 2001.

[109] Gregory J. Kolb and Vahab Hassani, "Performance of thermocline energy storage proposed for the 1 MW saguaro solar trough plant," in *ASME International Solar Energy Conference*, DEnver, Colorado, USA, 2006.

[110] P. Siangsukone and K. Lovegrove, "Modelling of a steam based paraboloidal dish concentrator using the computer source code TRNSYS," in *Annual Conference of the Australian and New Zealand Solar Energy Society*, Newcastle,Australia, 2002.

[111] S.A. Klein et al., "TRNSYS – a transient system simulation program. Version 15.1," Madison, Wisconsin, USA, 2000.

[112] Sargent & Lundy LLC Consoluting Group, "Assessment of parabolic trough and power tower solar technology cost and performance forecast," Chicago, Illinois, 2003.

[113] H. Zha, Y.J. Dai, and R.Z. Wang, "Energy and exergy analyses on a novel hybrid solar heating, cooling and power generation system for remote areas," *Applied energy 86 (2009) 1395–1404*.

[114] William B. Stine and Michael Geyer, *Power from the sun*.: www.powerfromthesun.net, 2001.

[115] Radiant & Hydronics. (2010) AZ Solar Station To Harnesses Sun's Heat For Power. http://www.radiantandhydronics.com

[116] International Information Technology and Applications. (2010) Home page. http://www.iitainc.com/

[117] Kai Nielsen, "Thermal Energy Storage. A State-of-the-Art," Trondheim, Norway, 2003.

Appendix A – In-house made TRNSYS types

Biomass furnace type subroutine

```
SUBROUTINE TYPE208 (TIME,XIN,OUT,T,DTDT,PAR,INFO,ICNTRL,*)
C************************************************************************

C ***
C *** Model Parameters
C ***
C                               Pnom    kW [0;+Inf]
C                               Pgen kW [0;+Inf]
C                               Tf_out1  C [0;+Inf]
C                               To_out1 C [0;+Inf]
C                               e       - [0;+Inf]
C                               C       - [0;100]
C                               H       - [0;100]
C                               O       - [0;100]
C                               S       - [0;100]
C                               u       - [0;100]
C                               Hi      kJ/kg.K [0;+Inf]
C           gammaSET [0;1]
C ***
C *** Model Inputs
C ***
C

C                               To_in    C [0;+Inf]
C           gamma Kg/s [0;+Inf]
C ***
C *** Model Outputs
C ***

C                               Am      kg/kg [0;+Inf]
C                               Gm      kg/kg [0;+Inf]
C                               mf      kg/h [0;+Inf]
C                               mc      kg/h [0;+Inf]
C                               To_out C [0;+Inf]
C           mo  Kg/h [0;+Inf]
C                               Qout kW [0;+Inf]
C ***
C *** Model Derivatives
C ***
```

```
C (Comments and routine interface generated by IISiBat 3)
C***********************************************************************

C       STANDARD TRNSYS DECLARATIONS
                        DOUBLE PRECISION XIN,OUT
                        INTEGER NI,NP,ND,NO
                        PARAMETER (NI=2,NP=12,NO=11,ND=0)
                        INTEGER*4 INFO,ICNTRL
                        REAL T,DTDT,PAR,TIME
                        REAL
Pnom,Pgen,Tf_out1,Tf_out,molio,C,H,O,S,u,Hi,Am,Gm
                        REAL
mf,mc,e,To_out1,To_out,To_in,gammaSET,n,cp,Qeff,gamma
                        REAL Atm
                        DIMENSION
XIN(NI),OUT(NO),PAR(NP),INFO(15)
                        CHARACTER*3 YCHECK(NI),OCHECK(NO)

C-----------------------------------------------------------------------

C       IF ITS THE FIRST CALL TO THIS UNIT, DO SOME
BOOKKEEPING
                        IF (INFO(7).GE.0) GO TO 100
                        INFO(6)=NO
                        INFO(9)=1
                        CALL TYPECK(1,INFO,NI,NP,ND)


                        RETURN 1

C-----------------------------------------------------------------------

C       VALUES OF THE PARAMETERS

100     CONTINUE
                        Pnom=PAR(1)
                        Pgen=PAR(2)
                        Tf_out1=PAR(3)
                        To_out1=PAR(4)
                        e=PAR(5)
                        C=PAR(6)
                        H=PAR(7)
```

```
                        O=PAR(8)
                        S=PAR(9)
                        u=PAR(10)
                        Hi=PAR(11)
                        gammaSET=PAR(12)

C       VALUES OF THE INPUTS
                        To_in=XIN(1)
                        gamma=XIN(2)
C-------------------------------------------------------------------------

C       COMPONENT EQUATIONS

        if (gamma.ge.gammaSET) go to 120

                gamma = gammaSET

120             cp=2.273
                dT=To_out1-To_in
                Qeff=Pgen*gamma
C               To_outk=To_out1+273.15
C               To_inK=To_in+273.15
                mo=Qeff*3600/(cp*dT)
C               mo=Qeff*3600/(cp_oo*To_out1-cp_io*To_in)
                mc=Pnom*gamma*3600/Hi
                Atm=0.11484*C+0.34204*H+0.4302*S-0.0431*O
                n=(e/100)+1
                Am=Atm*n
                Gm=Am+1
                mf=Gm*mc

                hf_out=(972.7+10.76*u)*Tf_out1/1000+(166.31-3.25*u)*
     *          (Tf_out1/1000)**2-(27.98-2.443*u)*(Tf_out1/1000)**3
                dhf=Qeff/mf
                hf_in=hf_out+dhf



C-------------------------------------------------------------------------

C       OUTPUTS

200     CONTINUE
```

```
OUT(1)=Am
OUT(2)=Gm
OUT(3)=mf
OUT(4)=mc
OUT(5)=To_out1
OUT(6)=mo
OUT(7)=Qeff


RETURN 1
END
```

Biomass furnace control

```
SUBROUTINE TYPE221 (TIME,XIN,OUT,T,DTDT,PAR,INFO,ICNTRL,*)
C************************************************************************

C ***
C *** Model Parameters
C ***
C                           Pgen     kW [0;+Inf]
C                           gammaSET        dimensionless [0;+Inf]

C ***
C *** Model Inputs
C ***
C                           mhftD    kg/hr [0;+Inf]
C                           mhtfSol  kg/hr [0;+Inf]

C ***
C *** Model Outputs
C ***
C                           gamma  - [0;+Inf]

C ***
C *** Model Derivatives
C ***

C (Comments and routine interface generated by IISiBat 3)
C************************************************************************

C                   STANDARD TRNSYS DECLARATIONS
                            DOUBLE PRECISION XIN,OUT
                            INTEGER NI,NP,ND,NO
                            PARAMETER (NI=2,NP=2,NO=1,ND=0)
                            INTEGER*4 INFO,ICNTRL
                            REAL T,DTDT,PAR,TIME
                            DIMENSION
XIN(NI),OUT(NO),PAR(NP),INFO(15)
                            CHARACTER*3 YCHECK(NI),OCHECK(NO)

C-----------------------------------------------------------------------

C                   IF ITS THE FIRST CALL TO THIS UNIT, DO SOME
BOOKKEEPING
                            IF (INFO(7).GE.0) GO TO 100
                            INFO(6)=NO
                            INFO(9)=1
                            CALL TYPECK(1,INFO,NI,NP,ND)

                            RETURN 1
```

```
C                    END OF THE FIRST ITERATION BOOKKEEPING

C-----------------------------------------------------------------------

C          VALUES OF THE PARAMETERS

100        CONTINUE
                              Pgen=PAR(1)
                              gammaSET=PAR(2)

C          VALUES OF THE INPUTS
                              mhftD=XIN(1)
                              mhtfSol=XIN(2)

C-----------------------------------------------------------------------

C                    COMPONENT EQUATIONS

                    if (mhftD.gt.mhtfSOL) then

                              mbio=mhftD-mhtfSOL
                              Pbio=(mbio+8595)*(136.33)/3600
                              gam=Pbio/Pgen

                                        if (gam.gt.1) then
                                             gamma=1
                                        else
                                             gamma=gam
                                        endif

                    else
                              gamma=gammaset
                    endif


C-----------------------------------------------------------------------

C          OUTPUTS

200        CONTINUE
C
                              OUT(1)= gamma

                              RETURN 1
                              END
```

Steam engine type subroutine

```
SUBROUTINE TYPE206 (TIME,XIN,OUT,T,DTDT,PAR,INFO,ICNTRL,*)
C************************************************************************
C
C ***
C *** Model Parameters
C ***
C                       ef      any [0;1]           singolo o doppio
effetto
C                       m_sel   kg/hr [2000;15000]          single effect
lower limit flowrate
C                       m_seh   kg/hr [2000;15000]          single effect
upper limit flowrate
C                       m_del   kg/hr [2000;10000]          double
effect lower limit flowrate
C                       m_deh   kg/hr [2000;10000]          double
effect upper limit flowrate
C                       ps      BAR [1;+Inf]                outlet
pressure
C                       r       - [0;+Inf]                  steam
admission degree
C                       n       any [0;+Inf]                rotational
frequency (rpm)
C                       V       m^3 [0;+Inf]                expansion
chamber volume
C                       XSI     - [0;1]                     pistons
shaft encumbrance

C ***
C *** Model Inputs
C ***
C                       mw      kg/hr [o;+Inf]              steam flow
rate
C                       Pa      BAR [0;+Inf]                inlet
pressure

C ***
C *** Model Outputs
C ***
C                       pmi     BAR [0;+Inf]        mean indicated
pressure
C                       Pi      kW [0;+Inf]         indicated power
```

```
C                       Pel     kW [0;+Inf]     electric power
C                       ETAo    - [0;1]         operational efficiency
C                       z       - [0;+Inf]      admission rate
C                       hout                    outlet enthalpy

C ***
C *** Model Derivatives
C ***

C (Comments and routine interface generated by IISiBat 3)
C**********************************************************************

C               STANDARD TRNSYS DECLARATIONS
                        DOUBLE PRECISION XIN,OUT
                        INTEGER NI,NP,ND,NO,ef
                        PARAMETER (NI=3,NP=10,NO=6,ND=0)
                        INTEGER*4 INFO,ICNTRL
                        REAL
T,DTDT,PAR,TIME,mw,pa,m_sel,m_seh,m_del,m_deh,ps,r,n
                        REAL pmi,Pi,Pel,ETAo,z,V,XSI,hin,hout
                        DIMENSION
XIN(NI),OUT(NO),PAR(NP),INFO(15)
                        CHARACTER*3 YCHECK(NI),OCHECK(NO)

C----------------------------------------------------------------------

C               IF ITS THE FIRST CALL TO THIS UNIT, DO SOME
BOOKKEEPING
                        IF (INFO(7).GE.0) GO TO 100
                        INFO(6)=NO
                        INFO(9)=1
                        CALL TYPECK(1,INFO,NI,NP,ND)


                        RETURN 1

C               END OF THE FIRST ITERATION BOOKKEEPING

C----------------------------------------------------------------------

C       VALUES OF THE PARAMETERS

100     CONTINUE
```

```
                    ef=PAR(1)
                    m_sel=PAR(2)
                    m_seh=PAR(3)
                    m_del=PAR(4)
                    m_deh=PAR(5)
                    ps=PAR(6)
                    r=PAR(7)
                    n=PAR(8)
                    V=PAR(9)
                    XSI=PAR(10)

C       VALUES OF THE INPUTS
                    mw=XIN(1)
                    Pa=XIN(2)
                    hin=XIN(3)

C-------------------------------------------------------------------------

C       COMPONENT EQUATIONS

                z= pa/ps
                ETAo=0.855

        IF (ef.eq.0) THEN ! if ef=0 then it is a single effect engine

                IF (((mw.ge.m_sel).and.(mw.le.m_seh)).and. ! m  in the
single effect range
    *           ((z.ge.2.5).and.(z.le.8)))    THEN    ! admission rate
range

                                c=-0.6558*(z**2)+9.5605*z+11.515 !(
angular coefficient)
                                Pel=c*mw/1000 ! line equation
                                Pt=Pel/ETAo
                                PtJ=Pt*3600
                                dh=PtJ/mw
                                hout=hin-dh
                                GO TO 500
                ELSE    Pel=0
                                Pt=0
                                hout=hin
                                GO TO 400
                ENDIF
```

```
        ELSE
                IF (((mw.ge.m_del).AND.(mw.le.m_deh)).and. ! m  in the
double effect range     *
        ((z.ge.6).and.(z.le.20))) THEN        ! admission rate range

                                        c=-0.084*(z**2)+4.0409*z+34.775
                                        Pel=c*mw/1000
                                        Pt=Pel/ETAo
                                        PtJ=Pt*3600
                                        dh=PtJ/mw
                                        hout=hin-dh
                                        GO TO 500
                ELSE    Pel=0
                                        Pt=0
                                        hout=hin
                                        GO TO 400
                ENDIF
        ENDIF


 400    Pt=0
        Pel=0
        hout=hin
        ETAo=0
        dh=0


C-------------------------------------------------------------------------

C       OUTPUTS

500      CONTINUE

                                OUT(1)=dh
                                OUT(2)=Pt
                                OUT(3)=Pel
                                OUT(4)=ETAo
                                OUT(5)=z
                                OUT(6)=hout

                                RETURN 1
                                END
```

Hot thermal fluid flow request calculator type subroutine

```
SUBROUTINE TYPE219 (TIME,XIN,OUT,T,DTDT,PAR,INFO,ICNTRL,*)
C************************************************************************

C ***
C *** Model Parameters
C ***

C ***
C *** Model Inputs
C ***
C                           LoadEl   kW [0;+Inf]
C                           Loadth

C ***
C *** Model Outputs
C ***
C                           mhtfel    kg/hr [0;+Inf]
C                           mhtfth    kg/hr [0;+Inf]

C ***
C *** Model Derivatives
C ***

C (Comments and routine interface generated by IISiBat 3)
C************************************************************************

C                   STANDARD TRNSYS DECLARATIONS
                            DOUBLE PRECISION XIN,OUT
                            INTEGER NI,NP,ND,NO
                            PARAMETER (NI=2,NP=0,NO=2,ND=0)
                            INTEGER*4 INFO,ICNTRL
                            REAL T,DTDT,PAR,TIME
                            DIMENSION
XIN(NI),OUT(NO),PAR(NP),INFO(15)
                            CHARACTER*3 YCHECK(NI),OCHECK(NO)

C-----------------------------------------------------------------------

C                   IF ITS THE FIRST CALL TO THIS UNIT, DO SOME
BOOKKEEPING
                            IF (INFO(7).GE.0) GO TO 100
                            INFO(6)=NO
                            INFO(9)=1
                            CALL TYPECK(1,INFO,NI,NP,ND)


                            RETURN 1
```

```
C                    END OF THE FIRST ITERATION BOOKKEEPING

C-----------------------------------------------------------------------

C          VALUES OF THE PARAMETERS

100        CONTINUE

C          VALUES OF THE INPUTS
                              LoadEl=XIN(1)
                              LoadTh=XIN(2)

C-----------------------------------------------------------------------

C          COMPONENT EQUATIONS

                    mhtfel=0.036*LoadEl**2.713
                    mhtfth=0.000002*LoadTh**3.289

                              if(mhtfel.le.0)then
                                        mhtfel=0
                              endif

                              if(mhtfth.le.0)then
                                        mhtfth=0
                              endif


C-----------------------------------------------------------------------

C          OUTPUTS

200        CONTINUE
C                    mhtf
                              OUT(1)=mhtfel
                              OUT(2)=mhtfth


                              RETURN 1
                              END
```

Appendix B – TRNSYS types parameters

Type 16 g - Solar radiation processor

Parameter	Value
Tracking mode	1
Tilted surface mode	3
Starting day	1
Latutude	41,91
Solar constant	4˙871 kJ/h m^2
Shift in solar time	O degrees
Solar time	-1

Type 115 – Economizer

Parameter	Value
Overall heat transfer factor	5˙500 kJ/h K
Reference pressure loss cold side	0 bar
Reference cold side flow	1˙850 kg/h
Power law exp for UA	0
Power law exp for DP	0

Type 116 – Evaporator, solar side

Parameter	Value
Overall heat transfer factor	70˙000 kJ/h K
Blow down fraction	0
Reference pressure loss	0 bar
Reference flow rate	1˙400 kg/h
Power law exp for UA	0
Power law exp for DP	0

Type 116 – Evaporator, biomass side

Parameter	Value
Overall heat transfer factor	120˙000 kJ/h K
Blow down fraction	0
Reference pressure loss	0 bar
Reference flow rate	1˙850 kg/h
Power law exp for UA	0
Power law exp for DP	0

Type 183 – Condenser

Parameter	Value
dT cool water out + condensing temp	53,58 °C
Temp increase in cool. water	30 °C

Type 202 – Biomass furnace

Parameter	Value
Pnom	1˙163 kW
Pgen	930 kW
Tf_out1	340 °C
To_out	300 °C
e	200
C	46,92
H	5,32
O	38,55
S	0,04
u	8
Hi	16˙944,86 kJ/kg
gammaSET	0,35

Type 206 – Steam engine

Parameter	Value
ef	1
m_sel	500 kg/h
m_seh	15˙000 kg/h
m_del	500 kg/h
m_deh	10˙000 kg/h
ps	3 bar
r	4
n	1˙000
V	0,015 m^3
XSI	0,15

Type 230 – Concrete storage

Parameter	Value
HTF specific heat	2,273 kJ/kg K
HTF density	839,19 kg/m^3
Total cross sec area of pipes	1,5 m^2
Lenght of storage	114 m
Concrete specific heat	0,9638 kJ/kg K
Concrete total mass	4˙543˙990 kg
Overall heat transfer coefficient at reference flowrate	124˙847,31 kJ/h K
Overall loss coefficient	10 kJ/h K
Reference flowrate	5˙489 kg/s
ak0 parameter for scaling of heat transfer coeff	0,6454905
ak1	2,255832
ak2	-6,842885
ak3	10,86112
ak4	-8,5377
ak5	2,618488

Type 231 – Stoco

Parameter	Value
Charge max oil bottom temp	300 °C
Discharge min oil temp	280 °C
Cp HTF	2,273 kJ/kg K

Type 296 - Solar field

Parameter	Value
A – loss coeff	68,86
B – loss coeff	-0,00684
C – loss coeff	-14,68
Cw – loss coeff	0
D – loss coeff	-0,1672
Clean reflectivity	1
Broken mirror fraction	0
Lenght of SCA	36 m
Aperture width of SCA	2,3 m
Focal lenght of SCA	0,76 m
Rowspacing	6,9 m
Total field area	2˙580 m^2
Pump max flowrate	31˙000 kg/h
Pump power coeff. 1	1,308
Pump power coeff. 2	4,28 E-3
Pump power coeff. 3	1,99 E-3
Tank heat loss rate at 275 °C	0 W
Piping heat loss/area at 343 °C	0 W/m^2
Field tracking parasitic/area	0 W/m^2
Field stow energy	0 J
Wind speed limit for tracking	13,7 m/s
Turn down ratio (min flow ratio)	0,03
Direction (S=0, W=90)	0 degrees
Tilt	0 degrees
Min tracking	-90 degrees
Max tracking	90 degrees
Typ (IAM-Ls3=0, IST Sandia =1; ST)	2